THIN FILM COATING OF GLASS FABRICS FOR RADAR ABSORBING COMPOSITES

A Thesis submitted to
the Graduate School of Engineering and Sciences of
İzmir Institute of Technology
in Partial Fulfillment of the Requirements for the Degree of

MASTER OF SCIENCE

in Physics

by
Mutlu Devran YAMAN

February 2015
İZMİR

We approve the thesis of **Mutlu Devran YAMAN**

Examining Committee Members:

_____

Prof. Dr. Lütfi ÖZYÜZER
Department of Physics, Izmir Institute of Technology

_____

Prof. Dr. Metin TANOĞLU
Department of Mechanical Engineering, Izmir Institute of Technology

_____

Assoc. Prof. Dr. Ekrem ÖZDEMİR
Department of Chemical Engineering, Izmir Institute of Technology

05 February 2015

_____

Prof. Dr. Lütfi ÖZYÜZER
Supervisor, Department of Physics,
Izmir Institute of Technology

_____

Prof. Dr. Nejat BULUT
Head of the Department of Physics

_____

Prof. Dr. Bilge KARAÇALI
Dean of the Graduate School of
Engineering and Sciences

ACKNOWLEDGMENTS

First of all, I would like to express my deepest gratitude to my supervisor Prof. Lütfi ÖZYÜZER for valuable discussions, endless support and giving me the possibility of carrying out this studies under his supervision. He always gave me a lot of freedom to perform and design my own experiment. I have really enjoyed working in his laboratory. Also, I am indebted to Prof. Metin TANOĞLU for his valuable comments on my thesis. Moreover, I am grateful to the thesis committee member Assoc. Prof. Ekrem ÖZDEMİR for his valuable comments on my thesis.

In addition, I am thankful to Prof. Metin TANOĞLU for his permission to use his laboratories during my experimental studies.

Furthermore, I am especially grateful to my laboratory colleagues, Adnan TAŞDEMİR, Metin KURT, Serkan KANGAL, Hasan KÖSEOĞLU and Fatime Gülşah AKÇA for their assistance and supporting in my studies. I would like to thank all OZYUZER Laboratory Members for their kindness and creating a nice and funny atmosphere while studying in laboratory. In addition, special thanks to Göksenin BOZDAĞ.

Finally, I would like to express my cordially thanks to my family. Of course I am very grateful to my wife, Zeynep Burçin YAMAN and to my son, Ahmet Deniz YAMAN. They are my biggest supporters in my life.

This thesis was partially supported by KOSGEB through facilities of TeknoMa Technological Materials Inc.

ABSTRACT

THIN FILM COATING OF GLASS FABRICS FOR RADAR ABSORBING COMPOSITES

By the invention of radio and micro wave range in electromagnetic spectrum, some radar systems were started to use to predict the range, altitude, direction or speed of objects. During the Second World War, the scenario changed significantly and this led to the development of the radar absorbing materials (RAM's). Then the stealth technology and Radar Cross Section (RCS) terminologies took place in science research area. To reduce of an objects detectability in the radar detection systems, the reduction of the radar cross section play an important role. For absorbing electromagnetic micro waves, radar absorbing materials have been developed and they consist dielectric and magnetic materials that has capacity for absorbing. In order to increase frequency range (bandwidth) of the absorbance, several materials have been already proposed by several researchers. But nowadays, studies on investigating the radar absorbing structures (RAS) using fiber reinforced polymeric composite materials, are becoming popular research field. The purpose of this study is to design, fabricate and characterize RAS's based on unidirectional E-glass fiber reinforced epoxy resin composites which can absorb microwave within 2-20 GHz frequency range. Several Jaumann design composite structures were manufactured to achieve radar wave absorbance. In this Jaumann structures, we use different designs in terms of different resistive values of sheets and different thickness of composites. In addition to this, we also focused on the different concentration of additives and distance between resistive sheets. Glass fiber / epoxy system were employed as a base structure. Carbonyl Iron powders were used to change permittivity, permeability and intrinsic impedance values of the structure. To functionalize the glass fibers and to make them conductive, surface of them was metalized by using large area planar magnetron sputtering system. These conducting layers act as a resistive sheet within the composite structure. Surface resistances of resistive sheets used in structures show diversity between ≈ 430 ohms and to 30 ohms.

ÖZET

RADAR SOĞURABİLEN KOMPOZİTLER İÇİN CAM ELYAFLARIN İNCE FİLM KAPLAMALARI

Elektromanyetik spektrumdaki radyo ve mikro dalga aralıklarının keşfinden sonra, nesnelerin büyüklüğünü, irtifalarını, yönlerini ya da hızlarını belirlemek için bazı radar sistemleri kullanılmıştır. İkinci dünya savaşı sırasında senaryo önemli ölçüde değişmiş ve bu olay Radar Soğurabilen Malzemelerin (RSM'ler) geliştirilmesine yol açmıştır. Bu sebeple görünmezlik teknolojisi ve radar kesiti terminolojileri bilim araştırma alanında yer almıştır. Radar tespit sistemlerinde, nesnelerin tespit edilebilirliklerini azaltmak istiyorsak, radar kesitinin azaltılası bunda önemli rol oynar. Mikrodalgaların soğurulması için, radar emebilen özelliklere sahip dielektrik ve manyetik malzemeler geliştirilmiştir. Emilimin frekans aralığını (bant genişliğini) arttırmak için, bu güne kadar araştırmacılar tarafından birçok malzeme önerilmiştir. Fakat bu aralar, cam elyaf katkılandırılmış polimerik kompozit malzemeler kullanılarak geliştirilen radar soğurabilen yapılar (RSY), popüler araştırma alanı olmaya başlamıştır. Bu çalışmanın amacı, 2-20 GHz aralığındaki dalgaları emebilen, tekyönlü cam elyaf katkılandırılmış epoksi bağlayıcı kompozitlerin tasarım, üretim ve karakterizasyonlarını yapmaktır. Radar dalgası soğurulması için, birçok Jaumann tipi kompozit yapılar üretilmiştir. Bu Jaumann yapılarda, farklı direnç değerine sahip katmanlar kullanılmış ya da farklı kalınlıklarda değişik tasarımlar yapılmıştır. Buna ek olarak, direnç katmanları arasındaki uzaklıklar değiştirilmiş ve farklı derişimdeki katkı maddelerine sahip yapılar üzerinde de durulmuştur. Cam elyaf / epoksi sistemi temel yapı olarak kullanılmıştır. Kompozit yapının elektrik ve manyetik geçirgenlik katsayıları ile empedansının değiştirilmesi için demir karbonil tozları kullanılmıştır. Cam elyafların fonksiyonelleştirilmesi ve üzerlerinin iletken olması için, geniş alan düzlemsel mıknatıssal saçtırma yöntemi kullanılarak yüzeyleri ince film kaplanarak metalize edilmiştir. Bu iletken yüzeyler kompozit yapı içerisinde direnç katmanı olarak davranırlar. Yüzey dirençleri ≈ 430 ohm'dan başlayarak 30 ohm'a kadar çeşitlilik göstermektedir.

To my Family

TABLE OF CONTENTS

LIST OF FIGURES

LIST OF TABLES

Table **Page**

CHAPTER 1

INTRODUCTION

1.1. Radar

Radar, which is an acronym for Radio Detection and Ranging that, is an object detection system. In this systems, for detection purposes, through the electromagnetic spectrum, ultraviolet, visible, infrared, microwave and radio frequencies can be used. This electromagnetic waves are used to determine the range, altitude, direction or speed of objects. For example; it can be used to detect aircraft, ships, spacecraft, guided missiles, motor vehicles, weather formations and terrain. In this spectrum, for radars, most used waves are microwaves. In this mechanisms, simply, there is a radar disk or antenna which emits pulses of radio waves or microwaves that bounce of any object in this path. And at the same time in the system there is receiver part which can detect the return wave energy from the tiny object. This parts are usually located at the same site as transmitter.

Radars are modern uses of many diverse areas such as air traffic control, radar astronomy, air defence systems, antimissile systems, marine radars to locate landmarks and other ships; aircraft anti-collision systems; ocean surveillance systems, outer space surveillance and rendezvous systems; meteorological precipitation monitoring; altimetry and flight control systems; guided missile target locating systems; and ground-penetrating radar for geological observations. In Figure 1.1 there is a radar ranges related to the using purposes.

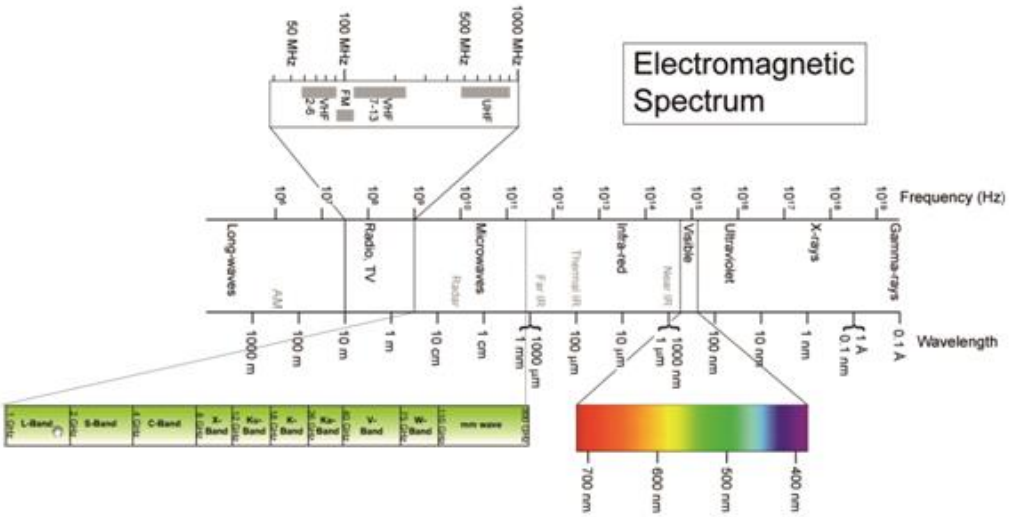

Figure 1.1. Illustration of electromagnetic wave spectrum

Band Designation	Frequency Range	General Usage
VHF (Very High Frequency)	30-300 MHz	Very Long Range Surveillance
UHF (Ultra High Frequency)	300-1000 MHz	Very Long Range Surveillance
L	1-2 GHz	Long Range Surveillance, Enroute Traffic Control
S	2-4 GHz	Moderate Range Surveillance, Terminal Traffic Control, Long Range Weather
C	4-8 GHz	Long Range Tracking, Airborne Weather Detection
X	8-12 GHz	Short Range Tracking, Missile Guidance, Mapping, Marine Radar, Airborne Intercept
K_u	12-18 GHz	High Resolution Mapping, Satellite Altimetry
K	18-27 GHz	Little Used (Water Vapor Absorption)
K_a	27-40 GHz	Very High Resolution Mapping, Airport Surveillance

Figure 1.2. Spectrum of the using RADAR waves

1.2. History

Radar absorbing material (RAM) has been widely proceeded in many papers (Severin 1956; Emerson 1973; Vinov and Jha 1995; Petrov and Gagulin 2001; Lederer 1986; Gaylor 1989) and book (Ruck 1981; Vinoy and Jha 1996) not only due to its applications but also due to high demand for necessity of improvement. It can be observed that RAM's begun to use in the 1930 followed by the rise of the investigation of radar. These structures have absorber design with combined materials including different loss mechanism. This mechanism required to be optimized in absorption over wide range bandwidth by using optics and physics science. Besides, there were other parameter playing role in limitation of absorbers such as different shapes and structures, ranging from thick pyramidal structures, to multilayer and single coatings. Afterwards, microwave absorbing materials have been used in commercial applications which are favourable for anechoic chambers and reducing the reflected signals from buildings and superstructures around radar installations. Recent communication technologies corresponding microwave frequencies are carrying forward the development of absorbers and frequency selective surfaces. In this section, I will give a brief look for development of RAM and it will help to examine the devices, materials and structures which is discussing here.

Electromagnetic wave absorbers started to research in the 1930's (Emerson 1973; Vinoy and Jha 1996). Then the first patent about electromagnetic wave absorber came out in 1936 in the Netherlands. It was a quarter-wave resonant type absorber and carbon black used as lossy resistive material and titanium dioxide used as its high permittivity to reduce the thickness.

Germany was one of the related country with radar camouflage for submarines and they developed a "Wesch" material around time of World War II. It was including a carbonyl iron powder loaded rubber sheet about 7.6 mm thick and a resonant frequency at 3 GHz. The front surface was waffled in order to produce a larger bandwidth in this material. A multilayer device of alternating resistive sheets and rigid plastic were produced as Jaumann Absorber. This prototype was nearly 7.62 cm thick and resistances were decreasing exponentially from the front to the back. Reflectivity in this device was successfully reduced to –20 dB over 2-15 GHz. During the same time period, "HARP" standing for Halpern AntiRadiation Paint was developed by Halpern at MIT Radiation

Laboratory in America. MX-410 is airborne version of HARP and it was including 0.64 mm thickness of for X-band resonance. The permittivity of base dielectric was 150 due to loading with highly oriented disk shaped aluminium flakes suspended in a rubber matrix and carbon black for loss. The reduction of reflectivity in this material was a 15-20 dB. Shipborne absorbers have 1.78 cm thickness (X-band) iron particle contain rubber with a permittivity of 20 and have enough permeability to produce resonance broadening (Halpern 1960; Otto, et al. 1960). The resonant Salisbury Screen was developed with about 25% bandwidth at resonance at the same time (Salisbury 1952). US Rubber Company marketing helped for production of Salisbury screens with resistive cloth called Uskon. At that time another absorber design was produced. It was a long pyramidal structure with the inside coated with Salisbury Screen and the apex in the direction of propagation. High attenuation was obtained from the absorber as a result of multiple reflections (Neher 1953). The importance of ferrites for RAM's was known. These devices are typically narrow band with the exceptions of the Jaumann device and the inverted pyramid.

Sharp pointed geometric shapes were used to produce a gradual transition into the absorbing material in the time period of post war (1945-1950) which was characterized by the development of broadband absorbers. The application in anechoic chambers was found by these materials (Tiley 1944; Salati 1954; Tanner 1961; McMillan 1958). Materials examined for microwave attenuation contain carbon loaded plaster of paris, graphite, iron oxide, powdered iron, powdered aluminium and copper, steel wool, water, powdered "Advance" and "Constantin" and metal wires (Carlton 1961). Supporting with a lot of air at the interface included foams, fibers and "excelsior", the binders included various plastics and ceramics. The patterned flat layered resistive sheets reproduce the pyramidal, or conical structures of above, so that more functional lossy broadband materials were created with a flat surface.

A commercial production of RAM called "Spongex" which is based on carbon coated animal hair is produced in 1950's by the Sponge Products Company becoming a division of B.F. Goodrich Company. This material with 5.08 cm thickness had –20 dB attenuation in the reflectivity over 2.4-10 GHz for normal incidence. By the following, 10.16 cm and 20.32 cm versions also produced for lower frequencies. Emerson and Cuming Inc and McMillan Industrial Corporation joined to this company in order to manufacture the absorbers. During this decade, Severin and Meyer started to research into circuit analog devices. Circuit analog first used for circuit theory to represent the

components/processes occurring in the absorber, and hence to model the reflectivity. This technique was accepted from research programs on acoustical absorbers. Severin and Meyer made experimental absorbers with various orientations including resistance loaded loops, slots in resistive foil, resistance loaded dipoles, strips of resistive material, strips of magnetic material, surface shaping and magnetic loading of resonant materials.

Frequency selective surfaces (FSS) was born as a new field by results of these kind of researches (Munk 2005). Important absorber thickness reductions were demonstrated by using ferrite under layers (Kunihiro 1971) and circuit analog materials continued to explore at 60's and 70's. Pyramidal shaped absorbers were being used for anechoic chambers resulted –60 dB at near normal incidence. With the screen printing (Connolly and Luoma 1977) control of the fabrication of Jaumann layers was demonstrated. Absorbers were being manufactured from foams, netlike structures, knitted structures, or honeycomb and coated with a paint containing particulate or fibrous carbon, evaporated metal or nickel chromium alloy. It was interesting that one patent described an absorbers that employing a plasma to absorb the microwaves. A radioactive substance generated the plasma requiring about 10 Curies/cm2 (Nahmias 1977).

The 1980's includes the absorber design process improvement by optimization techniques (Fante and McCormack 1988; Cloete and du Toit 1989; du Toit and Cloete 1990). A graded layer (Gaylor 1989; Nortier, et al. 1987) improved Jaumann absorbers' bandwidth and used for different resistive profiles to achieve maximum bandwidths. Computers and transmission line models were used to calculate reflectivity from material properties. The transmission line model are applied for frequency selective surfaces representing as equivalent circuits (Lederer 1986). Circuit analog materials are modelled (Kasevich and Broderick 1993) and the scattering of these materials is investigated based on the Floquet theorem (Vanderplas, et al. 1989). Carbon black or graphite, carbonyl iron and ferrites was continued to use for materials and though now artificial dielectrics are being evaluated by adding inclusions such as rods, wires, disc and spheres (Gaylor 1989). Helical inclusions are found to improve absorption and resulted in research into chiral materials (Jaggard and Engheta 1989). The desired permittivity and permeability of these new materials are calculated by mixing theory. One of the other potential radar absorbing materials is conducting polymers.

It is seen that dominant optimisation techniques for Jaumann structures including genetic algorithm optimization from 1990's to today (Chakravarty, et al. 2001; Chakravarty, et al. 2002; Cheldavi and Kamarei 1997; Foroozesh, et al. 2000; Johnson

and Rahmat 1997; Mosallaei and Rahmat 2000). Circuit analog and frequency selective surfaces are still hot topics in the literature (Meyer, et al. 1954; Kasevich and Broderick 1993; Vanderplas, et al. 1989; Chakravarty, et al. 2002; Bornemann 1993; Broderick, et al. 1996; Diaz and McKinzie 2003; Simovski, et al. 2000; Terracher and Berginc 2000; Heafey, et al. 1993) These materials with Conducting polymers and composite materials are found along with conducting polymer coated fibers and fabrics for creating devices (Adams, et al. 1994; Barry and Carey 1993; Bjorklund and Lunströem 1984; Child 1998; Child and DeAngelis 1999; Collins and Buckley 1996; Child, et al. 1997; Child, et al. 1998; Genies, et al. 1991; Gregory, et al. 1989; Cuddihee, et al. 1992; Kimbrell, et al. 1989; Kimbrell and Kuhn 1991; Kuhn 1992; Kuhn, et al. 1995; Machell and Thomas 1975; Marchant, et al. 1998; Newman, et al. 1986; Oh, et al. 1999; Olmedo, et al. 1995; Kuhn, et al. 1992; Rhode and Sparks 2001; Kocsik and Rowe 2000; Thieblemont, et al. 1993; Truong and Ternan 1995; Warren, et al. 1986; Wettermark and Worrell 1996; Woldanski 2001). A new class of absorbers and their roots in conducting polymers is that of dynamic RAM (Chambers and Tennant 2003; Chambers and Tennant 1996) where the resonant frequency of the absorber is tunable through variation of resistive and capacitive elements in the absorber.

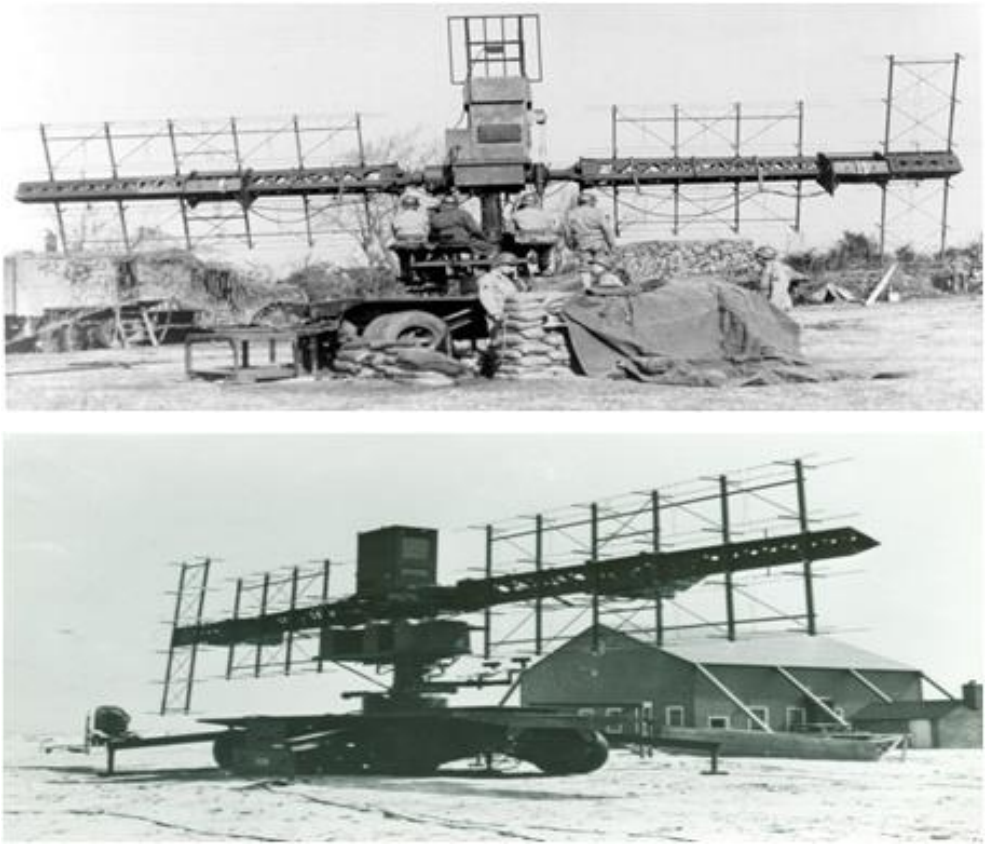

Figure 1.3. Examples of first radar applications system

1.3. Radar Cross Section (RCS)

Radar is a very sensitive long-range detection technique that is deployed in many locations and on many platforms including missiles. Radar cross section is a measure of the how much electromagnetic radiation is scattered from an object. The signature received by a radar from a target is determined by the radar cross section of the target. The magnitude of the radar cross section is indicative of the objects detectability. Low radar cross section means that a platform is less detectable and can operate a closer ranges. Reducing the RCS reduces the detection range of a platform. The optimum means of reducing the RCS of an object is in the design phase, where low scattering materials and angular shapes can be used to reduce the signal returned to a radar receiver. The RCS of a platform can be determined on a range, in an anechoic chamber with a scale mode, or by modelling. The factors affecting radar cross section are the target's shape, size and the materials from which it is manufactured. Radar Cross Section reduction relies on shaping, low reflectivity and on the use of radar absorbing materials.

1.4. Reflectivity Minimization

The interaction between material and electromagnetic wave is important thing here. Firstly, if you want to low radar cross section, it means, the wave reflected from an object should be minimized. This reflectivity minimization can be done by several ways. In this section, I will focus on some points for minimize the reflection.

In an attempt to minimize the reflection from surface of an object, it is useful to consider the physical equations that represent the reflection process. It can be said that, there are three conditions about the reflection minimization to achieve the minimum reflection process.

The first equation of interest is that describing the reflection coefficient at an interface.

$$r = \frac{\eta_M - \eta_0}{\eta_M + \eta_0} = \frac{Z_M - Z_0}{Z_M + Z_0} \tag{1.1}$$

Where r is the reflection coefficient and η admittance of the propagating medium (subscript o for incident medium or air and M for substrate). It can be said in this equation, the admittance of an object can be replaced with intrinsic impedance ($Z = 1/\eta$). We can easily see from the equation that, reflection coefficient falls to zero when $\eta_0 = \eta_M$, or in other words the material in the layer is impedance matched to the incident medium. The intrinsic impedance of free space is effectively given by

$$Z_o = \frac{E}{H} = \sqrt{\frac{\mu_0}{\varepsilon_0}} \approx 377\ ohms \tag{1.2}$$

Where E and H are the electric and magnetic field vectors and μ_o and ε_o are the permeability and permittivity values of free space, respectively. Thus if we achieve to manufacture a material with an intrinsic impedance of 377 ohms, this type of materials will not reflect microwaves. Of course it provided that the incident medium is free space.

The second way to minimize the reflection is to have equal electric permittivity and magnetic permeability values. This second condition also will give the result of minimum in the reflection coefficient. In this case equation 2.1 can be rewritten as;

$$r = \frac{\frac{Z_M}{Z_0} - 1}{\frac{Z_M}{Z_0} + 1} \tag{1.3}$$

The normalized intrinsic impedance is

$$\frac{Z_M}{Z_o} = \sqrt{\frac{\mu_r^*}{\varepsilon_r^*}} \tag{1.4}$$

Where $\varepsilon_r^* = \frac{\varepsilon' - i\varepsilon''}{\varepsilon_0}$ and$\mu_r^* = \frac{\mu' - i\mu''}{\mu_0}$. The prime and double prime superscripts represent the real and imaginary components of the complex numbers, respectively.

If the incident medium is free space and the reflectivity is zero, then it follows that$\mu_r' = \varepsilon_r'$. If we make research and think on it, we can easily say, it would be so hard to manufacture such kind of materials which have this values of permittivity and permeability. But the implication is if both the real and imaginary parts of the permittivity and permeability are equal, then the reflectivity coefficient is zero.

In the third consideration, we can talk about the attenuation of the wave as it propagates in to the absorbing medium. The power of the wave decays exponentially with distance, x, by the factor $e^{-\alpha x}$. α is the attenuation constant of the material and can be expressed as

$$\alpha = -\sqrt{\varepsilon_0 \mu_0}\omega(a^2 + b^2)^{\frac{1}{4}} \sin(\frac{1}{2}\tan^{-1}(-\frac{a}{b})) \tag{1.5}$$

Where $a = (\varepsilon_r'\mu_r' - \varepsilon_r''\mu_r'')$ and$b = (\varepsilon_r'\mu_r' + \varepsilon_r''\mu_r'')$.

What we have to do here is to achieve large amount of attenuation in a small thickness. For this reason α must be large, which implies that attenuation will be large. For large α values, $\varepsilon_r', \varepsilon_r'', \mu_r' \; and \; \mu_r''$ must be large. It is noted here that this condition must be tempered with the first condition (Equation 1.1), where large values of permittivity and permeability would result in a large reflection coefficient.

1.5. Transmission Line Theory

Transmission line theory has been used to model and optimize absorbers and essentially follows the logic of the reflectivity calculation. A multisection transmission line is shown in Figure 2.1.

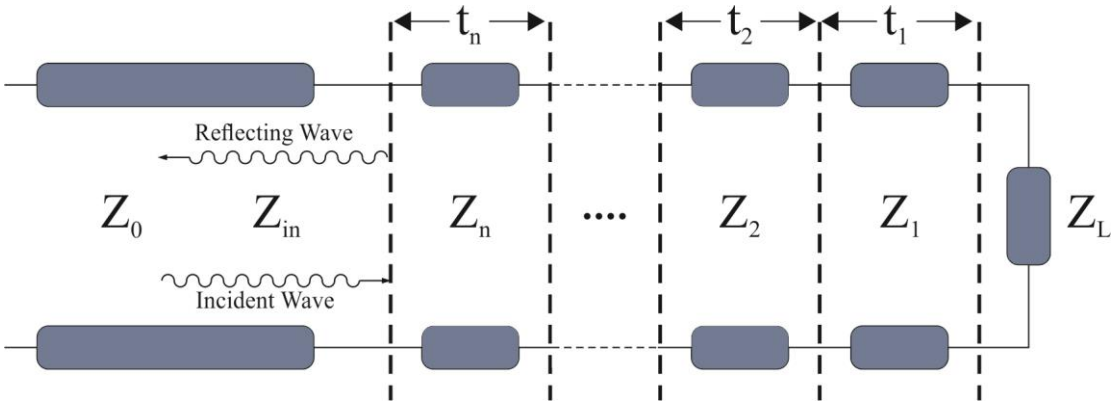

Figure 1.4. Multi-section transmission line

Under these hypothesis we can use the transmission line theory in order to calculate the microwave Reflection Coefficient (RC) at the air-composite material layer interface. The electromagnetic wave absorbing property can be evaluated by the following equation (Ramo 2007);

$$RC = 20\log_{10}\left|\frac{(Z_i - Z_0)}{Z_i + Z_0}\right| \tag{1.6}$$

Where RC is the reflection coefficient (dB), Z_0= 377 ohm is free space impedance, and Z_i is the input impedance at the air-absorber interface. This latter can be expressed as

$$Z_i = \eta_k \frac{Z_L \cos(\beta t) + j\eta_k \sin(\beta t)}{\eta_k \cos(\beta t) + jZ_L \sin(\beta t)} \tag{1.7}$$

Where t is the thickness of the absorber layer, and the propagation number β is given by

$$\beta = j2\pi f\sqrt{\mu_0\varepsilon_0}\sqrt{\mu_r\varepsilon_r} = 2\pi f\sqrt{\mu_0\varepsilon_0}\sqrt{\mu_r(\varepsilon' - j\varepsilon'')} \tag{1.8}$$

The equivalent electric circuit is shown in Figure 2.2.

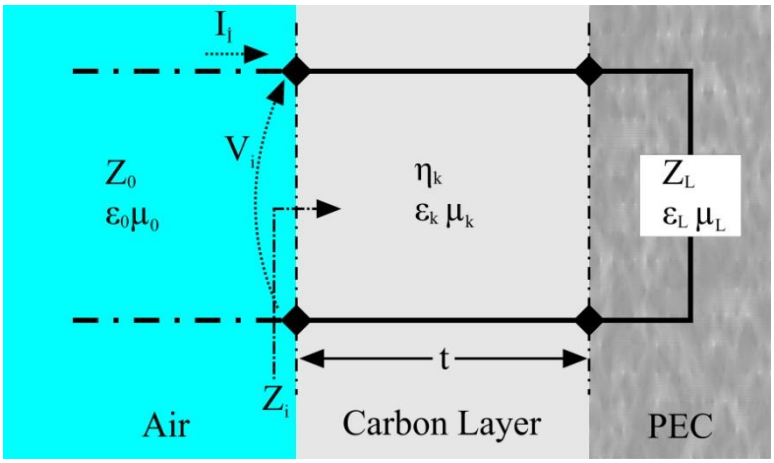

Figure 1.5. Microwave absorbing layer equivalent electric circuit

The absorption capability of a thin layer is mainly due to both dielectric losses within the material and impedance matching condition. The dielectric losses are mainly function of the imaginary part of the permittivity, while the matching condition are to be studied by taking in to account the microwave wavelength too. From Equation 2.7 it is possible to observe that the imaginary part of Z_i vanishes for certain multiple values of the quantity βt. In such a case, if the real part of Z_i is close to Z_0 the matching condition is verified, and the RC quantity goes to zero (i.e. -∞ in dB). Since βt depends on frequency, permittivity and thickness, there will be some combinations and also periodic values of such parameters for which the impedance matching condition is close to be verified (Micheli, et al. 2010).

In particular, when the thickness is an odd multiple of the composite quarter wavelength

$$t = n\frac{\lambda}{4}\ (with\ n = 1, 3, 5, \dots.)$$

$$\lambda = \frac{\lambda_0}{[|\mu_r||\varepsilon_r|]^{1/2}}\ where\ \lambda_0 = \frac{c}{f} \cong \frac{3.10^8}{f} \qquad (1.9)$$

The incident and reflected waves are out of phase (Deng and Han 2007).

If we think on multilayer RAM structures, using equation (2.7) iteratively we can find the corresponding input impedance at each layer interface; by this way we contemporary take into account of the other layers which in turn become the new load impedances. The several input impedances are then expressed by

$$Z_{i_1} = \eta_1 \frac{Z_{PEC}\cos(\beta_1 t_1)+j\eta_1 \sin(\beta_1 t_1)}{\eta_1 \cos(\beta_1 t_1)+jZ_{PEC}\sin(\beta_1 t_1)} \quad (1.10)$$

$$Z_{i_2} = \eta_2 \frac{Z_{i_1}\cos(\beta_2 t_2)+j\eta_2 \sin(\beta_2 t_2)}{\eta_2 \cos(\beta_2 t_2)+jZ_{i_1}\sin(\beta_2 t_2)} \quad (1.11)$$

$$Z_{i_3} = \eta_3 \frac{Z_{i_2}\cos(\beta_3 t_3)+j\eta_3 \sin(\beta_3 t_3)}{\eta_3 \cos(\beta_3 t_3)+jZ_{i_2}\sin(\beta_3 t_3)} \quad (1.12)$$

$$Z_{i_4} = \eta_4 \frac{Z_{i_3}\cos(\beta_4 t_4)+j\eta_4 \sin(\beta_4 t_4)}{\eta_4 \cos(\beta_4 t_4)+jZ_{i_3}\sin(\beta_4 t_4)} \quad (1.13)$$

And the resulting impedance matching condition between free space and RAM structure is $RC = 20\log_{10}\left|\frac{(Z_{i_4}-Z_0)}{Z_{i_4}+Z_0}\right|$.

CHAPTER 2

RADAR ABSORBING

2.1. Classification of Radar Absorbing Materials

In sections 1.4 and 1.5 some theoretical background about the radar absorbing or reflection conditions were given. Now it will be useful to consider how these theories have been put in to practice by considering the types of absorbers that have been produced (Severin 1956; Emerson 1973; Lederer 1986; Gaylor 1989). Absorbers can be classified in to impedance matching and resonant absorbers, though it will be shown in the following discussion that many absorbers have features of both of these classifications. These features typically are a graded interface to match impedance or a gradual transition in material properties for impedance matching, and tuned or so called quarter wavelength resonant layers.

2.1.1. Graded Interfaces-Impedance Matching

If we consider the first condition of the reflectivity minimization equation, it can be said that a propagating wave that impinges upon an interface will experience some reflection that is proportional to the magnitude of the impedance step between incident and transmitting media. With this consideration three classes of impedance matching RAM, pyramidal, tapered and matched, have been devoloped to reduce the impedance step between the incident and absorbing media. For complete attenuation of the incident wave one or more wavelengths of material are required, making them bulky and adding weight.

2.1.1.1. Pyramidal Absorbers

This type absorbers are typically thick materials with pyramidal or cone shapes extending perpendicular to the surface in a regularly spaced pattern (Emerson 1973; Tanner 1961). The height and periodicity of the pyramids tend to be on the order of one wavelength. For shorter structures, or longer wavelengths, the waves are effectively met by a more abrupt change in the impedance. In that reason, these absorbers have a minimum operating frequency above which they provide high attenuation over wide frequency and angle ranges. We can say, pyramidal absorbers provide the maximum performance. Hovewer, the thickness and tendency to be fragile is the disadvantages of these absorbers. Thus, they are usually used for anechoic chambers. A more robust flat pyramidal absorber can be fabricated using multilayers with a pyramidal type structure being described by resistive sheets (McMillan 1958). Pyramidal and wedge shaped absorbers have been designed using Tschebyshev transformer technique (Gau 1997) and have been investigated with Finite Element Methods (Jiang 1999).

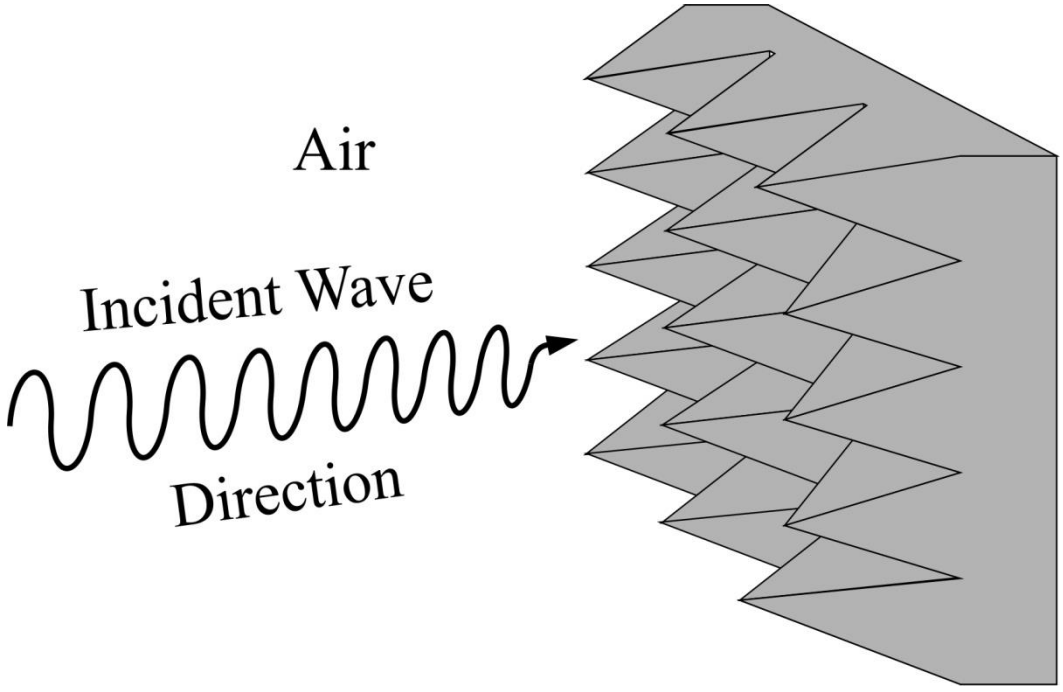

Figure 2.1. Pyramidal absorber

2.1.1.2. Tapered Loading Absorbers

In this type it is typically a slab composed of a low loss material mixed with a lossy material. The lossy component is homogeneously dispersed parallel to the surface, with a gradient perpendicular to the surface and increasing into the material. (Otto, et al. 1960; Tanner 1961). It is difficult to produce this type materials. Because adjusting the gradient is important here and it is not an easy work. These materials are much thinner than the pyramical absorbers, it could the advantage, but the absorbance performances are poorer.

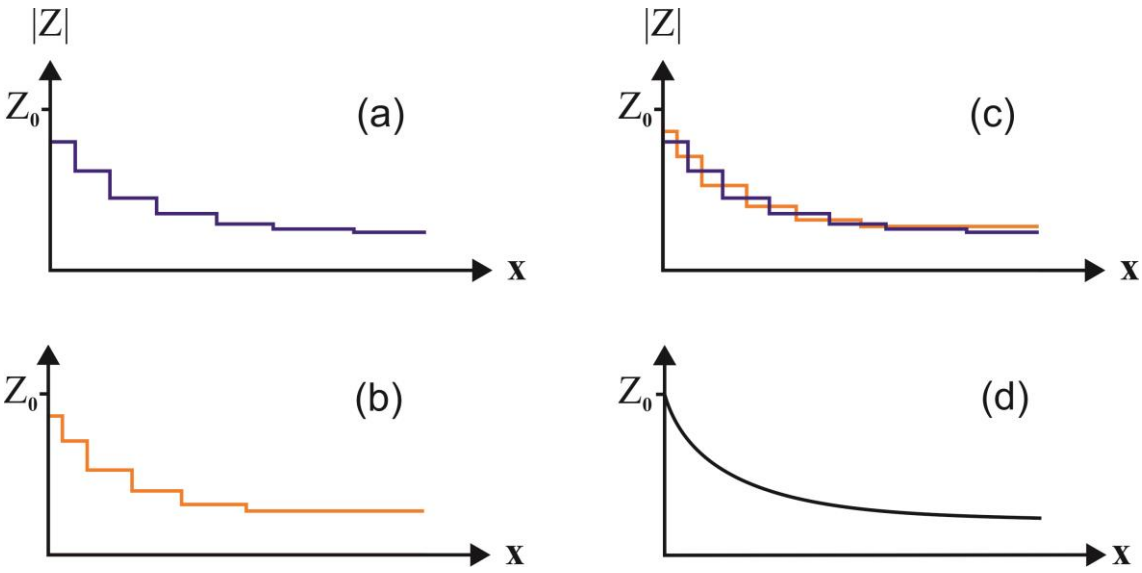

Figure 2.2. Tapered loading absorber a and b) stepped type c) combination of a and b d)smooth type

2.1.1.3. Matching Layer Absorbers

To get rid of the thickness problems of the absorbing materials, the matching layer absorbers can be used for gradual transition materials. Transition matching layer is placed between the incident and absorbing media. The thickness and impedance values of transition layer is important. These values are between the two impedances to be matched (i.e. the absorber and incident media). The idea is to have the combined impedance from the first and second layers to equal the impedance of the incident medium, Figure 2.5. If

the thickness of the matching layer is one quarter of a wavelength of the radiation in the layer, then we can say, matching occurs and

$$Z_2 = \sqrt{Z_1 x Z_3} \tag{2.1}$$

If the frequency of the wave is equal to the optical thickness of the structure, it can be seen that impedance matching. Because of this condition, we can that matching layer materials narrow band absorbers. In microwave frequency range, these absorbers are made using an intermediate impedance and quarter wavelength thickness for absorbtion.

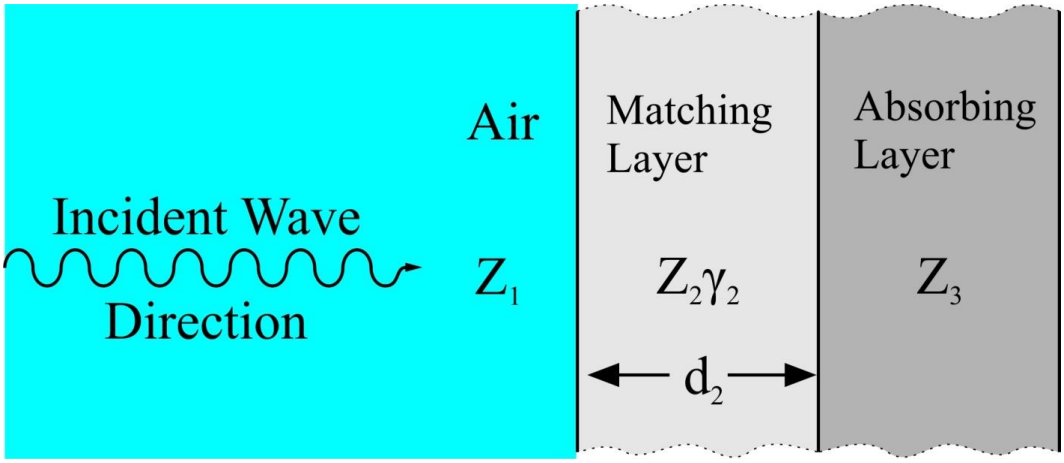

Figure 2.3. Matching layer

2.1.2. Resonant Materials

In this section we will focus on three type of absorbing layers. We can say to this materials tuned or quarter wavelengtth absorbers. These include Dallenbach layers, Salisbury screen and Jaumann layers. In this class most of the coming waves are absorbed but this is not the all power of incident wave. Because the impedance is not matched between incident and absorbing media. And addition to this, the material is thin so that not all the power is absorbed.

2.1.2.1. Dallenbach (Tuned) Layer Absorber

A Dallenbach layer (Dallenbach and Kleinsteuber 1938), is a homogeneous absorber layer with a perfect conducting plane which placed back side of layer. To minimize the reflection for desired wavelength, it is possible to adjust thickness, permittivity and permeability of the layer. In this type of absorbers, destructive interferance of waves occurs between the first and second interfaces. For the reflectivity to result in a minimum, the effective impedance of the layer, Z_L, must equal the incident impedance Z_0.

$$Z_L = Z_1 \tanh \Upsilon_1 d_1 \tag{2.2}$$

However, since Z_L is complex and Z_0 real there is a requirement that the sum of the phase angles in Z_1 and $\tanh \Upsilon_1 d_1$ is zero (destructive interference) and the product of their magnitudes is equal to Z_0. This Dallenbach layer is expressed by five parameters which are Ɛ', Ɛ'', μ', μ'' and d.

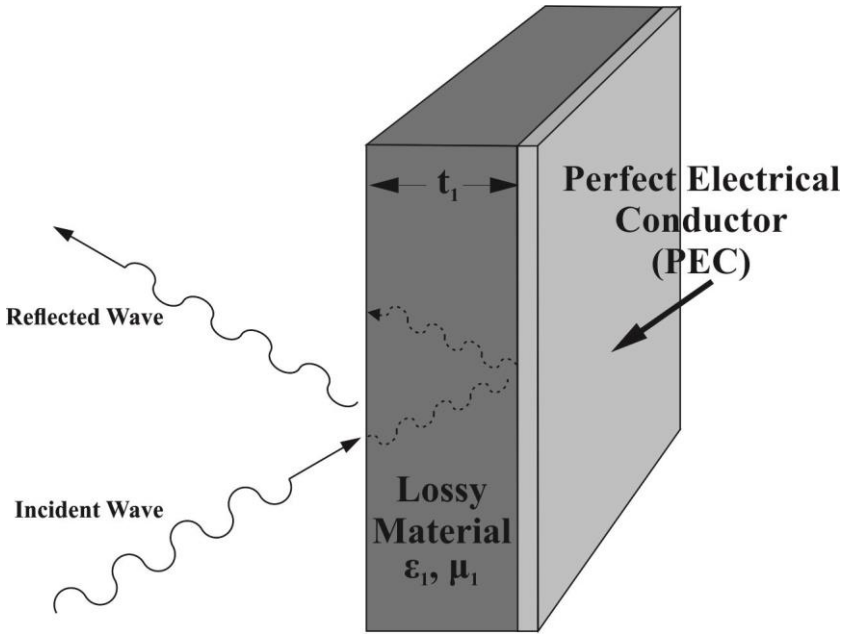

Figure 2.4. Dallenbach layer

2.1.2.2. Salisbury Screen

Unlike the tuned (Dallenbach) absorber, Salisbury Screen does not depend on the permittivity and permeability of the bulk layer but it is an absorber layer as well (Salisbury 1952). In Salisbury Screens, there are resistive sheets which are positioned in front of a metal and odd multiples of ¼ wavelength apart from each other, and separation gaps are filled by air. When air filled gap is re-filled by a material with higher permittivity, the required gap thickness decrease at the expense of bandwidth. The quarter wavelengths transform the short circuit at the metal into an open circuit at the resistive sheet according to transmission line theory. Then, sheet resistance is the effective impedance of the structure. If the gap is a half wavelength then the short circuit reappears and perfect reflection occurs. As a result, good impedance matching can be obtained if sheet resistance is equal to 377 ohms/square. Obtained in an analogous thin electrical display device will be in a magnetic layer on the metal surface. 25 % resonant frequency of the Salisbury Screen corresponds to -20 dB bandwidth of it.

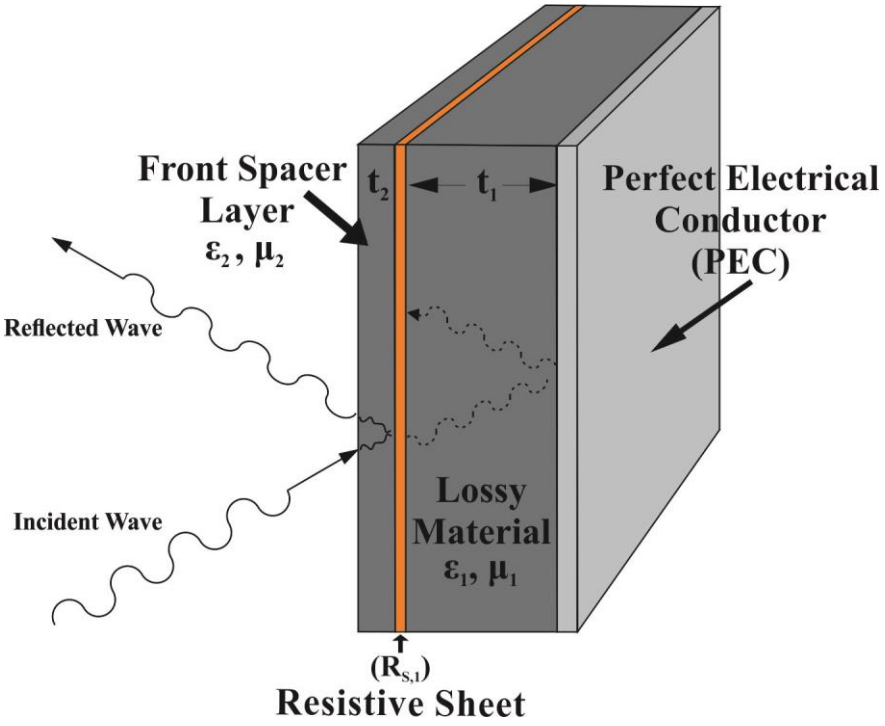

Figure 2.5. Salisbury Screen

2.1.2.3. Jaumann Type

To increase the bandwith of the Salisbury Screen, Jaumann layers (1943) have started to use in composite structures. In other words, the Salisbury Screen is the simplest form of the Jaumann device (Severin 1956). The first Jaumann device consisting two equally spaced resistive sheets in front of the conducting plane was mathematically shown to produce two minima in the reflectivity, thus increasing the bandwidth. In multilayer Jaumann device, it has low loss dielectric sheets seperating by poorly conductive sheets. These sheets conductivities are increase towards metal plane (1948) (Severin 1956).

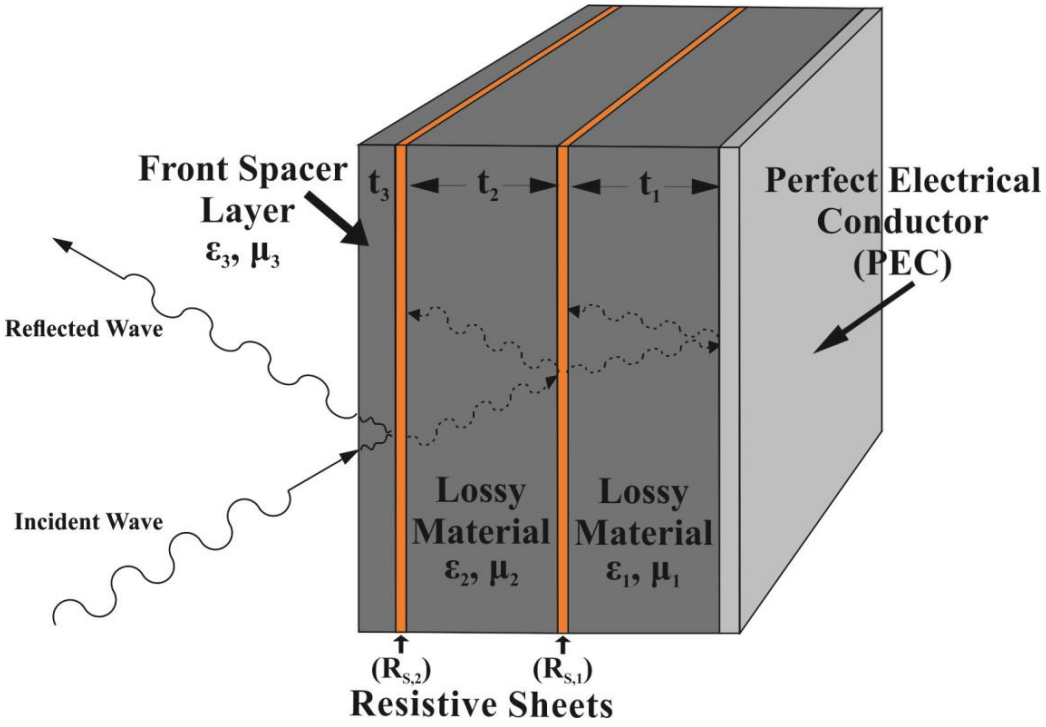

Figure 2.6. Jaumann Layers

2.1.3. Circuit Analog RAM

If we want to improve the bandwidth and attenuation of the resonant absorbers in Jaumann layers or Salisbury Screen, we can use the advantage of other loss mechanisms by employing materials. In first manufactures of Jaumann layers and Salisbury Screens, purely resistive sheets were used to design these types of structures. Replacement of the

resistive sheets with materials also containing capacitance and inductance gives added scope for making broadband absorbers. Resistive-capacitive materials have been made in the form of conducting polymer coated fibers, (Wright, et al. 1994), and resistive-inductive materials have been made with helical metal coils imbedded in a dielectric layer (Kuehl, et al. 1997). However, the field of circuit analog absorbers generally refers to materials where the resistive sheet has been replaced with lossy materials deposited in geometric patterns on a thin lossless sheet (Severin 1956). If we change the thickness of the lossy material, this will effect the resistance and the shape, geometry and spacing of the patterns control the effective inductance and capacitance. With these, reflectivity and bandwidth performance will increase and also the structure tend to be thinner absorber.

In Figure 2.7. we can see the simplest view of a circuit analog material and how it works. The resistive loss comes from the conductivity of the material used for the patterns. The spacing between the elements of the patterns gives rise to a capacitance and the length of the element gives rise to an inductance (Munk 2000).

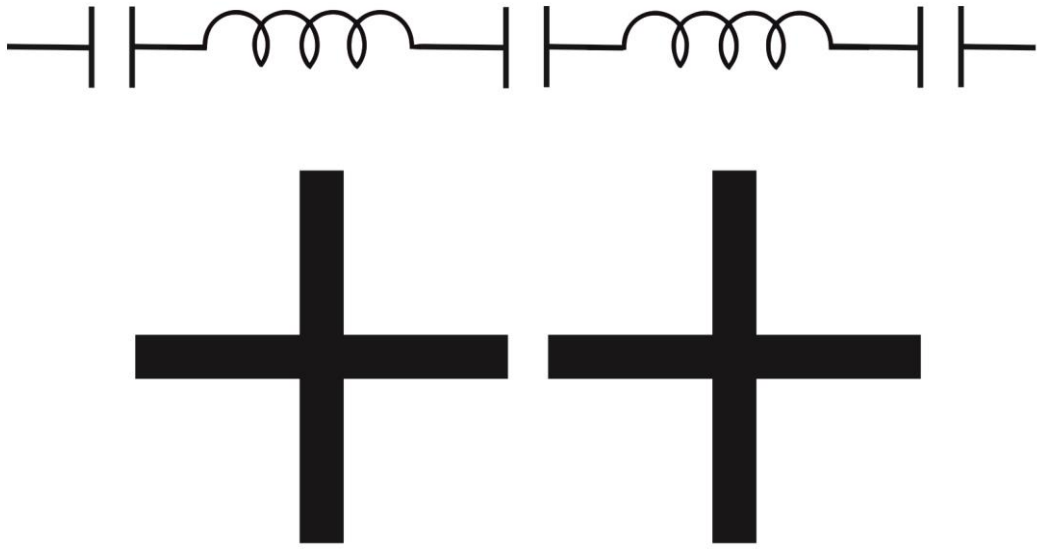

Figure 2.7. Circuit analog RAM

We can use the transmission line theory to see the circuit analog equivalent of the Salisbury Screen. In this circuit, it contains elements of resistance, capacitance and inductance. In Figure 2.8 this circuit elements can be seen. We can adjust the input

impedance of the device to that of free space by changing the distance between elements or by changing the element size.

When we compare the frequency selective surfaces, FSS, with the circuit analog absorber, we can say that they are similar. However, in FSS, the patterned elements are made from metallic materials. These are typically used as bandpass filter for radomes. A FSS acts differently from a circuit analog absorber. Consider a FSS of metallic dipoles or slots with a dielectric spacer of ¼ wavelength or more. In this system the slots act as an open circuits and the dipoles act as a short circuits. For the slotted layer, there is a resonant frequency and varies around $\frac{f_0}{\sqrt{\varepsilon_r}}$, and dielectric slab thickness is not responsible for dipoles f_0. Stacking frequency selective surfaces improves transmission or reflection bandwidth. Placing dielectric slabs on either side of a FSS also increases bandwidth.

It is difficult to model and optimize the circuit analog and frequency selective surfaces because of the complexity of the patterns. For analytic solution, transmission line models can be used to create broadband microwave absorber.

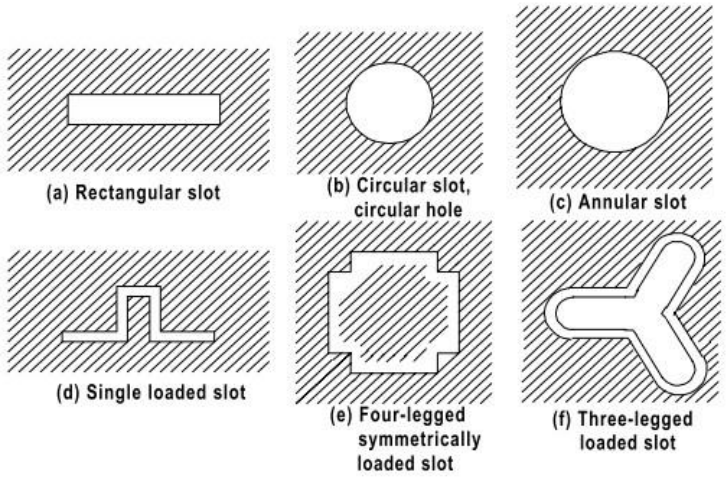

Figure 2.8. Examples of patterns for frequency selective surfaces
(Source: Barton and Leonov 1998)

Multilayer grid devices are used for microwave absorption in FSS. Another thing is, multi-layered arrays of disks or squires which is also used in FSS. These two are used for Jaumann type circuit analog absorber designs (Kasevich and Broderick 1993). These designs are reported to reflect less than -15 dB over a bandwidth of 2-18 GHz. The other

novel design is a polymeric material blended with conducting materials such as carbon, metal powder, ferrites or conducting polymers (Narang 1999).

2.1.4. Magnetic RAM

Carbonyl iron and hexaferrites, which have magnetic property, have been used in magnetic RAM's. When we use these materials in structures, they have absorb in the MHz and GHz ranges. It can be said that, the resonance frequency is related to sintering temperature and particle size which is used in structure. For instance, M-type hexaferrites can be used for higher frequencies (5-20 GHz) to absorb the electromagnetic wave (Sugimoto 1999; Cho 1999). So, with this approach two different layers can be used with different property, to increase the bandwidth of the absorption.

2.1.5. Adaptive RAM (Dynamically Adaptive RAM)

Adaptive absorbers have many potentials and have been explored by many researchers. Lossless dielectric fluid filled cell can be used behind the resistive sheet in mechanical devices. Actually, this methodology is similar to circuit analog materials where the capacitance and resistance of the impedance sheet can be tuned.

2.2. Composite Structures

2.2.1. Polymeric Composites

A composite is a structure with two or more components that are combined at macroscopic level and they do not decompose in each other. Composite include such components as reinforcement and matrix. Reinforcement is embedded into the matrix. The reinforcement can be made up of continuous fibers, short fibers, particles, or flakes. Fiber-reinforced materials good value of strength and modulus by comparison with many traditional metals and structure with metallic compounds. Composite materials are crucially preferable to conventional materials because of their good properties such as

their low density, high strength and modulus. Moreover, fatigue strength as well as fatigue damage tolerance of many laminated composites are the other counted properties. Therefore, fiber reinforced materials feasible for major class of structural materials and they are considered for use as substitution for metals in many weight-critical components in aerospace, automotive, and other industries (Mallick 1993).

Table 2.1. Mechanical property comparison of most common reinforcement fibers (Source: Campell 2003)

Fiber	*Density Ib/in^3*	*Tensile Strength (ksi)*	*Elastic Modulus (msi)*	*Strain to Failure (%)*	*Diameter (Mils)*	*Thermal Expansion Coefficient 10-6 in/in/ F*
E-glass	0.090	500	11.0	4.8	0.36	2.8
S-glass	0.092	650	12.6	5.6	0.36	1.3
Quartz	0.079	490	10.0	5.0	0.35	1.0
Aramid (Kelvar 49)	0.052	550	19.0	2.8	0.47	–1.1
Spectra 1000	0.035	450	25.0	0.7	1.00	–1.0
Carbon (AS4)	0.065	530	33.0	1.5	0.32	–0.2
Carbon (IM-7)	0.064	730	41.0	1.8	0.20	–0.2
Graphite (P-100)	0.078	350	107	0.3	0.43	–0.3
Boron	0.093	520	58.0	0.9	4.00	2.5

Aramid, carbon, graphite and glass are most common fiber reinforcements. Every type of fiber reinforcement has its own vital advantages over other and used for according to suitable applications (Long 2005). A comparison between these fibers can be found in Table 2.1.

It can be said that glass fibers are the most abundant and relatively cost efficient type of fiber reinforcements according to good strength and modulus per cost ratio (Campbell 2003).

Carbon fibers used for application often requiring high-modulus and high-strength such as aircraft components, etc. High specific strength and modulus, low coefficient of thermal expansion, and high fatigue strength are indicative properties by using as advantages over others. High cost, low impact resistance, and high electrical conductivity are disadvantages of carbon Fibers (Mallick 1993).

The aramid fiber is an aromatic organic material which is composed of carbon, hydrogen, oxygen, and nitrogen. Low density, high tensile strength, low cost, and high

impact resistance are the attractive properties of aramid fibers. On the contrary, low compressive properties and degradation in sunlight are undesired properties of them. Aramid fibers consist of two main types such as Kevlar 29® and Kevlar 49®. Despite the similarity in specific strength of both type, Kevlar 49 is different in having higher specific stiffness. Kevlar 29 can be exclusively employed in bulletproof vests, ropes, and cables. The aircraft industry has performance applications area for Kevlar 49 (Campbell 2003).

Large number of polymeric composites contain matrix which is made of polymers. These polymers can be preferable by advantages and disadvantages by according to desired structure and epoxy, phenolic, acrylic, urethane, and polyamide can be given as illustration for these polymers. (Campbell 2003).

Desired applications or structures force us to use particular resin systems specified by their advantages and disadvantages. Mechanical strength, cost, smoke emission, temperature excursions, resistance to corrosion are substantial criteria's for choosing resin structures (Mazumdar 2001). Table 2.2 gives a summary of most commonly used resin systems.

Table 2.2. Comparison of most commonly used resin systems
(Source: Campbell 2003)

Polyesters	Used extensively in commercial applications. Relatively inexpensive with processing flexibility. Used for continuous and discontinuous composites.
Vinyl Esters	Similar to polyesters but are tougher and have better moisture resistance.
Epoxies	High performance matrix systems for primarily continuous fiber composites. Can be used at temperatures up to 250-275F. Better high temperature performance than polyesters and vinyl esters.
Bismaleimides	High temperature resin matrices for use in the temperature range of 275-350F with epoxy-like processing. Requires elevated temperature post cure.
Polyimides	Very high temperature resin systems for use at 550-600F. Very difficult to process.
Phenolics	High temperature resin systems with good smoke and fire resistance. Used extensively for aircraft interiors. Can be difficult to process.

2.2.2. Glass/Epoxy Polymeric Composite Systems

Glass / epoxy systems can be classified by high strength, cost efficient and high modulus structures. These systems are widely used in industry, from aerospace applications to protective equipment.

Glass fibers are one of the most common reinforcement among the materials using in the industry. The main types of glass fibers are E-glass (fiber glass) and S-glass. The "E" in E-glass account for electrical because of its design for electrical applications. Also, it is used for many other purposes such as decoration and structural applications. The "S" in S-glass account for to higher content of silica. S-glass fibers have fatigue strength than E-glass and they hold their strength at higher temperatures. They have wide applications area for aerospace sector. To classify other types; C-glass (Corrosion) used in chemical environments commercially available such as storage tanks; R-glass used in structural applications such as construction; D-glass (Dielectric) used for applications requiring low dielectric constants, such as radomes; and A-glass (Appearance) used to improve surface appearance. E-CR glass (Electrical and Corrosion resistance) and AR glass (Alkali Resistant) are good examples for combinational types (Mallick 1993).

As a matrix binder, epoxy is the most commonly used in polymeric composite matrix, however it is more expansive than other polymer matrices. Epoxy based polymer matrices structures are generally more than two-thirds layer used in aerospace applications. During processing, high strength, low viscosity and low flow rates allow good wetting of fibers and prevent misalignment of fibers. Moreover, low volatility during cure, corrosion resistance, and low shrink rates reduce the tendency of gaining large shear stresses of the bond between epoxy and its reinforcement. Epoxy resins are the most widely held polymeric composite matrix and existing in more than 20 grades to meet specific property and processing requirements (Mazumdar 2001).

2.2.3. Manufacturing Methods

Manufacturing plays most important role for quality of our structure. Phenomena like Void formation, wetting, and degree of curing, resin flow, processing time and reinforcement ratio hugely affect the final product especially in polymeric composites. A

hand lay-up technique is used in early manufacturing method for fiber-reinforced composite structural. Hand lay-up is a reliable process, but it is very slow and labor-intensive by its nature. In recent years, there is more demand on the development of manufacturing methods that can support mass production rates particularly due to the interest generated in the automotive industry.

Another manufacturing method is resin transfer molding (RTM) that has resulted significant advancing in both aerospace and automotive industries. It has favorable ability to produce complex composite parts shapes at relatively high production rates (Long 2005; Campbell 2003; Mazumdar 2001).

In RTM, several layers of dry continuous fiber reinforcement are positioned in the bottom half of a two-part mould which is closed. A catalyzed liquid resin is injected into the mould via a centrally located channel. The range of injection pressure is about 0.7 – 7 bars. Resin fills the space between the fiber yarns in the dry fiber preform, displaces the entrapped air through the air vents in the mould, and coats the fibers, when it flows and spreads throughout the mould. Curing depends on the type of the resin-catalyst system and can be perform either at room temperature or at an elevated temperature in an air-circulating oven. It is essential to trim the part at the outer edges to conform to the exact dimensions after the cured part is pulled out of the mould. (Long 2005). RTM process is depicted step by step schematic illustration in Figure 2.9.

Several variations of the basic RTM process are described earlier. Vacuum-assisted RTM (VARTM) is one of these variations and corresponding vacuum is used in addition to the resin injection system to pull the liquid resin into the preform.

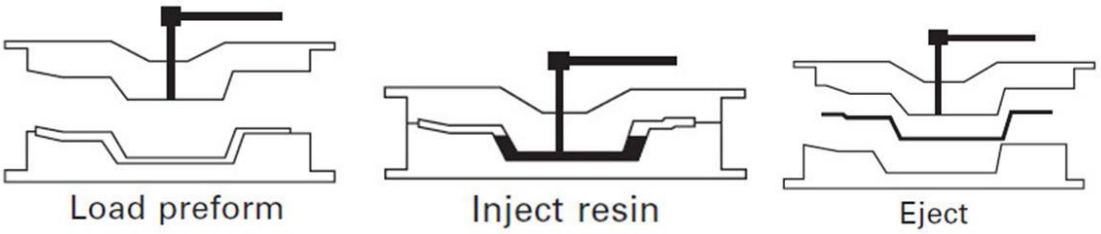

Figure 2.9. Step by step schematic illustration of RTM process
(Source: Long 2005)

Another type of process is vacuum infusion that compared to RTM, the upper half of the mould pair is shifted with a vacuum membrane. This minimizes the tooling cost

vitally and offer a significant fabrication route for large structures where the throughput requirement is small (Long 2005). The main advantages over open-mould variants are management of volatiles, thickness and fiber volume fraction (V_f) and resin consumption. The usual infusion set-up contains a mould employed at room temperature. The fabric is laid-up by hand, followed by the ancillary materials–peel ply, breather felt, infusion mesh and vacuum membrane. As with conventional vacuum bag moulding, sealing relies on mastic tape and the facility to pull an effective vacuum. While the impregnation process is relatively fast for most set-ups (owing largely to the infusion mesh), the overall manufacturing time may be quite similar to those for hand lay-up laminated products (Long 2005). This is because the mould preparation are all critical, manual operations. Cross section of a vacuum infusion process is schematically shown in Figure 2.10.

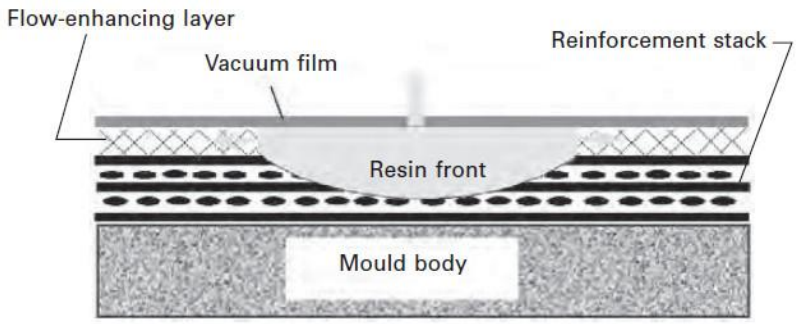

Figure 2.10. Schematic illustration of Vacuum Infusion process
(Source: Long 2005)

2.2.4. Hand Lay-Up with Compression

One of the simplest and oldest open moulding method of the composite fabrication processes is hand lay-up or as some called it wet lay-up. Besides, it needs compression which is supplied by labor force. It is generally used for large components but low volume and it is labor intensive method suited especially, such as boat hulls. Basically reinforcing fabric such as fiber glass is placed manually in the open mould, and resin is poured, brushed, or sprayed over and into the glass plies. Trapped air is evacuated manually with squeegees or rollers to complete the laminates structure which is corresponding "compression" in the title. The most commonly used matrix resins are room temperature curing polyesters and epoxies. Curing is inducted by a catalyst in the

resin system, which hardens the fiber reinforced resin composite without external heat. A pigmented gel coat can preferably be perform to the mold surface to get high quality part surface (Campell 2003).

A step by step description of hand lay-up with compression process is illustrated in Figure 2.11.

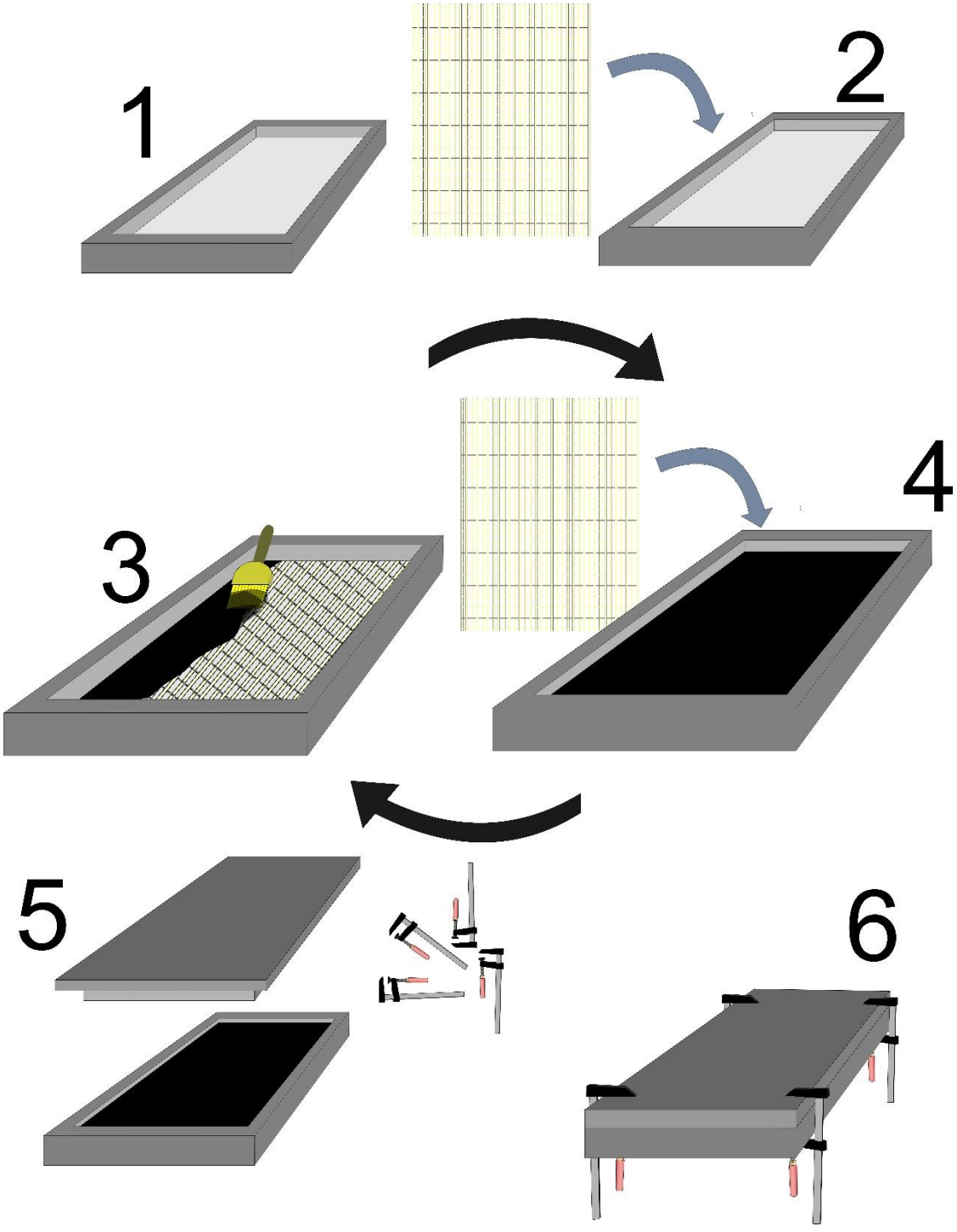

Figure 2.11. Illustration of Hand Lay-up with compression process

2.3. Absorbing Additives in Composite Structures

The goal of absorbing materials is to soak electromagnetic energy forms such as radar wave and to reduce the net available energy for reflection. (Barton and Leonov 1998). These materials have many layers and these layers behaves like resistor, capacitor or inductor in a simple electric circuit to absorb energy from incident electromagnetic energy by converting to heat or to any other form of energy.

Besides all, permittivity and permeability properties of material demonstrate the dielectric and magnetic behavior of the material, respectively (Gama and Rezende 2010). Basically, permittivity is the materials tolerance to electric and show how electric field affected by it. Permeability has same definition for material in terms of magnetic field. In simple terms, permeability shows the magnetization degree of material resulted by applied magnetic field. There are some expression to define both as in Equation 2.15 and 2.16 respectively.

$$\varepsilon = \varepsilon_0 \varepsilon_r = \varepsilon_0 (\varepsilon_r' - j\varepsilon_r'') \tag{2.3}$$

$$\mu = \mu_0 \mu_r = \mu_0 (\mu_r' - j\mu_r'') \tag{2.4}$$

Dielectric permittivity (ε) can be expressed as relative permittivity of the material (ε_r) to the permittivity of vacuum ($\varepsilon_0 = 8.8541878175\ x\ 10^{-12}\ F/m$). Relative permittivity can be dissociated into real and imaginary parts (ε_r' and ε_r'') that can be tested.

Magnetic permeability (μ) can be expressed similar to permittivity, as relative permeability (μ_r) of the material to the permeability of free space ($\mu_0 = 4\pi\ x\ 10^{-7} \left(\frac{N}{A^2}\right) \cong 1.2566370614\ x\ 10^{-6}\ H/m$). Similar mentality to permittivity, relative permeability can be dissociated into real and imaginary parts (μ_r' and μ_r'') that can be detected.

First absorber designs were considered perfectly desired materials and ε_r and μ_r were taken as positive integer numbers. Unfortunately, when theoretical design was intended to convert in real applications, it is seen that all materials behave as a lossy medium. Despite the fact that some materials may have dominant dielectric or magnetic properties, these properties may vary significantly with changing frequency of the incident wave. Furthermore, real and imaginary parts of permittivity and permeability can

be measured in frequency domain and designs based on measurements became more viable with real life circumstances (Jenn 2005; Park 2011).

Absorbent materials generally have a particulate formation which generally consisted of rubber, silicone, or thermo set resin and these particulate materials act as filler in a matrix (Park 2011; Lee, et. al 2006; Qing 2009; Xu 2013; Qing 2010). There are mainly two types of particulate absorbers which are carbon based absorbers and magnetic absorbers. Carbon based absorbers have dominant dielectric properties compared to nearly steady permeability in frequency domain. Magnetic absorbers have significant magnitude of relative permeability compared to dielectric absorbers.

2.3.1. Carbon

Carbon had been used to manufacture the early absorbers due to its unsufficient conductive property and it is still being used as a basic and important materials in this purpose (Knott 2004). With convenient crystal structure and magnificent property, carbon nanostructures have good match for study in radar absorbing materials and their applications. Graphite, carbon black, single and multi-walled carbon nanotubes, short carbon fibers, carbon nanofibers can be given as examples of carbon based absorbers (Oh 2004; Rosa, et. al 2010; Micheli 2010). These absorber are classified in microwave lossy materials which are identified according to the electrical permittivity, which is general in a complex quantity (ε) and reveals the interaction between an electric field and material.

An electromagnetic field propagation within a dielectric material induces two types of electrical occurrences which are conduction and displacement currents according to the theory of complex permittivity. As a result of conduction current, there occur an increase in imaginary permittivity (ε_r''), power loss, which is proportional to the affiliation with displacement current induction of the polarization effect expressed by the real permittivityε_r'. So that, the dielectric relaxation and space charge polarization effect can be connected to the increase of the real part of the complex permittivity. On the other hand, the rise in the imaginary part of the complex permittivity is predicated to the increase in electrical conductivity of the material (Micheli 2010; Micheli 2011).

Carbon based absorbers are generally very low dense materials and they have very low mixing ratios when compare to magnetic absorbers. As a matter fact that high thickness is required to promote them resonant in radar wave frequencies (Barton 1997).

2.3.2. Magnetic Materials

Iron, iron oxides, cobalt, nickel, manganese, and zinc are most common magnetic materials that are capacity to absorb electromagnetic wave (Knott 2004; Qing 2009; Qiu 2007). For instance, carbonyl iron and iron oxide based ferrites are two most common materials used in radar absorbing structures as an additive (Meshram 2004; Feng 2006).

The loss mechanism is firstly comes from the magnetic dipole moment. It has permanent magnetization in some ceramics, denominated as ferrimagnetism which is defined as magnetism with unbalanced antiparallel magnetic alignment (Jenn 2005). In the view of electrical properties, these materials are semiconductors or insulators, unlike the metallic magnetic materials which are electrical conductors (Knott 2004).

The hexaferrites or M-type ferrites are the most important absorbing additives in radar absorbing structures which characterized by the compound $MeFe_{12}O_{19}$, where Me can be replaced as barium, strontium or lead. M type ferrites are most common used materials as permanent magnets (Meshram 2004; Parida 2007).

Magnetic materials are a piece of the thickness of dielectric absorbers, so they offer the advantage of compactness. On the other hand, magnetic absorbers are heavy due to their iron content or in other words because of their densities, and mostly used at high mixing ratios. Because of that reason, most of the magnetic absorbers have high aerial weight (Meshram 2004; Kim, et. al 2008).

2.3.3. Conducting Polymers

In a polymer, for instance in polypyrrole, partial axidation of the polymer (doping) causes it to become conducting through the formation of polarons and bipolarons; the charge carriers along the chains. The conductivity of a conducting polymer is modelled by phonon assisted hoping between the randomly distributed localized states (that result from the partial oxidation (Capaccioli, et. al 1998).

The main problem in conducting polymers is that they are ordinarily resistable. Compression can be done to these polymers in to the shapes like polyaniline, PANI. Another method is, using thermoplastic to form a composites. Polypyrrole, PPy, has been polymerised on the surface of PVA, PVC and within it to form composites. Emulsion

polymerisation has also been used. PANI is soluble in solvents such as DMF, or the solubility of monomers has been increased by chemicall modification though usually at the expense of conductivity. Textile materials have been used as substrates for a number of materials and have been coated with conducting polymers by soaking them with oxidant and then exposing them to monomer (Bjorklund and Lunströem 1984). This procedure was also reversed soaking in the monomer and then adding oxidant (Newman 1986). The first investigation of PANI and PPy deposition onto fabric by an in situ polymerization technique was reported in 1989 (Gregory, et al. 1989).

2.3.4. Polypyrrole

Solely polypyrrole does not possess much useful physical properties so that such materials like latex, fibers or polymer blends are used to generate polypyrrole composites. Polypyrrole is very feasible in use according to its relative stability in air.

2.3.5. Polyaniline

Polyaniline, PANI, is a cheap, simple and quick formable conducting polymer that has convenient properties to manufacture an absorber. Polyaniline is a poor soluble polymer and its monomer has very derivatives. Therefore, it has a large capability to change or arrange the setting absorbent properties of this materials.

2.3.6. Tubules and Filaments

Radar absorbing structures can be constructed by adding conducting filaments or tubules to an insulating polymer matrix. The length of the filaments should be less than ½ λ of the median frequency to be absorbed. In these type materials, ε' reaches a maximum when the additives increases and starts to fall off at the percolation threshold, the composite becomes macroscopically conducting. ε'' increases with loading around the percolation threshold and continues to increase to saturation value at higher filling. This is the because of the dependence of ε'' on the conductivity.

2.3.7. Chiral Materials

A plausible amount of work has been handled on chiral inclusions in a matrix as an additive in radar absorbing structures. For instance, Dallenbach layers have been prepared with metal inclusions such as right of left handed metal wire helices (Jaggard and Engheta 1989; Kuehl, et. al 1997; Varadan 1994). This helix is called as chiral (It's mirror image is not superimposable). With these chiral materials, structures have shown efficient effect in microwave attenuation. For this reason, they have been patented (Jaggard and Engheta 1989). Because of the optical activity and circular dichroism of the material, the propagation constant for these materials is modified from isotropic materials. A term is attached for the chirality admittance similar to the permittivity and permeability that gives another method of fine tuning the reflectivity. When chiral materials passes through the media, they have the effect of rotating linearly polarized electromagnetic radiation to the left or right. This property has been noted for microwaves (Kuehl, et al 1997; Varadan 1994). Because of the chirality parameter β, the chirality of the material has been thought to lead to enhanced lead to increased loss and major design capability. This β parameter is complex like a relative permittivity and permeability volues of materials.

It can be said from theoretical (Bohren, et. al 1992) and experimental (Kuehl, et. al 1997) studies that, chiral additions are not necessary in the formulation of RAM. The chiral and racemic mixtures both showed rotation and ellipticity, possibly from improper mixing of the racemic mixture. At the resonant point, it was a few dB reflection loss for the chiral medium. Chiral materials will not produce thinner RAM than achiral materials (Bohren, et. al 1992). Because of the interaction of the electric field with the metal helices, producing a magnetic field through induction and hence a complex permeability, it can be talked about absorption properties of the chiral materials. These chiral materials could be categorized as circuit analog.

Latterly, it is accepted that chiral additives are not necessary, whereas, helical additives can be useful in the design of radar absorbing structures (Reinert 2001).

2.4. Optimization of Jaumann Type Radar Absorbing Structures

Optimization of Jaumann absorbers is more complex because of the number of parameters involved. Because, when we increase the number of layers, it means, the number of parameters like resistance, permittivity, and permeability or thickness values will also increase. Empirical procedures and numerical optimization techniques have been used for designing Jaumann absorbers (Cloete and Dutoit 1989).

2.4.1. Maximally Flat Design

The main purpose of using maximally flat design, or binomial expansion, is to have the exact possible bandpass in the wanted frequency region. It can be achieved by stacking up a few Salisbury screens (Fante and Mccormack 1988). An approximation with this expression for such a quarter wave stuck is;

$$\Gamma = \Gamma_0 + \Gamma_1 e^{-2j\theta} + \Gamma_2 e^{-4j\theta} + \cdots + \Gamma_n e^{-2nj\theta} = \sum_{n=0}^{N} \Gamma_n e^{-2nj\theta} \qquad (2.5)$$

Where Γ_n is the reflection coefficient from an interface and

$$\theta = \beta_n d_n = \frac{2\pi}{\lambda_n}\frac{\lambda_{n_0}}{4} = \frac{\pi f}{2f_0} \qquad (2.6)$$

2.4.2. Tschebyscheff (Equal-Ripple) Design

The objective of this design is to interfere fringes from the quarter wavelength positioned resistive sheets are dictated to approximate an equal amplitude ripple, with one ripple for each resistive layer. That is revealed by replacing the summation in equation 2.7 with a Tschebyscheff polynomial (Liu 1993).

$$\Gamma = e^{-jN\theta}\frac{T_N \sec\theta_m \cos\theta}{T_N \sec\theta_m} \qquad (2.7)$$

Where $T_N \sec \theta_m = p_m^{-1}$ and p_m is the ripple magnitude in dB, N is the number of ripples and layers,

$$\theta = \frac{\pi}{2(1+F)} \; and \; F = \frac{f - f_0}{f_0} \tag{2.8}$$

This method has a wider bandwidth than the governing maximally flat solution. Beside, Tschebyscheff polynomials are utilized to optimize the bandwidth of a Jaumann Device as well (Liu 1993). It is proved that choosing the optimal spacer yield a big effect on the bandwidth of the absorber. The Tschebyscheff technique has still been operated to the design of tapered absorbers (Gau 1997).

2.4.3. Gradient Methods

A Newton-Raphson method is employed to solve for maximally flat and equi-ripple designs to stacks up to 20 resistive sheets (Toit 1989; Toit 1990). When the number of layers increase, the optimum maximum relative dielectric constant of the spacer tends to 1. The absorber design has been performed to optimize by optimal control method which has been compared to solutions from simulated in order to overcome local optimum traps (Presque 1992). A huge number of thin layers with set thicknesses is subdivided by the coating in simulated annealing. A prescribed set of suitable materials is fixed a material chosen for each layer. Random perturbations of the material were concluded to optimal solution. This optimization technique usually leads to thinner, less reflective material than the optimal control approach. All mathematically governing equations were processed for optimizing the absorber properties.

2.4.4. Genetic Algorithm

The former optimization methods have produced significant reduction in bandwidth and minimization in reflectivity. These methods do not generate the optimal absorbing materials which are based on a number of parameters such as minimum thickness, weight, and type of minima. Therefore, the Genetic Algorithm (GA) has been studied as an optimization technique for RAM. Utilization of genetic algorithms in

engineering electromagnetics supply a good view of the genetic algorithm with some examples containing the design of microwave absorbers (Johnson and Rahmat 1997).

The first use of GA were encountered in 1993 for the optimization of Jaumann absorbers (Michielssen 1992; Michielssen 1993) and operated in the approaches for the optimal control method (Preque 1992). There are many parameters to determine the absorbers in GA such as a set of available materials, their frequency dependent optical properties (permittivity and permeability), and the layer thicknesses. A genetic algorithm was operated to normalize the absorber design against practical functions containing reflectivity, thickness and weight. Both TE and TM polarisations of the reflection coefficient were also calculated to optimise the absorber as a function of incident angle as well. The reflectivity was obtained by employing a recursion relationship and the permittivity, permeability of the materials. Several Pareto Genetic Algorithms were confronting with the nondominated sorting genetic algorithm, NSGA, generating the best outputs (Weile 1996). The genetic algorithm is tried optimise Jaumann absorbers based on transmission line theory (Chambers and Tennant 1996; Chambers and Tennant 1995; Chambers 1994). Absorber bandwidth is generally increased with increase in number of resistive layer before asymptotically approaching the maximum bandwidth as the layer number approached infinity.

2.4.5. Other Methods (Finite Element, FDTD and Taguchi Methods)

Scattering from cylindrical absorbers has been simulated by performing finite element method, FEM, and for single layer Jaumann (Salisbury Screen) the numerical method yields outcomes akin to the analytic results (Charles, et. al 1996).

The early FDTD calculations of the RCS of tapered Salisbury Screens and Jaumann the layers have illustrated that the capacity of the device is not restricted to resonant nature (Charles, et. al 1999).

The Taguchi method of optimization is performed as a means of invastigating less parameter space to analyse the sensitivity and interaction of parameters in the design of flat and curved Jaumann Absorbers (Charles, et. al 1999).

CHAPTER 3

EXPERIMENTAL

3.1. Materials

In this study, radar absorbing polymeric composite structure was constructed by using hand lay-up compression technique. Glass fiber reinforced epoxy matrix was used. Fiber reinforcement was non-crimp unidirectional glass fabrics purchased from Metyx Composites. The product coded as L300 E10B-0. Unidirectional E-Glass fabric that has about 330 g/cm^2 area weight. Despite being branded as unidirectional, fabric was multiaxial as it contains fibers both in 0^o and 90^o directions. The fabrics contain fibers dominantly at 0^o, having about 287 g/cm^2 areal weight and fibers at 90^o, having about 37 g/cm^2 areal weight. Stiches are tricot and contribute to area weight about 10 g/cm^2. The photo of back and front side of the fabric used within the study shown in Figure 3.1.

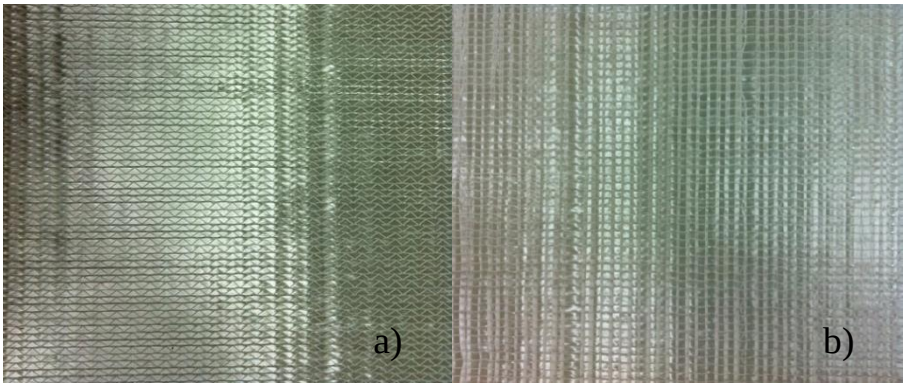

Figure 3.1. Photo of non-crimp E-Glass fabric, (a) front side, (b) back side, used within the study

In the manufacturing process, the epoxy resin was used as a matrix binder in structure. It was purchased with the brand name of Momentive laminating resin MGS L 160 and hardeners MGS 160 and 260 S. It was chosen as a suitable combination specifically for processing lamination time and glass transition temperature (T_g).

As an additive Carbonyl Iron (CI) micro sized particle was chosen because of its radar absorbing features. CI was purchased from Sigma Aldrich. Density of the CI reported as 7.86 g/mL at 25 ^{o}C. The CI was blended within epoxy matrix and mixed to disperse the micro particles. Different weight ratios of CI additives were used and the effect of the contributed particles was observed.

3.1.1. Thin Film Coating with Magnetron Sputtering

In our study, high vacuum based magnetron sputtering system was used to create metallized glass fibers to use them in absorbing structures as a resistive sheet. To adjust the resistance of the sheets, some parameters should be taken into account. The growth conditions such as oxygen partial pressure, substrate temperature and bias voltage are strongly important parameters for the thin film coatings.

Several deposition techniques such as thermal evaporation, chemical vapor deposition, electron beam evaporation, sol-gel, spray pyrolysis, pulsed laser deposition, sputtering and magnetron sputtering have been experienced for many years, in order to prepare high quality thin film. The magnetron sputtering methods are the most preferred technique among others.

In DC & RF sputtering, the efficiency of ionization from energetic collisions between the electrons and gas atoms is low. Most electrons lose energy in non-ionizing collisions or are collected by the electrodes (anode). Oscillating RF field increases ionization efficiency marginally. Hence, deposition rates are low. To increase deposition rates, magnets are used to increase the percentage of electrons that take part in ionization events, increasing the ionization efficiency by increase probability of electrons striking noble gas atoms or molecules. A magnetic field is applied at right angles to the electric field by placing large magnets behind the target. This traps electrons near the target surface and causes them to move in a spiral motion until they collide with a noble gas atom which is generally argon (Ar). This increases electron path length, so the ionization efficiency is increased significantly. Deposition rate increases up to 10-100 times faster than without magnetron configuration. A lower Ar pressure (to 0.5 mTorr, can still sustain plasma) can be utilized since ionization efficiency is larger which can improve film quality as less argon will be incorporated into the film. Magnetron sputtering can be done in DC or RF, but more often it is done in DC as cooling of insulating targets is difficult

in RF systems. Target erodes rapidly in the ring region resulting in a deep groove in the target face, which cause to non-uniformity film. Another reason to use magnets are lower voltage needed to strike plasma. Because, formation of magnetic field makes an electron go in curved path (helix) and it leads longer more collisions. More collisions make more ions easier to strike plasma. Other advantage is that uniformity of thin film growth can be controlled. Electrons path and collision region over the target is specified by magnetic field. Due to this specification, sample can be positioned or mobilize according to desired uniformity.

By using magnetron sputtering technique, E-glass fabrics surfaces were coated with Indium Thin Oxide (ITO) thin film to gain them conductivity property. It can be seen from the Figure 3.2 that, we have uncoated and coated parts of glass fiber fabric.

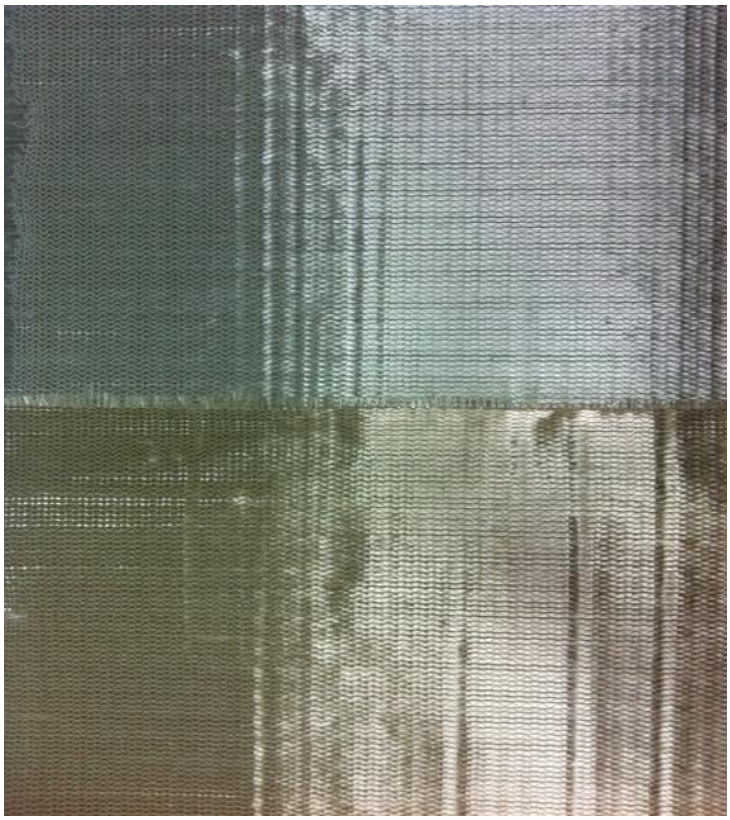

Figure 3.2. Unmodified (top) vs. Metallized (bottom) E-glass fabric

In Figure 3.3 we can clearly see the magnetron sputtering system which is used to coat the surface of the resistive sheet fabrics with thin film ITO.

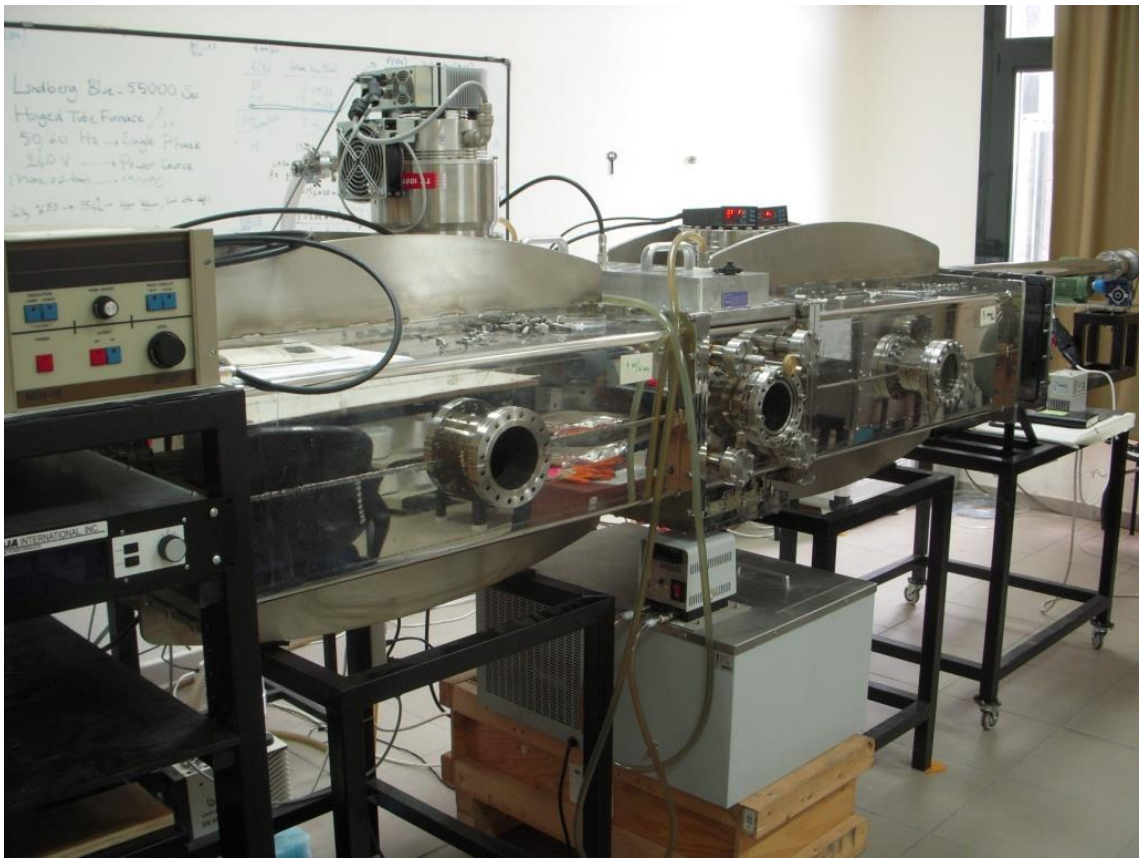

Figure 3.3. Photo of Magnetron Sputtering unit used for metal coating of fabrics

In this sputtering system, a tray shaped sample holder is slowly moved under target via frequency controlled switchable feed through system. It is aimed to control uniformity of thin film growth by mobilizing of sample. The deposited film thickness depends on the applied power and angular velocity of the feed through mechanism. Glass fiber fabrics was used as substrate to grow thin films on it. We used rough pump and turbo molecular pump, respectively and vacuum chamber was evacuated 10^{-6} torr as base pressure for this system. Ar and O_2 gases were flowed into the chamber using mass flow controller maintaining the working gas pressure of about 10^{-4} torr. For plasma formation, DC power around 1kW applied to target which has purity of 99.99%. During the thin film deposition, we moved the sample holder. Glass Fiber fabrics is coated according to desired electrical properties by controlling thin film thickness. All in all, we got metalized thin film coated glass fiber fabrics in order to use as resistive sheets in Jaumann design structure.

As it seen in Figure 3.4 glass lamellas were used to characterize the surface resistance of fabrics. For each metallization, we put lamella on the fabric and after

deposition we were able to measure the resistance of the lamella by using four probe measurement and thereby the resistance of the fabric.

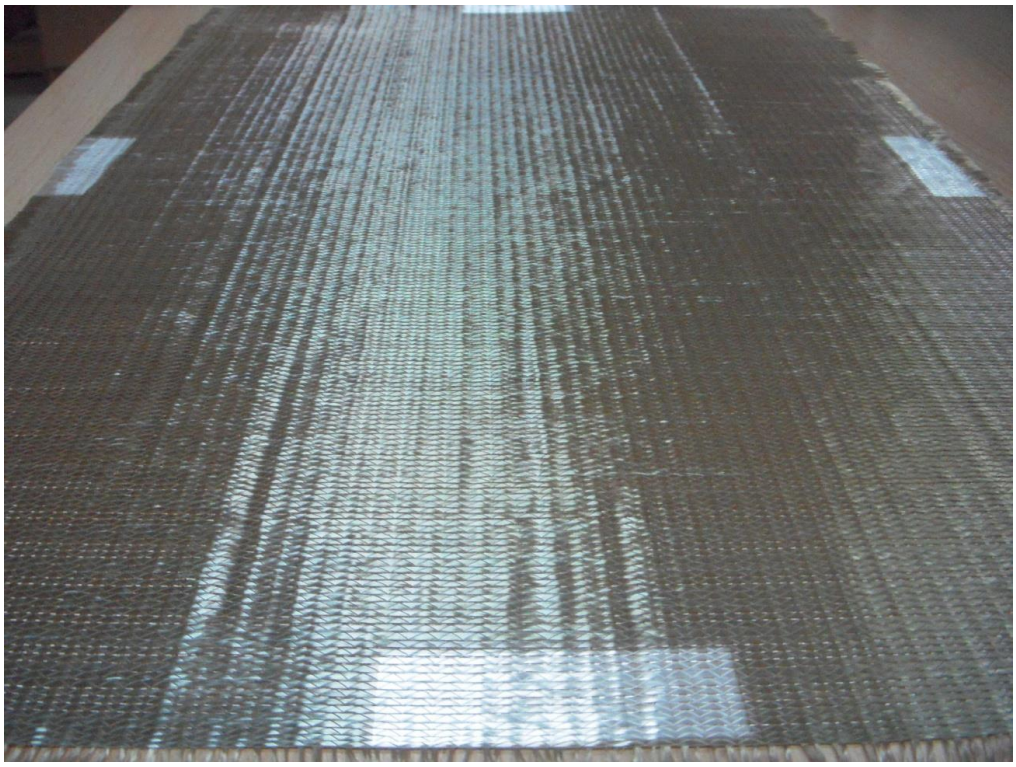

Figure 3.4. ITO coated glass fiber fabric image

3.2. Mathematical Background for Jaumann Type Structure

3.2.1. Construction of Related Equations for RAS's

Related equations used for simulation and optimization for radar absorbing structures derived from Transmission Line circuit equivalent of the proposed design.

For the Dallenbach layer, it consists only single layer which is a lossy material. It can be thought that it has CI additive or it is just simple fiber reinforcement epoxy resin polymeric composite structure. Equation 3.1 used for simulation and optimization purposes.

$$Z_1 = \eta_1 \tanh(\beta_1 t_1) \tag{3.1}$$

Z_1denotes input impedance of first layer, η_1 refers to characteristic impedance of first layer and β_1 is the propagation constant of again first layer. The only design variable is the thickness of the lossy material (first layer, and in this condition it is just one layer) (t_1) and also intrinsic impedance of lossy material. This intrinsic impedance of the lossy material is related to the permittivity and permeability values. As thickness changes, resonant frequency of the layer, as well as the bandwidth of absorbance through within 2-20 GHz range changes. The schematic illustration and circuit equivalent of Dallenbach layer are shown in Figure 3.5.

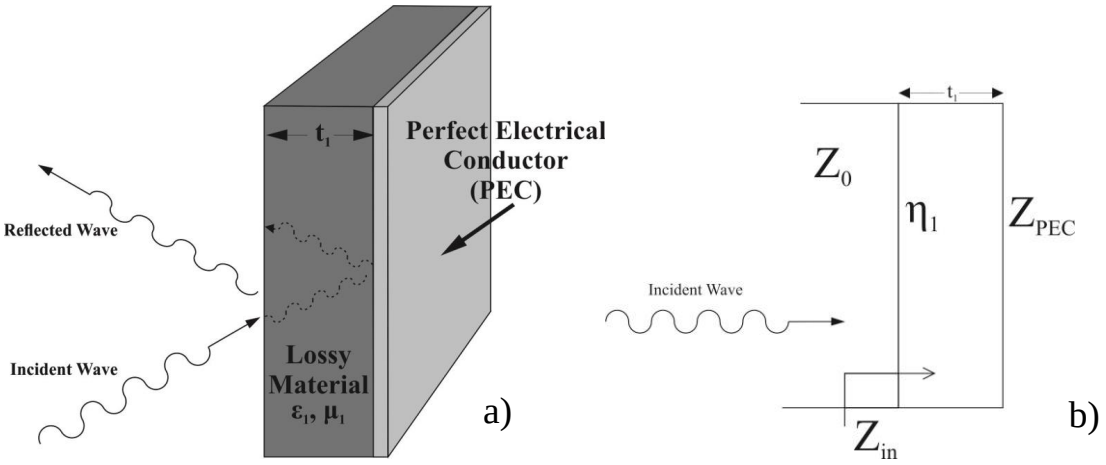

Figure 3.5. Schematic illustration of (a) Dallenbach layer and (b) circuit equivalent

The differences between Dallenbach and Salisbury Screen type, Salisbury screen consists of resistive sheet in the structure. The manufactured structures have ITO coated resistance fabric and it should be added into transmission line equations. In addition to resistive sheet, a front spacer layer for protecting the resistive sheet was added into structure. For the optimization purposes, Equations 3.1, 3.2 and 3.3 were derived. Schematic illustration and circuit equivalent of Salisbury Screen with front spacer layer and resistive sheet are shown in Figure 3.6.

$$Z_1 = \eta_1 \tanh(\beta_1 t_1) \tag{3.1}$$

$$Z_2 = \frac{Z_1 R_{s,1}}{Z_1 + R_{s,1}} \tag{3.2}$$

$$Z_3 = \eta_2 \frac{Z_2 + \eta_2 \tanh(\beta_2 t_2)}{\eta_2 + Z_2 \tanh(\beta_2 t_2)} \tag{3.3}$$

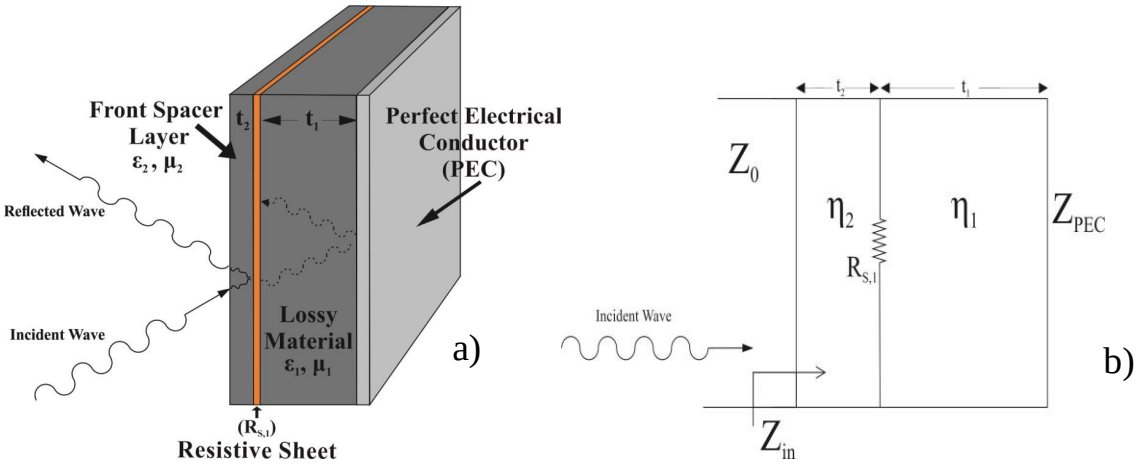

Figure 3.6. Schematic illustration of (a) Salisbury screen and (b) circuit equivalent

Jaumann absorbers include additional resistive sheets into the radar absorbing structure (more than one resistive sheet), so the bandwidth of the absorbance can be increased with this approach. Because of the increasing in resistive sheets, the complexity of the simulation will increase. Because the thicknesses between sheets can be changed and also resistances could be different. So with the so many parameters, the complications certainly will increase.

In this study, in each manufactured structure, four resistive sheets were used with the different resistance values. And also, the thicknesses between sheets were different. So, each time the microwave absorbance characteristic of structure will be different. So, Equations 3.1 to 3.6 can be written for Jaumann absorbers in general, as given below.

$$Z_1 = \eta_1 \tanh(\beta_1 t_1) \tag{3.1}$$

$$Z_2 = \frac{Z_1 R_{s,1}}{Z_1 + R_{s,1}} \tag{3.2}$$

$$Z_3 = \eta_2 \frac{Z_2 + \eta_2 \tanh(\beta_2 t_2)}{\eta_2 + Z_2 \tanh(\beta_2 t_2)} \tag{3.3}$$

$$Z_4 = \frac{Z_3 R_{s,2}}{Z_3 + R_{s,2}} \tag{3.4}$$

.

.

.

$$Z_{i-1} = \frac{Z_{i-2} R_{s,n}}{Z_{i-2} + R_{s,n}} \tag{3.5}$$

$$Z_i = \eta_i \frac{Z_{i-1} + \eta_i \tanh(\beta_i t_i)}{\eta_i + Z_{i-1} \tanh(\beta_i t_i)} \tag{3.6}$$

Schematic illustration for multilayer Jaumann absorber structures containing two and four resistive sheets are shown in Figure 3.7 and 3.8.

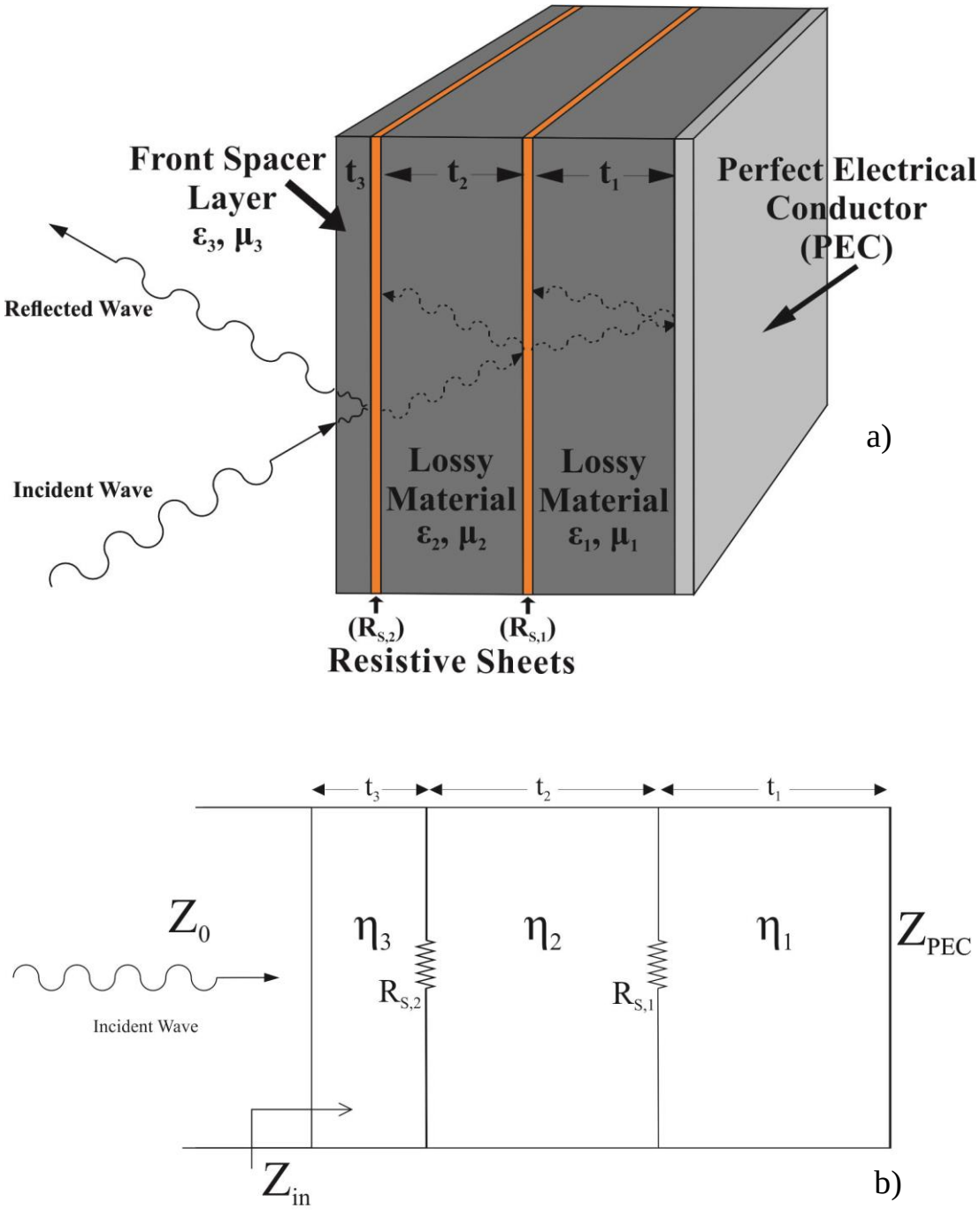

Figure 3.7. Schematic illustration of (a) Jaumann absorber with 2 resistive sheets and (b) circuit equivalent

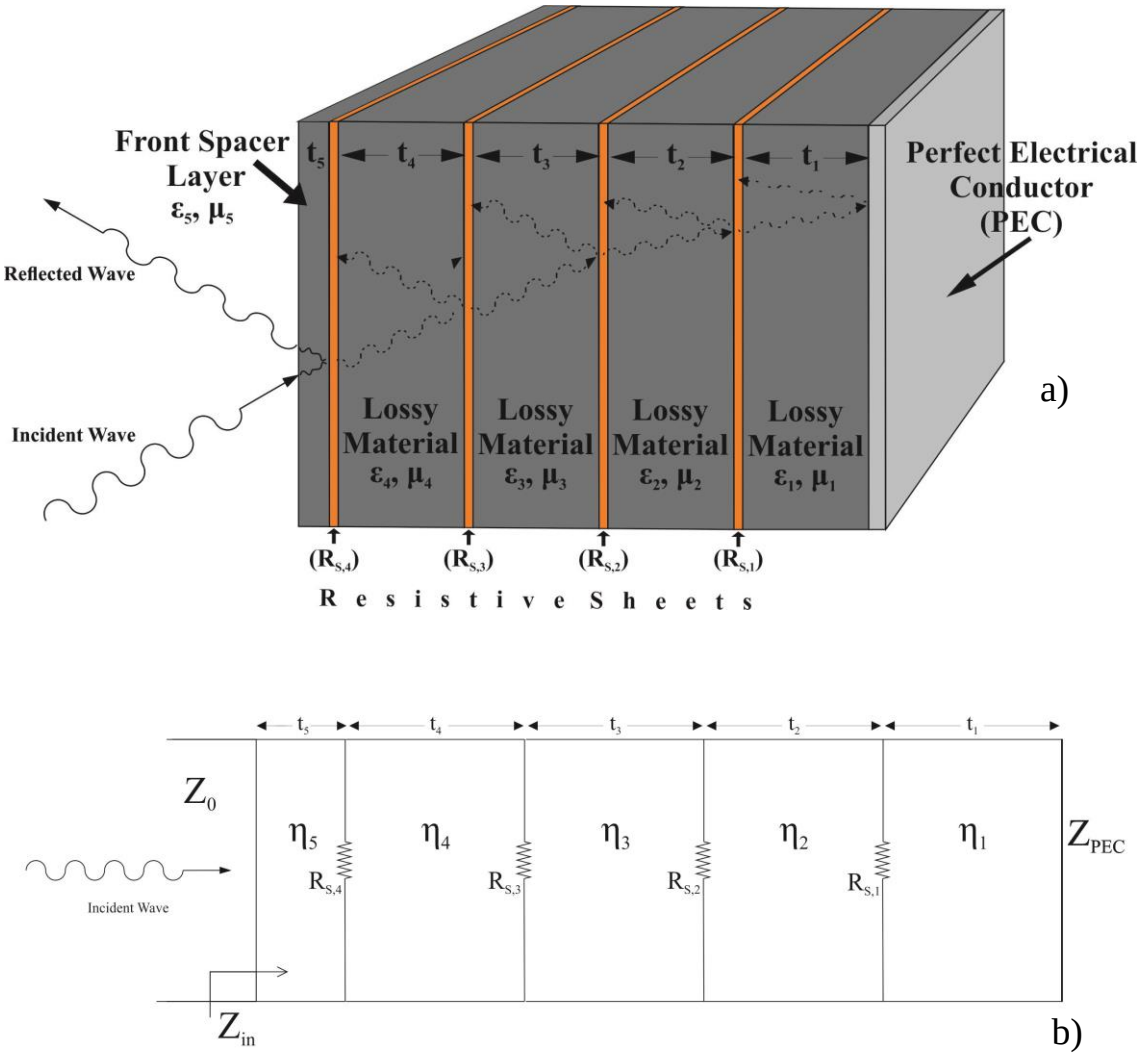

Figure 3.8. Schematic illustration of (a) Jaumann absorber with 4 resistive sheets and (b) circuit equivalent

3.2.2. LabVIEW Modelling of Jaumann Type RAS

In order to decide thickness, resistance or any other parameters of the structure to get maximum microwave absorbance, it should be followed some certain ways. At that point, we can get help from simulation or genetic algorithm (GA) programmes.

In our study, to have an idea for the thicknesses and the resistance of sheets, or about thicknesses between sheets, reflection loss simulation and genetic optimization codes were written in MATLAB software package. Governing equations for structures were implemented into the code with absorbance calculation.

By taking some parameters result from the Matlab, structures were manufactured. Then reflection loss measurements were done for all structures. And for the conformity,

LabVIEW simulation programming was written by using governing transmission line theory formalization. Parameters taken from the structure used in LabVIEW simulation programme and reflection loss graphs were drawn. Then, experimental measurement results and theoretical reflection loss measurements were compared.

3.3. Fabrication Process of Polymeric Composite Structures

Glass fiber reinforced polymeric composites structures were fabricated for microwave absorbance. Epoxy and hardener was used as a matrix binder. Among the fabrication methods, Hand lay-up technique was applied with a compression for manufacturing purpose. For this aim, a closed metal mould was used by stacking and pressurizing the resin impregnated fabrics.

In this study, we not only focused on absorbance properties of manufactured structures, but also concentrated on mechanical properties. For that reason, a symmetrical stacking sequence was chosen. Sixteen layers of glass fabrics were used to prepare composite samples for mechanical property testing. Fabrics were stacked $[0^o/90^o]_{2S}$ orientation. This orientation provides 0^o direction on both surfaces which is recommended for ASTM D 3039 tensile test and ASTM D 6641 compression test. Also, center of symmetry provides appropriate condition for interlaminar peel testing.

Before the starting the fabrication, four resistive sheet layer are adjusted to use them in structure. Theirs resistances are changing between 35 ohm to 430 ohm. As it was mentioned in section 3.1.1, these resistive sheets were prepared by using magnetron sputtering system. Then, nonmetalized fabrics were cutted properly in the dimensions of the mould used. The epoxy resin was prepared by mixing of resin and hardener 80:20 weight ratio. After the sufficient mixing of resin and hardener, carbonyl iron (CI) micro particle additives was added to prepared resin system. CI particles have much higher densities than those of matrix. So, to prevent segregation of CI particles in resin, constant mechanical stirring was applied throughout the hand lay-up process. It can be seen fabrication process step by step in Figure 3.9.

In order to increase the fiber volume ratio and improve surface properties of the composites for perfect finish of both surfaces of the samples, the impregnated fabrics were placed in a metallic mould and the mould was closed and clamped firmly. The laminates were cured for 24 hours at room temperature within the mould under pressure.

After remoulding the composite parts, post curing was applied in a ventilated drying oven at 80 ^{o}C for 24 hours.

The continuing manufacturing process and fabricated structure is schematically illustrated in Figure 3.9 and Figure 3.10 respectively.

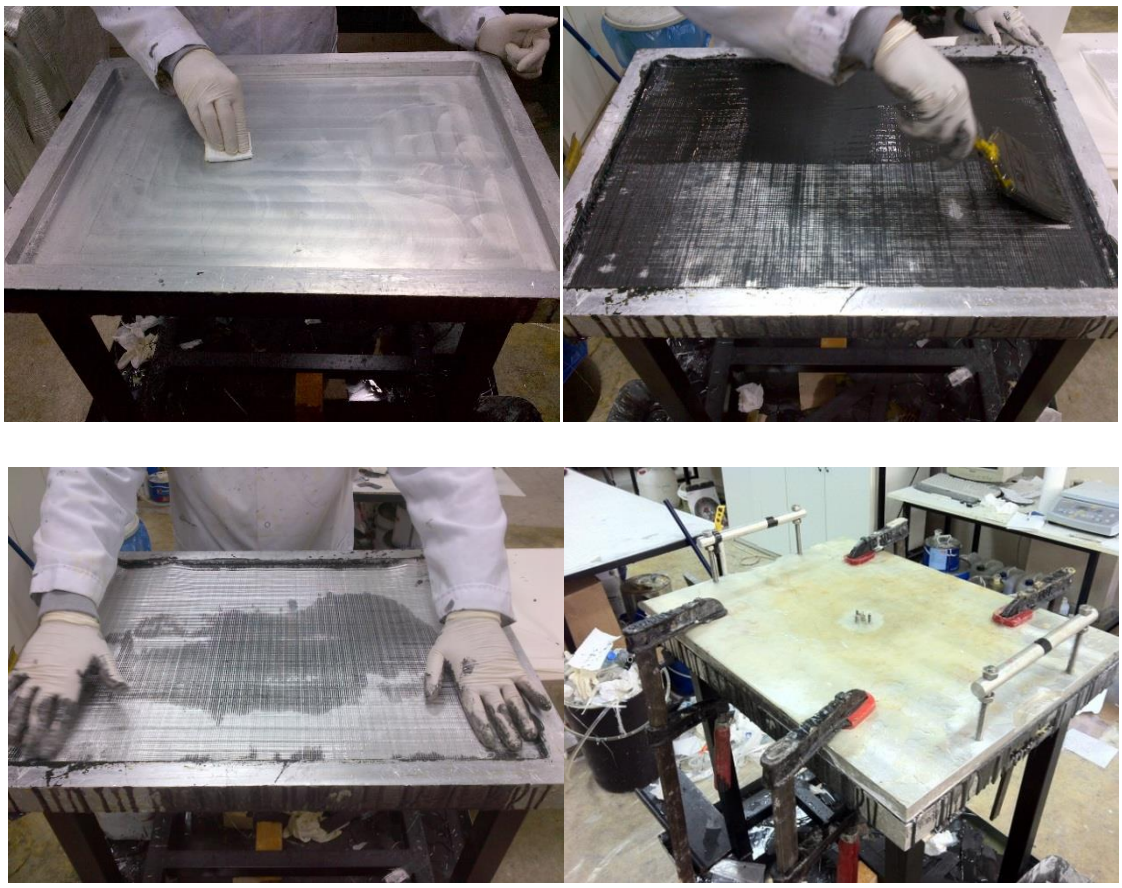

Figure 3.9. Step by step manufacturing of composites by hand lay-up technique

Figure 3.10. Fabricated one Structure

In Figure 3.10 post curing process can be seen after construct the structure. After all these preparations, the composite samples were sectioned using a diamond saw for the mechanical tests and absorbance tests. In Figure 3.11, there are manufactured and also prepared by cut with diamond saw to measure absorbance properties.

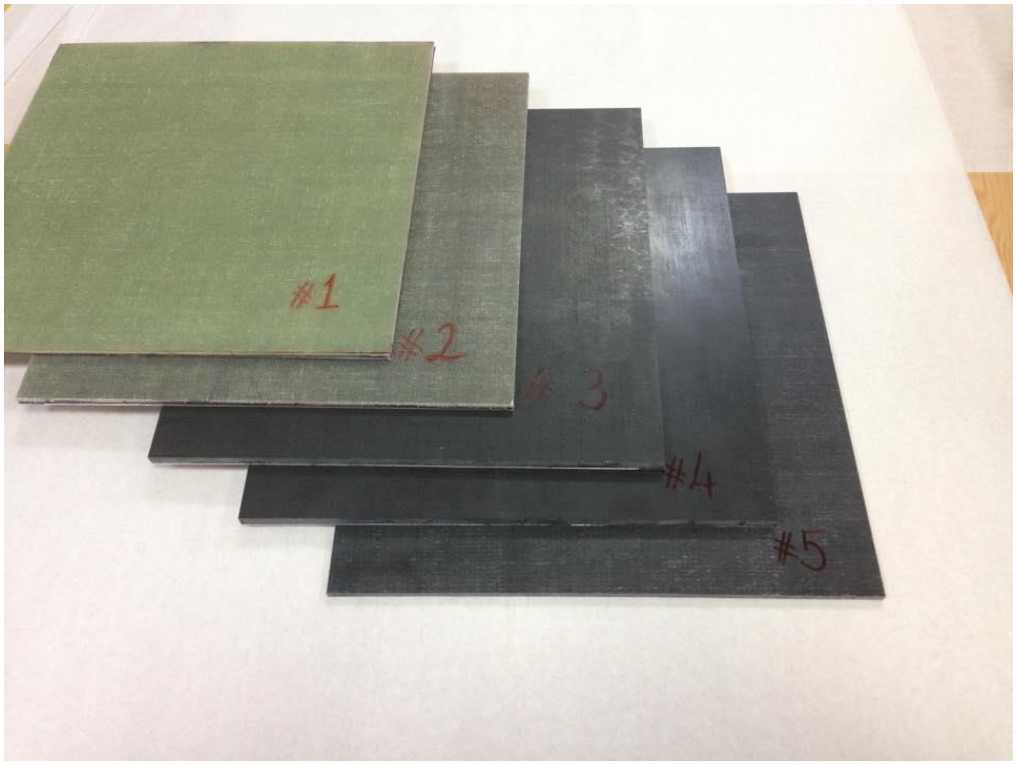

Figure 3.11. Photographs of all manufactured specimens for electromagnetic absorbance measurements

3.4. Characterization of Radar Absorbing Structures

Some characterization techniques were applied to manufactured composite structures. We looked SEM and Optical microscopy images of the samples. Mechanical tests were done and also radar absorbing properties of structures were measured.

3.4.1. Microstructural Property Characterization

3.4.1.1. Determination of Fiber Weight and Volume Ratio

The test standard of ASTM D 2584-02 was used for determining the fiber weight and volume ratio of radar absorbing polymeric composite structure by ignition loss of cured resins. To achieve this, small pieces of samples were cutted and prepared about 1cm^3 volumes. Then these pieces were burned off in a high temperature oven at 700 ^{o}C. After the burn off epoxy resin, the fiber and carbonyl iron residues were weighted and based on the weight and density of fiber, additive and polymer matrix, volume ratios were calculated by Equation 3.7.

$$V_f = \frac{v_f}{v_f + v_m + v_p} = \frac{\frac{m_f}{\rho_f}}{\frac{m_f}{\rho_f} + \frac{m_m}{\rho_m} + \frac{m_p}{\rho_p}} \tag{3.7}$$

In this equation, $v_f$indicates the volume of fiber, $v_m$is the matrix volume and $v_p$is the filler volume. With the same analogy, $m_f$is the mass of fiber, $m_m$indicates the mass of matrix and lastly $m_p$is mass of additive (here mass of carbonyl iron). Moreover, ρ_f, ρ_m, and ρ_p are the densities of fiber, matrix and radar absorbing filler material, respectively.

There are four structures which are containing carbonyl iron and Indium Tin Oxide thin film, but ITO thin films can be neglected because it is in the range of nanometers. So, if we compare the weight of ITO with others, it hardly affected the weight. After the burn off epoxy, its weight were known as residue weight subtracted from initial sample weight. Assuming epoxy matrix mixture ratio was homogeneous throughout the matrix, CI weight calculated from epoxy weight. Then calculated CI weight subtracted from residue weight to obtain remaining fiber weight. After weight calculations, by knowing densities of the materials in the structure, volumes and volume ratios were calculated.

3.4.1.2. Morphological Analysis by SEM

Firstly, Scanning Electron Microscopy (SEM) images of fiber fabrics were taken. Also, ITO coated parts of fabric surfaces were investigated by using Energy-Dispersive X-Ray (EDX) mapping. Moreover, as an additive, CI micro particles was used and SEM images of CI were taken. Then CI was added to structure. After manufacture the radar absorbing structure, samples prepared and SEM, EDX mapping were performed on cross sections. For all these, Quanta 250FEG scanning electron microscope at IZTECH Material Research Center was used.

Both back scattering electron and ETD modes were used through SEM analysis. For some samples, back scattering electron mode provides identification of materials based on their atomic number, thus creating a contrast between higher and lower atomic numbered elements. However, mostly ETD mode was used for our samples because of the better contrast and images.

3.4.1.3. Optical Microscopy Images and Confirmation

From the cross sectional area, the thickness of the samples were determined by using optical microscopy. Four resistive sheets were used in each sample. From second to fifth structures, for each sample, the thicknesses between resistive sheets were examined. We decided the parameters and used these parameters in LabVIEW programming to confirm the measured reflection loss with the theoretical (simulation) one.

Before the optical imaging, the structure surfaces were prepared and polished by starting from 320 number of sandpaper to 1200, then diamond solutions were performed from 9 micron to 3 micron. After these operations, optical images were captured from cross sectional areas of manufactured structures. Then, thicknesses which were taken from images, were used for the confirmation. In Figure 3.12, it can be seen optical microscopy which was used for images.

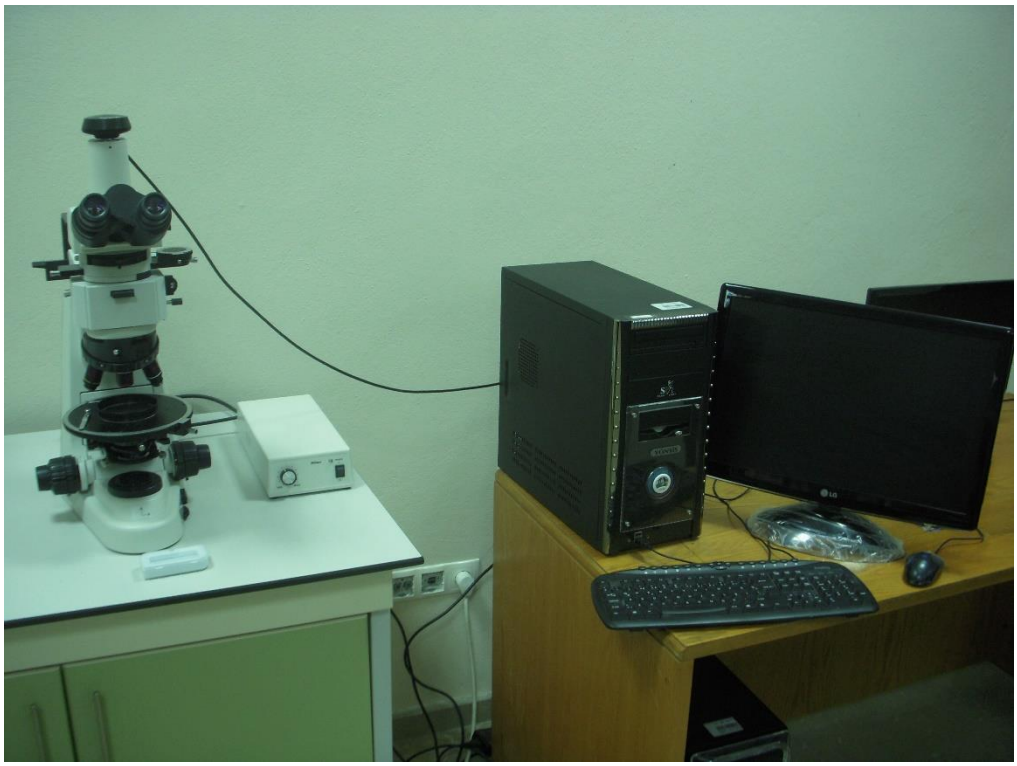

Figure 3.12. Photographs of all manufactured specimens for electromagnetic absorbance measurements

3.4.2. Mechanical Property Characterization

Some mechanical properties of microwave absorbing structures were examined to compare the mechanical performance of RASs with the conventional glass fiber reinforcement epoxy resin polymeric composite structure. And by using these results, the effect of the additive CI particles and ITO coated fabrics on the integrity of the composite was investigated. Quasi-static tests such as tensile, bending and compression tests were performed on the specimens sectioned from composite plates. Also, impact strength test were done based on standard procedures.

3.4.2.1. Tensile Properties of Structures

For determination of tensile properties, tensile strength, tensile modulus and strain at failure of samples manufactured, ASTM D 3039-00 test standard was used.

Test specimens was cut with the dimensions of 250 mm length and 25 mm width by using diamond saw. For each composite configuration, five samples were prepared at least. The specimens were tested at room temperature using universal mechanical testing machine, Shimadzu AG-IC 100KN at a cross head speed of 2 mm/min. Video extensiometer was used to measure the strain values. In Figure 3.13, it can be seen the tensile grips and specimen during tensile testing.

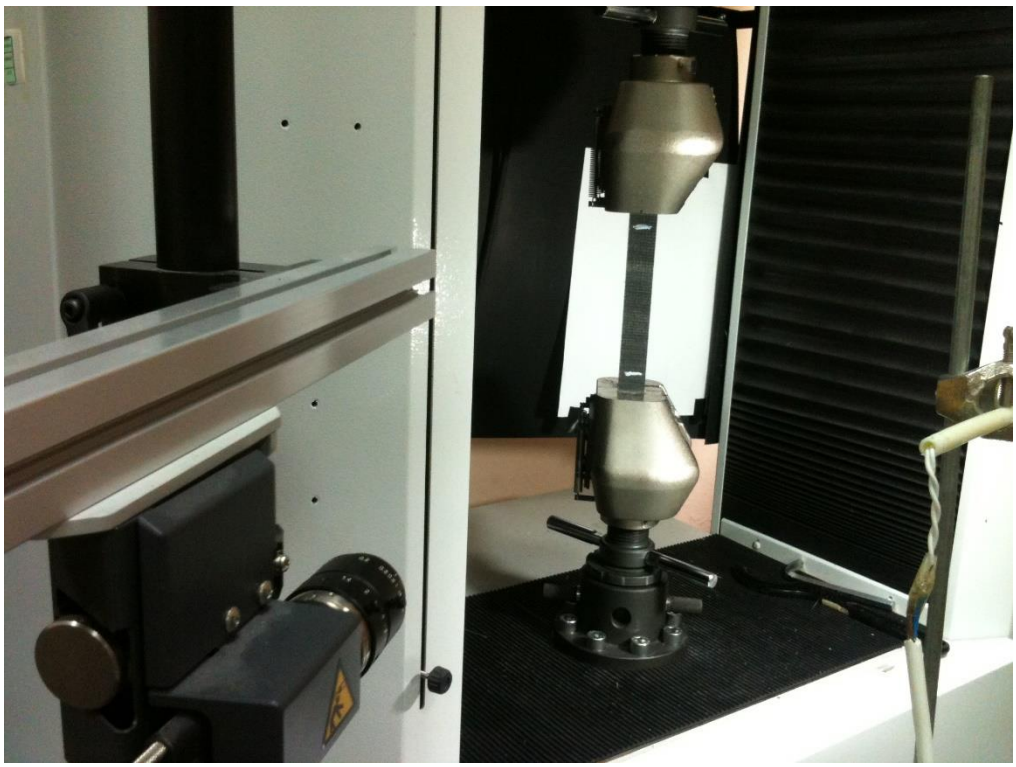

Figure 3.13. Photo of captured during the tensile test

From the following equations, tensile stress and strain values can be calculated easily;

$$\sigma = \frac{F}{A} \tag{3.8}$$

$$\varepsilon = \frac{(L - L_0)}{L_0} \tag{3.9}$$

In Equation 3.8 and 3.9, F is the ultimate load, A is the cross sectional area of the specimen tested, L_0 is the original distance between gauge marks and L is the distance between gauge marks at any time. Elastic modulus (E) was obtained from the initial slope of the stress-strain curves.

3.4.2.2. Flexural Properties of Structures

ASTM D 790-03 test standard was used for the specimen preparation and flexural tests. Specimens were tested in 3-point bending configuration with a span to thickness ratio of 16. Specimen thicknesses was important because they were used in correlation between specimen length, span distance and test speed which comprised in test standard. Through all bending tests, all specimens were cut 13 mm wide. At least from each radar absorbing structures, five specimens were prepared and tested using the universal testing machine. Force and deflection values at the center of the beam was recorded. Flexural test setup can be seen in Figure 3.14.

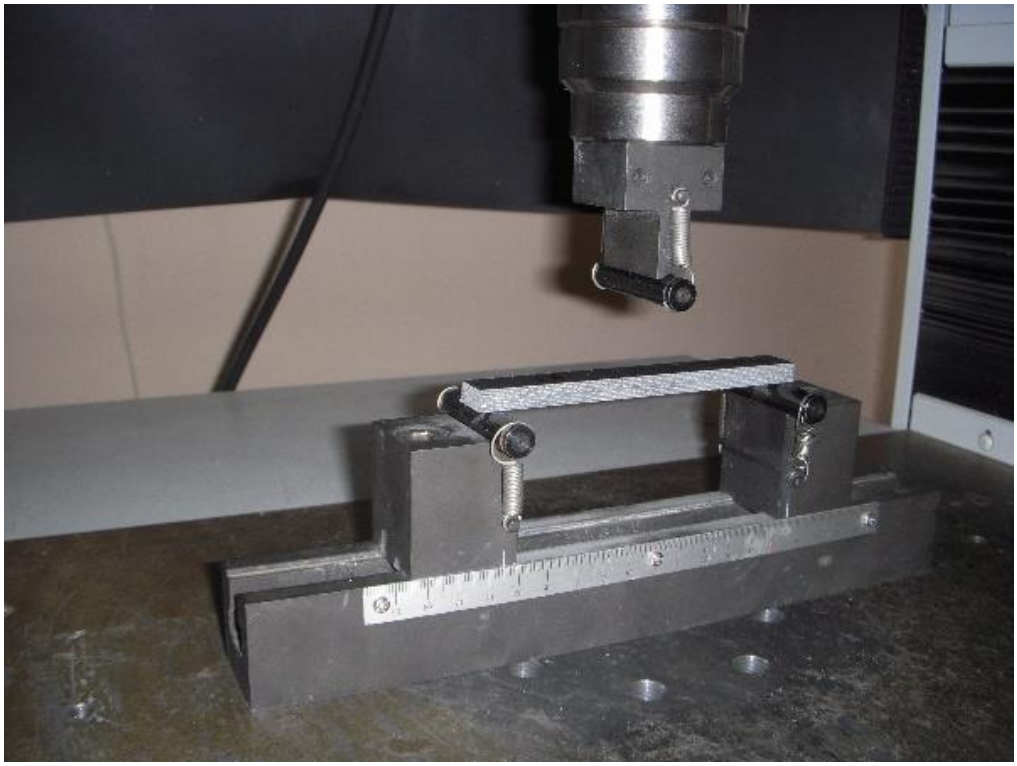

Figure 3.14. When the flexural test was performing

3.4.2.3. Compressive Properties of Structures

ASTM D 6641-01 compression test method was utilized to measure in-plane compressive strength, compressive modulus and strain at break values of the composite panels was manufactured. For this purpose, 140 mm length and 12 mm width specimens were cut from fabricated radar absorbing panels, and compression tests were applied to them. Compression tests along in-plane loading direction were performed using the universal test machine with test fixture shown in Figure 3.15, at a cross speed of 1.3 mm/min. On each set, five specimens were used to test the compressive property of structures and force vs. stroke data were recorded. The load values were divided to the cross sectional area of the specimens to obtain the compressive stress values. Moreover, the stroke values were divided to the initial specimens' thickness to estimate the strain values of structures. Finally, it can be reached to the modulus by using the slope of the strain-stress graph.

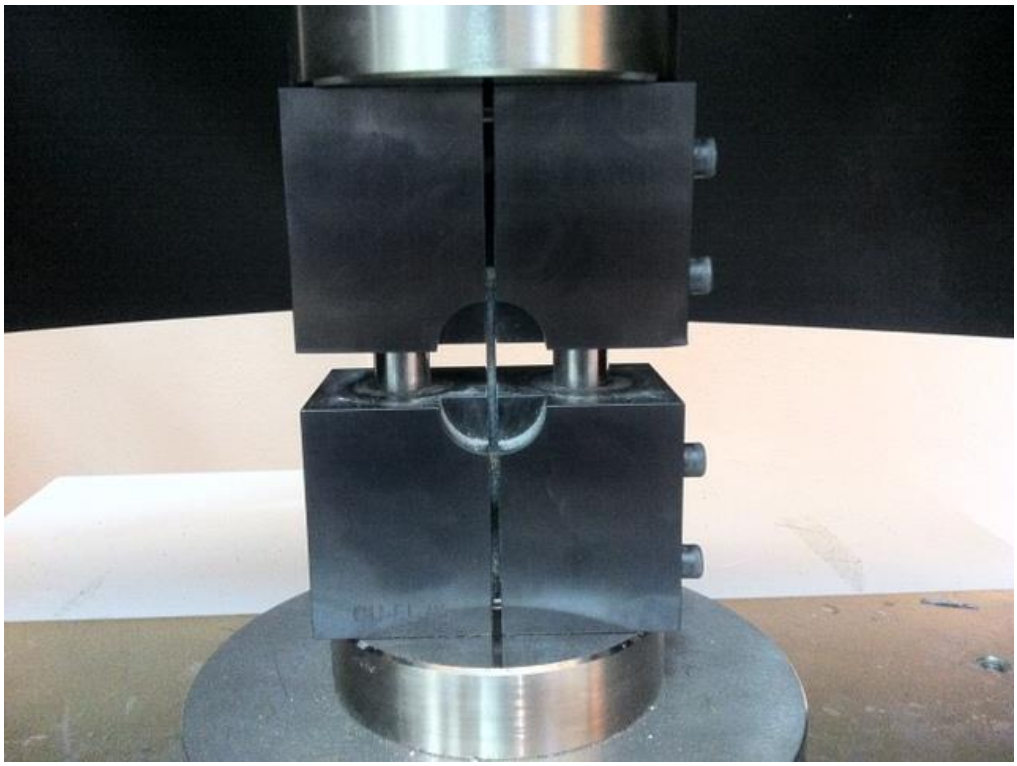

Figure 3.15. Picture of experimental setup for compression tests

3.4.2.4. Charpy Impact Strength Properties of Structures

In Charpy impact test, the impact toughness of a material can be measured then the information can be taken about the strength of the material. A swimming pendulum was used in the Charpy test to initiate and propagate cracking in a notched sample. The pendulum was realised from the known height and therefore from the known potential energy level. It rotates to the bottom position. At the bottom, the pendulum impacts the sample that setup in single-edge notched specimen and then the pendulum swings up to a final height, which is recorded. The differences between initial and final heights of the pendulum mass were used to calculate the potential energy loss of the pendulum, which is primary measurement in a typical Charpy test.

The potential energy loss of the pendulum, is equal to the fracture energy which is the amount of energy absorbed by the sample that fractures. Energy to initiate the crack, propagate the crack, elastically and plastically deform, the material around the crack and contact surfaces, and accelerate the sample are all the energy measured are sum of components. As a result, the Charpy test provides a measure of these combined mechanisms.

Dimensions of specimens were cut with the dimension of 80 mm length and 10 mm width by using the test standard of ISO 179. Moreover, all specimens were notched 2 mm in plane direction in accordance with ISO 179. For each sample plate, five specimens were tested at least. Impact energy values were recorded from CEAST 6545 Charpy Impact Energy Test Instrument shown in Figure 3.16.

Figure 3.16. Photo of experimental setup for Charpy impact tests

3.4.3. Absorption Measurement Properties of Structures

Five different type of composite structures were manufactured for microwave absorption purposes. One of them is Dallenbach layer with the 16 uncoated fiber and it did not contain any additive in it. Actually, this was just conventional fiber reinforced epoxy polymeric composite structure. In the second structure, from the 16 fibers, four of them were used as resistive sheet by coating surface of them with ITO, with magnetron sputtering system. Resistance of each sheet was different. In the remaining other 3 structures, still four resistive sheets was used for each structure and in addition to Salisbury Screen, also CI additive was used. Additive percentage and resistance of the sheets were different.

When the percentage of additives were changed or resistance of or number of the sheets changed, the intrinsic impedance of structure should be change. So, permittivity and permeability values acquired from literature (Qing 2009) for the simulations and optimizations. Results obtained from these optimizations had given preliminary design for manufactured samples. Composite structures based on optimization results were

manufactured and reflection loss measurements were performed and those experimental results were compared with simulation results. Moreover, by using related transmission line theory for Jaumann type structures, LabVIEW simulation programming were written. The experimental graph results were confirmed with the LabVIEW programming results which using data were taken from the literature and thicknesses between resistive sheets were measured by using optical microscopy.

Figure 3.17. Radar Absorbing Experimental Set-up

CHAPTER 4

RESULTS AND DISCUSSIONS

In this chapter, manufacturing the radar absorbing structures are introduced. Experimental results are compared with the simulation and optimization approaches. Moreover, microstructural and mechanical properties of the manufactured structures are given. Also, there is an absorbance performance of the microwave absorbing composite structures. Lastly, confirmation is done between LabVIEW modelling programme and the microwave absorbance results of the experimentally manufactured structures.

4.1. What We Manufactured

Five radar absorbing structures were fabricated which have the different properties for increase the bandwidth and capability of the structure. Also, mechanical properties are evaluated. The configuration of the samples can be seen from Table 4.1.

Firstly, just polymeric epoxy resin composite structure was manufactured with any modification or additives. It was 16 layers of glass fabric with $[0^o/90^o]_{2S}$ orientation. Of course, in absorbance measurement, it acts like a Dallenbach layer. Also, it is used as a reference in mechanical tests and the structures with additives or with some modifications, are compared with this structure. Thickness of first structure was measured about 5.6 mm.

In the 2nd sample, four resistive sheets (Indium Tin Oxide coated fabric layers) were used without any additives. These resistive sheets acted like a Salisbury Screen in the composite structure. So, it can be said that, this configuration was Jaumann type microwave absorbing structure. Thicknesses between resistive sheets and thickness between surface and resistive sheet, also resistances of sheets were very important. The measurements were done in two ways. Firstly, by using the total thickness, it divided to 16, then thickness between each layer was calculated. Of course, we had known the location of the resistive sheets in the structure. Then, we multiplied it with the number of layers so, found the associated thickness. The second way, which was more accurate but nearly same with the first, was, using the optical microscopy. Under the optical

microscopy, layers were seen clearly. So, thicknesses between sheets and surface were measured easily. Resistances of the layers were measured by using four probe measurement system. They included diversity between 45 ohms/square and 410 ohms/square. The total thickness of the structure was about 4.9 mm.

For preparation of 3rd sample, 25 wt% carbonyl iron (CI) additive was used as a filler in to epoxy matrix with four resistive sheets. This was Jaumann structure. Carbonyl iron served as a ferrimagnetic absorber and resistive sheets (ITO coated layers) assumed to increase the reflection loss. Resistance of the ITO coated fabric surfaces were measured and they showed variety between 75 ohms/square and 430 ohms/square. Again with the same method in sample 2, thicknesses between resistive sheets were measured and total thickness of the structure was nearly 6.2 mm.

In the 4th Jaumann absorber, 25 wt% carbonyl iron filler and four resistive sheets were used but with different resistances and different thicknesses. Again this was Jaumann absorber. Resistances were changing between 30 ohms/square and 245 ohms/square. Total thickness of the structure was about 6.5 mm.

Lastly, 5th Jaumann type radar absorbing structure was manufactured. In this structure, 13 wt% carbonyl iron additive for absorbance and four resistive sheets with different resistances for increase the bandwidth was used.

In all Jaumann type structures, resistive sheets were placed according to optimization results calculated from Matlab genetic algorithm programming.

Table 4.1. Configurations of radar absorbing structures fabricated

Sample #	# of Layers	Additive	Resistive Sheets	Orientation	Modelling Structure
1	16	No	No	$[0^o/90^o]_{2S}$	Dallenbach
2	16	No	4 ITO Coated Fabric	$[0^o/90^o]_{2S}$	4 Resistive Sheet Jaumann
3	16	25 wt% CI	4 ITO Coated Fabric	$[0^o/90^o]_{2S}$	4 Resistive Sheet Jaumann
4	16	25 wt% CI	4 ITO Coated Fabric	$[0^o/90^o]_{2S}$	4 Resistive Sheet Jaumann
5	16	13 wt% CI	4 ITO Coated Fabric	$[0^o/90^o]_{2S}$	4 Resistive Sheet Jaumann

4.2. Electrical Characterization of Fabrics

For the creation of resistive sheets to use them in Jaumann type radar absorbing structures, large area magnetron sputtering system was used, and surface of the fiber fabrics were coated with indium tin oxide thin film. Whereby, surface of the fabrics was functionalized and it was gained conductivity. It was not an easy work as thought. Because, electrical characterization of the surface was very important. In other words, to use them in structure as a resistive sheet, resistances should take some certain values which came from the optimization. And they are related to the thickness of the structure and thickness between resistive sheets.

There are so many techniques to get intended resistance values from the surface. For example, the speed of sample can be changed when it passes through the plasma, or the power of the plasma can be adjusted. In our study, to characterize the resistance, power was kept constant, the speed of feed through mechanism was changed. With the values taken from the optimization, we tried to obtain the required resistance values.

All in all, for the electrical characterization, four probe method was used to measure surface resistance of the coated fabrics. To get the accurate result, surface of the fabrics cannot be measured so glass lamellas were used to get correct electrical

measurements. In each deposition, lamellas were put on some part of fabric so that lamellas were coated with the fabric as the same parameters. Then, measurements were done from the surface of the lamellas. So, desired resistance parameters were obtained by changing speed of the feed through. In Figure 4.1, four probe method can be seen and there are resistance parameters of the Salisbury Screens of Jaumann layers in Table 4.2.

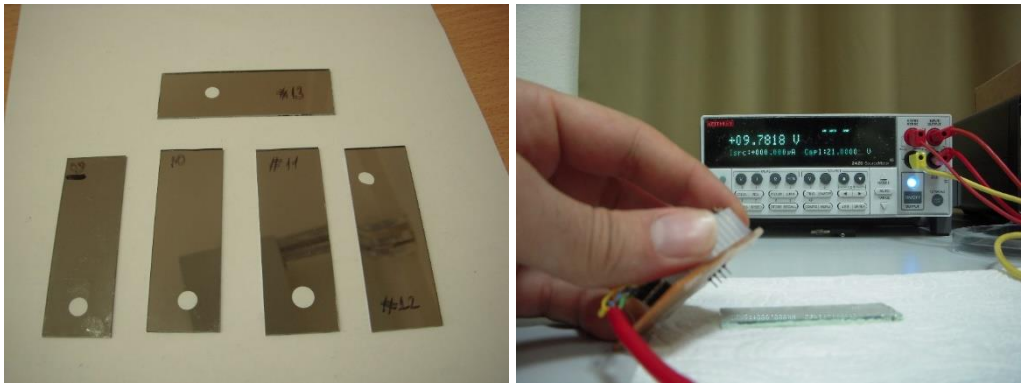

Figure 4.1. Coated Lamellas and Four Probe Method for Electrical Characterization

Table 4.2. Resistance values of used Sheets in Structure

Sample #	**1st Sheet**	**2nd Sheet**	**3rd Sheet**	**4th Sheet**
2	45 Ω/sqr	100 Ω/sqr	340 Ω/sqr	410 Ω/sqr
3	75 Ω/sqr	120 Ω/sqr	300 Ω/sqr	430 Ω/sqr
4	30 Ω/sqr	35 Ω/sqr	41 Ω/sqr	245 Ω/sqr
5	75 Ω/sqr	110 Ω/sqr	330 Ω/sqr	350 Ω/sqr

In Figure 4.2, sorting of the resistive sheets were given. First resistive sheet means, nearest to the meal back. In other words, for each sample, maximum resistance was placed closest to the surface of the structure. When wave comes, it will impinge on maximum resistance surface.

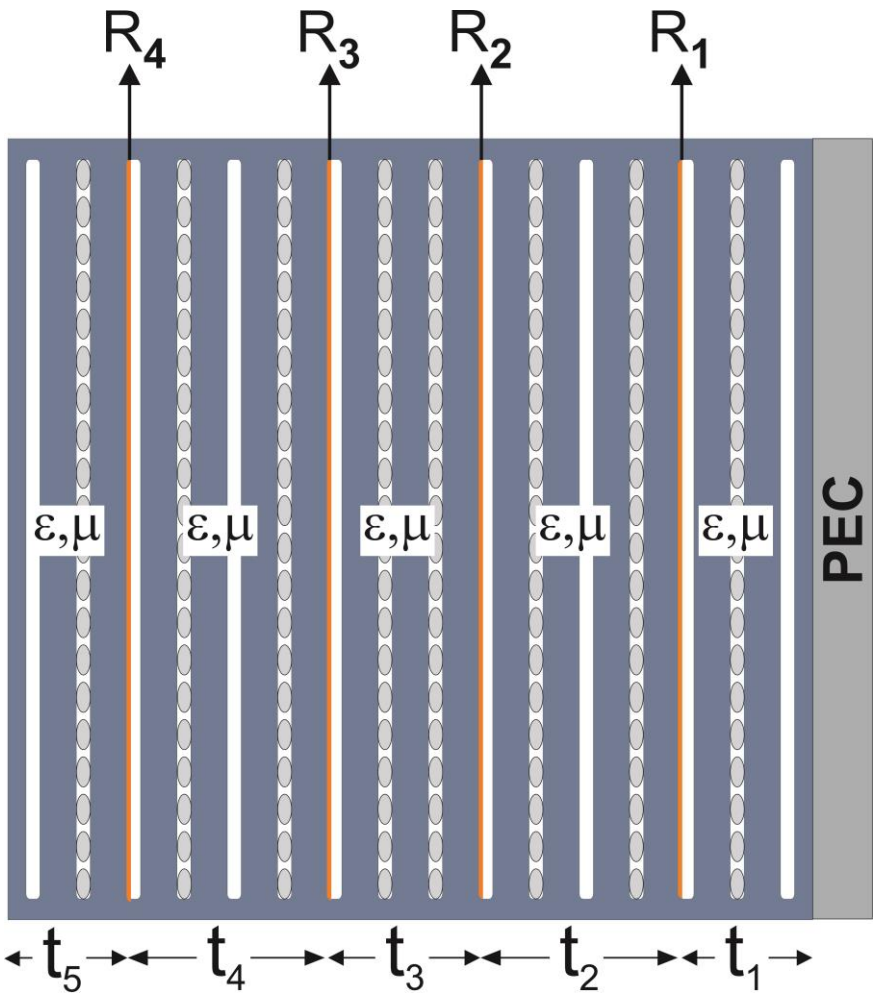

Figure 4.2. Illustration of Resistive Sheets in Composite Structure

4.3. Microstructural Characterization

4.3.1. Fiber Weight and Volume Ratio

Fiber volume ratio is one of the most important thing in composite structures. Because it is directly affects the physical properties of structures. Before comparing mechanical properties of the manufactured samples, their fiber volume content should be taken into account. Because fiber fabrics are the main mechanical load bearing elements of the composite structure, and when the volume of the reinforcement fiber is increased, mechanical properties of the structure gets well remarkably.

It can be seen fiber weight and volume ratio tables from 4.3 to 4.7 for each sample. It is observed that fiber volume ratio may change because of the manual compression of

the mould. In hand lay-up manufacturing process, fiber volume ratio cannot be fully controlled because it is an open mould process. Moreover, mould is pressurized by clamping and clamping force directly affects the fiber volume ratio.

Table 4.3. Fiber weight and volume ratios for 1st Structure

3 Samples from the 1st Structure	**Fiber Weight Ratio (%)**	**Fiber Volume Ratio (%)**
1	60.37	39.73
2	59.25	38.62
3	58.29	37.69
Average	**59.30**	**38.68**
Std. Dev.	**1.04**	**1.02**

Table 4.4. Fiber weight and volume ratios for 2nd Structure

3 Samples from the 2nd Structure	**Fiber Weight Ratio (%)**	**Fiber Volume Ratio (%)**
1	62.40	41.81
2	62.23	41.63
3	62.92	42.34
Average	**62.52**	**41.93**
Std. Dev.	**0.36**	**0.37**

Table 4.5. Fiber weight and volume ratios for 3rd Structure

3 Samples from the 3rd Structure	**Fiber Weight Ratio (%)**	**Fiber Volume Ratio (%)**
1	55.45	40.65
2	54.80	40.03
3	54.70	39.93
Average	**54.98**	**40.20**
Std. Dev.	**0.40**	**0.39**

Table 4.6. Fiber weight and volume ratios for 4th Structure

3 Samples from the 4th Structure	Fiber Weight Ratio (%)	Fiber Volume Ratio (%)
1	51.81	37.18
2	51.08	36.50
3	49.75	35.27
Average	**50.88**	**36.31**
Std. Dev.	**1.05**	**0.97**

Table 4.7. Fiber weight and volume ratios for 5th Structure

3 Samples from the 5th Structure	Fiber Weight Ratio (%)	Fiber Volume Ratio (%)
1	63.18	45.58
2	62.62	44.98
3	63.24	45.64
Average	**63.01**	**45.40**
Std. Dev.	**0.34**	**0.36**

Moreover, besides all these calculations, densities of the structures were calculated by using fiber weight and volume ratios of samples. The densities of carbonyl iron, glass fiber and epoxy has already known. Also, volume ratios calculated. Then the densities of structures can be calculated easily by using volume, mass and density relation equation. By using this technique, some density calculations were done. In addition, from the manufactured structures, nearly 1 cm^3 samples were cut from structures and masses were measured. Then densities were calculated with this second way. Comparisons were given in Table 4.8.

Table 4.8. Comparison between measured and calculated densities

Samples from the 1st Structure	**Densities Calculated from Fiber Weight and Volume Ratios**	**Density Calculated by Measuring Mass and Volume**	**Difference (%)**
Average	1.66964 g/cm^3	1.64736 g/cm^3	% 1.352
Samples from the 2nd Structure	**Densities Calculated from Fiber Weight and Volume Ratios**	**Density Calculated by Measuring Mass and Volume**	**Difference (%)**
Average	1.71676 g/cm^3	1.70974 g/cm^3	% 0.410
Samples from the 3rd Structure	**Densities Calculated from Fiber Weight and Volume Ratios**	**Density Calculated by Measuring Mass and Volume**	**Difference (%)**
Average	1.87175 g/cm^3	1.84366 g/cm^3	% 1.524
Samples from the 4th Structure	**Densities Calculated from Fiber Weight and Volume Ratios**	**Density Calculated by Measuring Mass and Volume**	**Difference (%)**
Average	1.82700 g/cm^3	1.7422 g/cm^3	% 4.867
Samples from the 5th Structure	**Densities Calculated from Fiber Weight and Volume Ratios**	**Density Calculated by Measuring Mass and Volume**	**Difference (%)**
Average	1.84456 g/cm^3	1.72828 g/cm^3	% 6.728

When the fiber weight and volume ratios were used, exact values of the densities were used for carbonyl iron, glass fiber and polyester from the literature. For carbonyl iron it was used 7.62 g/cm^3, for glass fiber it was 2.56 and lastly for polyester it was 1.108 g/cm^3.

4.3.2. SEM Images and EDX Mapping of the RAS

In this study micro sized Carbonyl Iron (CI) particles were used as an absorbing additives in composite structures. Scanning Electron Microscope images were taken and micrographs show that CI particles are nearly perfectly spherical and particle sizes about 5 μm. SEM images can be seen in Figure 4.3.

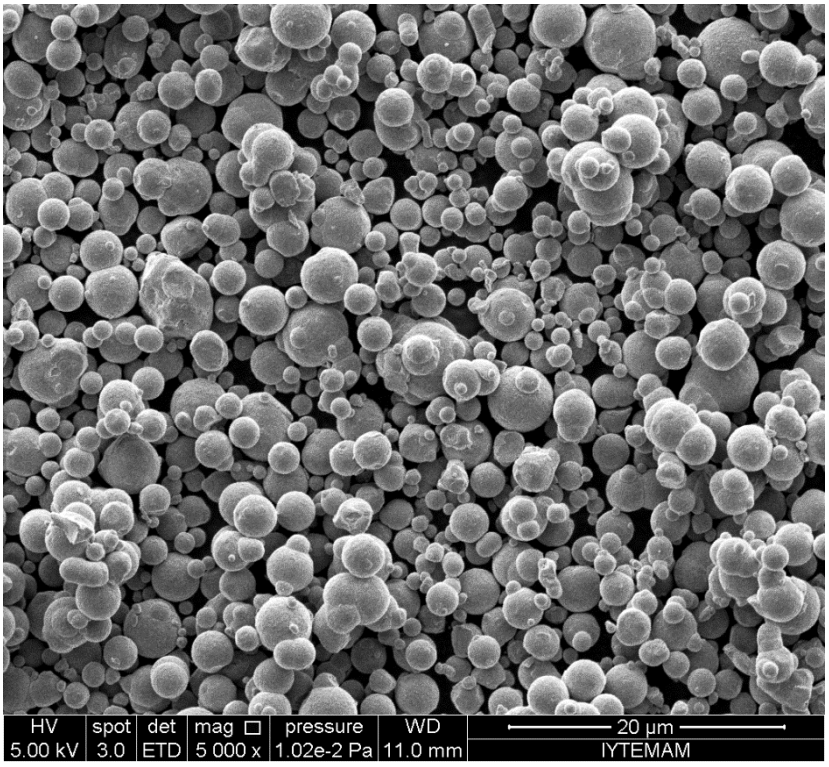

Figure 4.3. Electron micrograph of carbonyl iron powder (5000X)

The surface properties of the unmodified and modified fabrics that were used in these study were also analysed by SEM. Figures from 4.4 to 4.6 show the images of conventional E-glass fabric at 500X, 1000X and 2000X magnification, respectively. Also, Figures 4.7 to 4.9 show ITO coated fabrics at 500X, 1000X and 2000X magnification, respectively. It does not seen any significant changes on the surface of the fabric because of the thickness of the ITO thin film. But the main difference can be seen in the elemental analysis of the surface of the uncoated and coated glass fabrics.

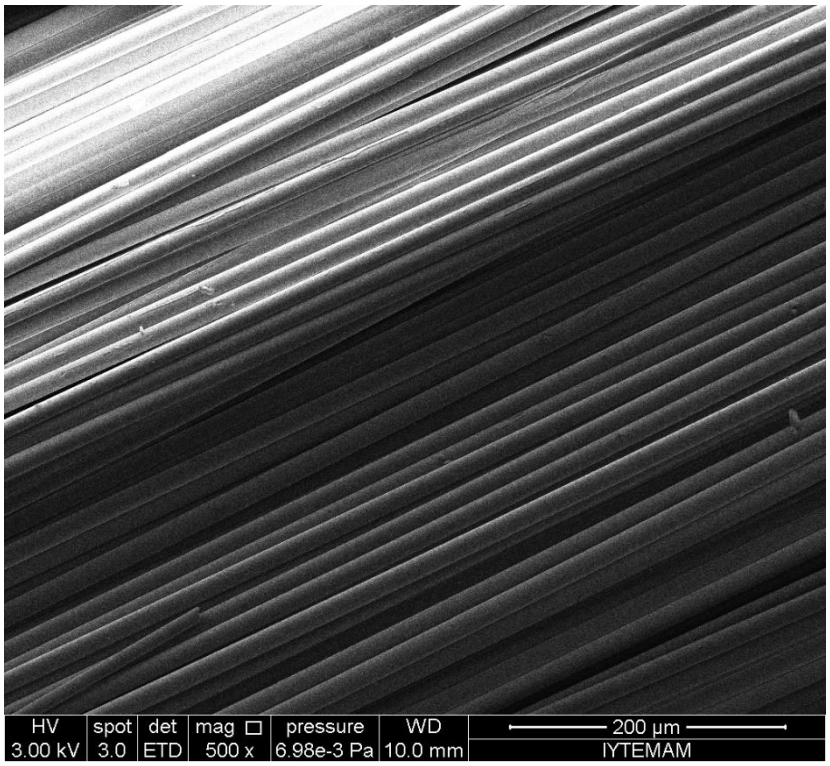

Figure 4.4. SEM Image of E-glass fabric with ETD detector (500X)

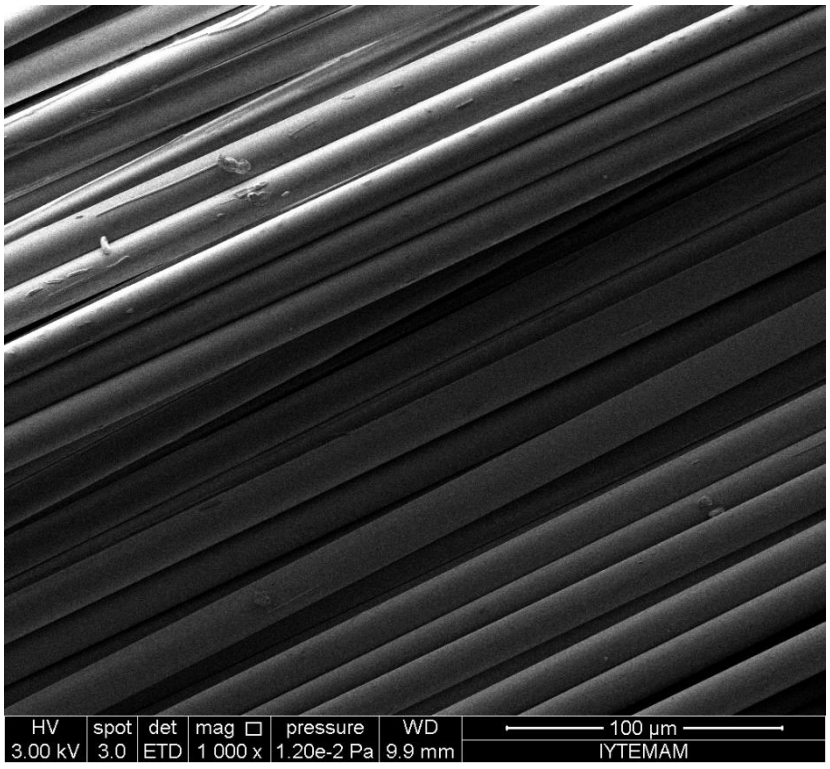

Figure 4.5. SEM Image of E-glass fabric with ETD detector (1000X)

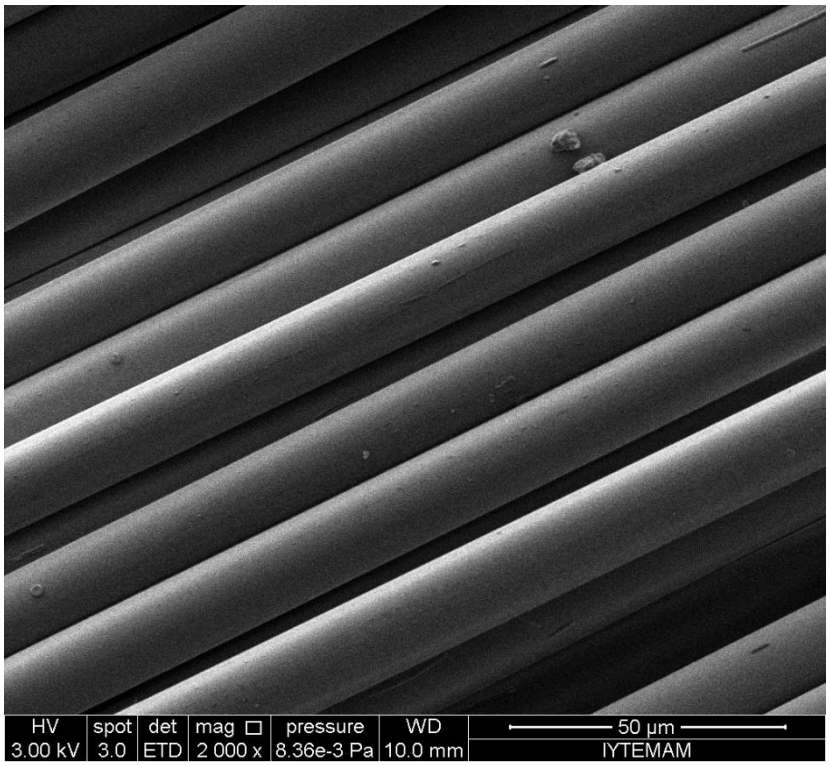

Figure 4.6. SEM Image of E-glass fabric with ETD detector (2000X)

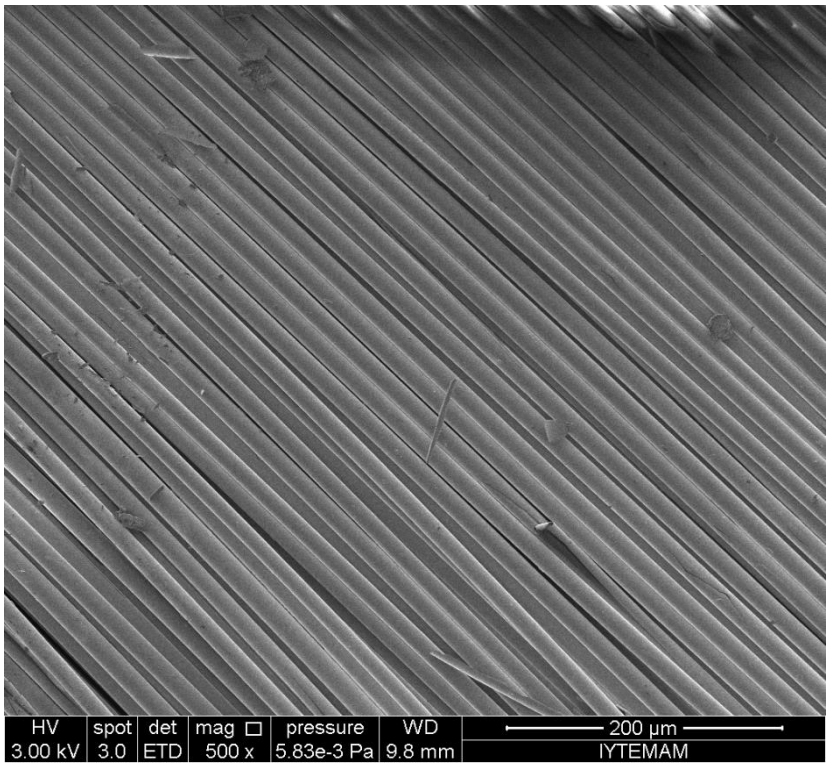

Figure 4.7. SEM image of E-glass fabric with ITO coating (500X)

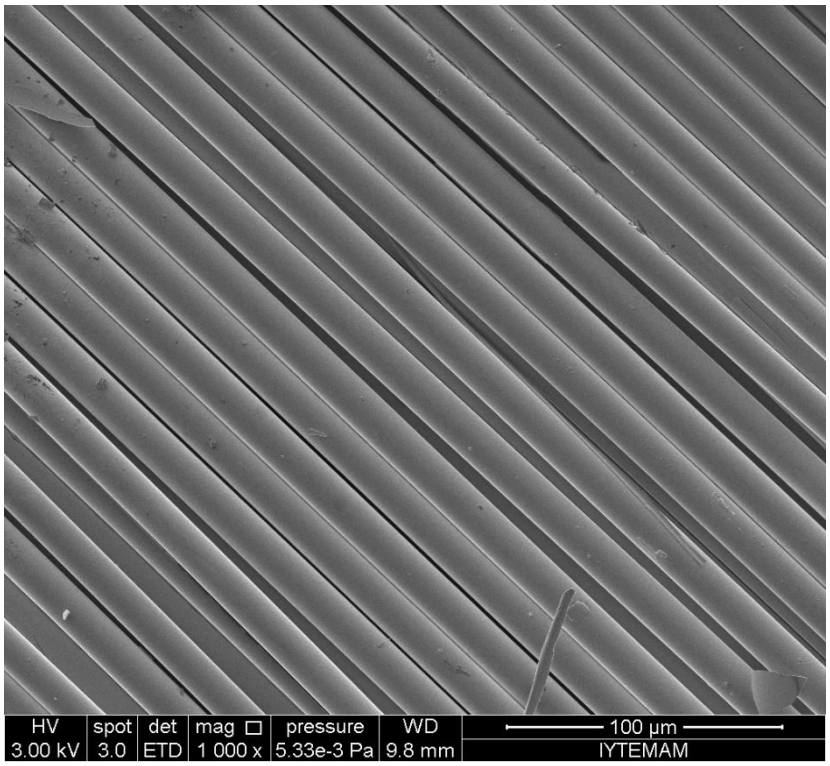

Figure 4.8. SEM image of E-glass fabric with ITO coating (1000X)

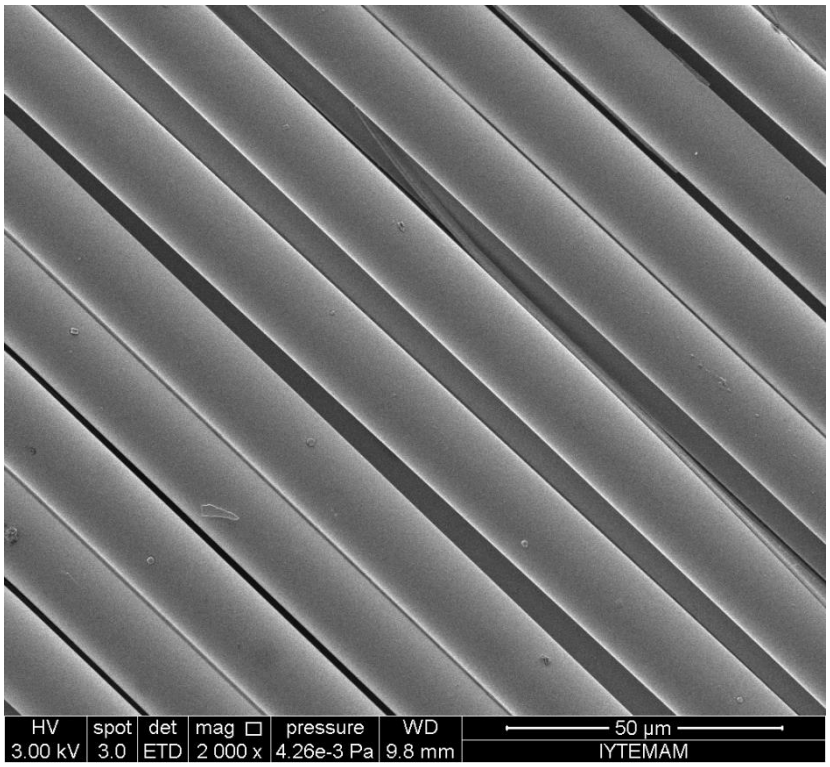

Figure 4.9. SEM image of E-glass fabric with ITO coating (2000X)

In addition to the glass fabrics, manufactured structures cross sectional SEM images were taken. ETD detector was used. This was performed for all manufactured structures. Each sample contain 0^o and 90^o fibers. In 3^{rd}, 4^{th}, and 5^{th} samples, there was a carbonyl iron micro particles. Also, except the first structure, other four has ITO coated resistive sheets.

It was observed that, the distribution of carbonyl iron particles are not perfectly homogeneous throughout the matrix phase. But it is likely homogeneous.

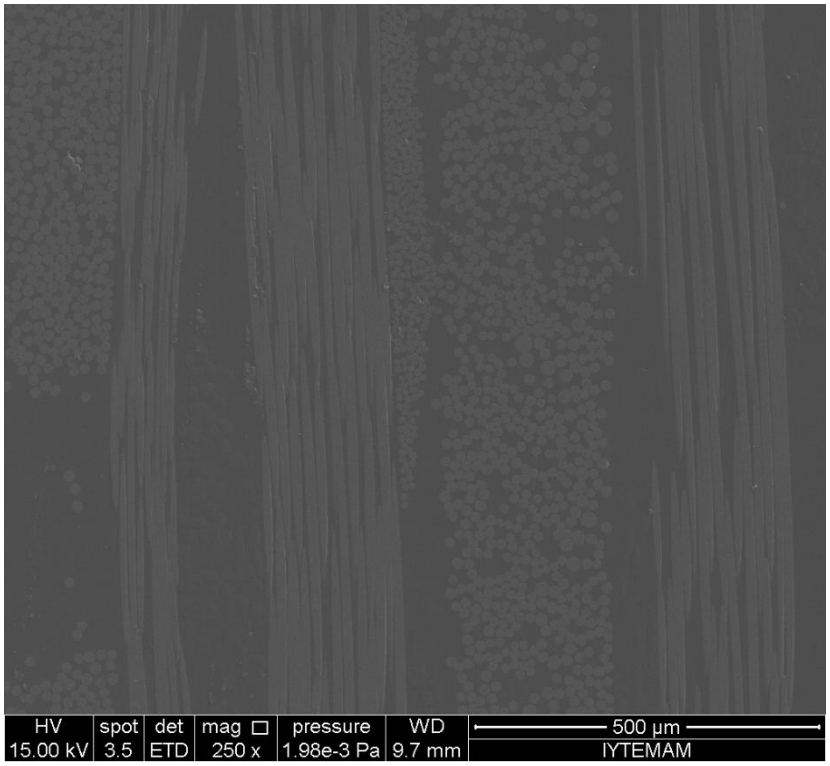

Figure 4.10. SEM image from glass fiber / epoxy based laminated composite cross-section, 1^{st} sample (250X)

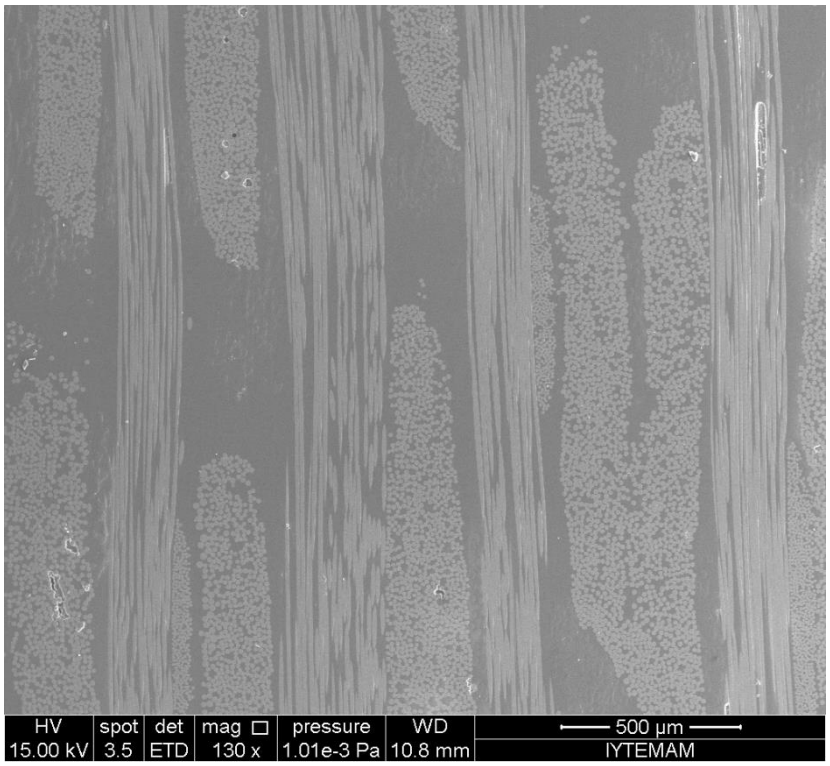

Figure 4.11. SEM image from glass fiber / epoxy based laminated composite cross-section, 2nd sample (130X)

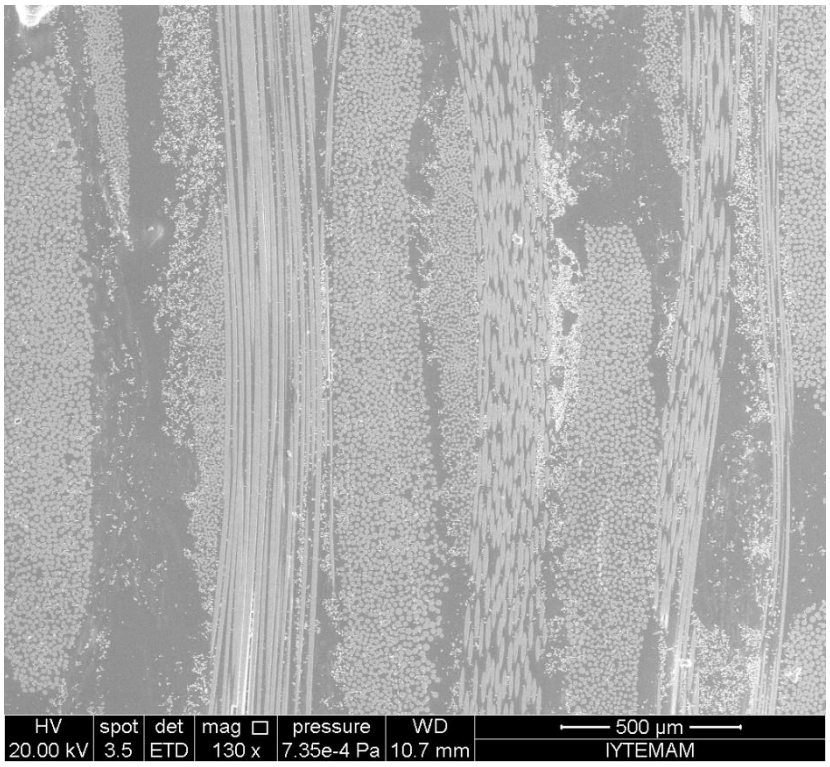

Figure 4.12. SEM image from glass fiber / carbonyl iron / epoxy based laminated composite cross-section, 3rd sample (130X)

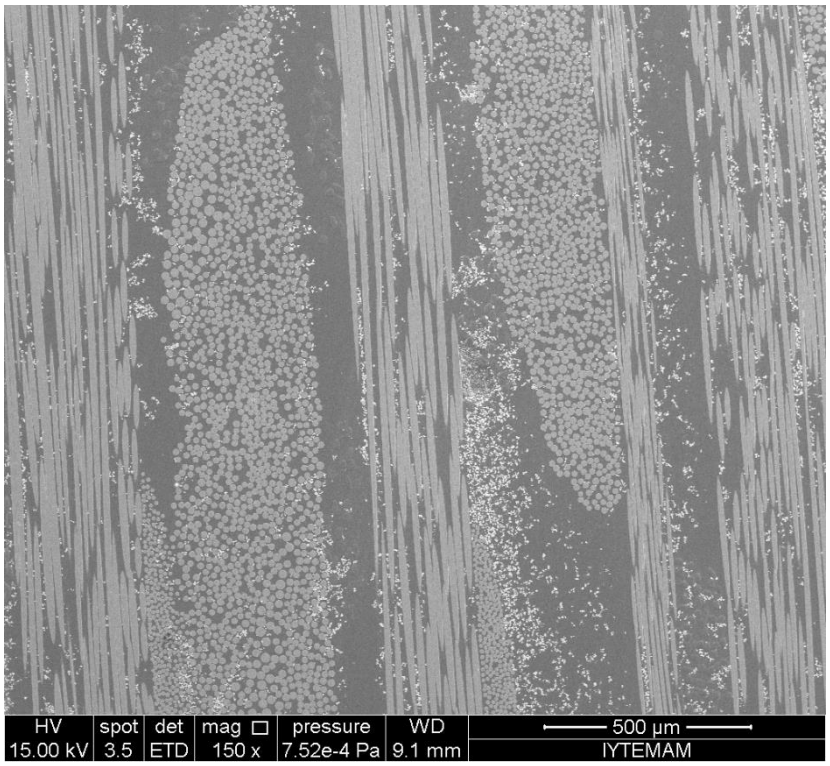

Figure 4.13. SEM image from glass fiber / carbonyl iron / epoxy based laminated composite cross-section, 3rd sample (150X)

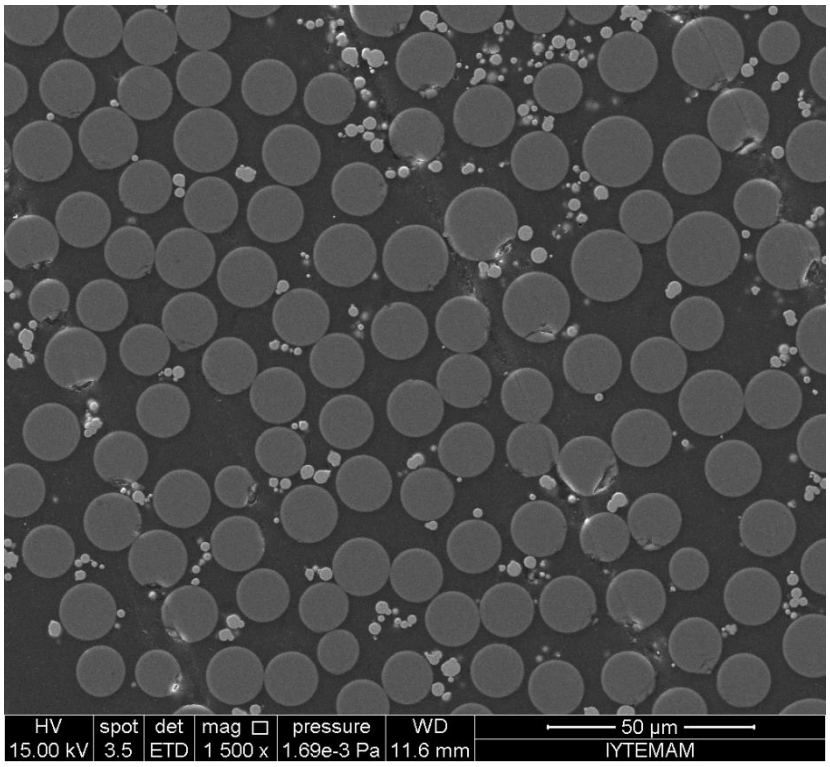

Figure 4.14. SEM image of CI distribution in 3rd sample (1500X)

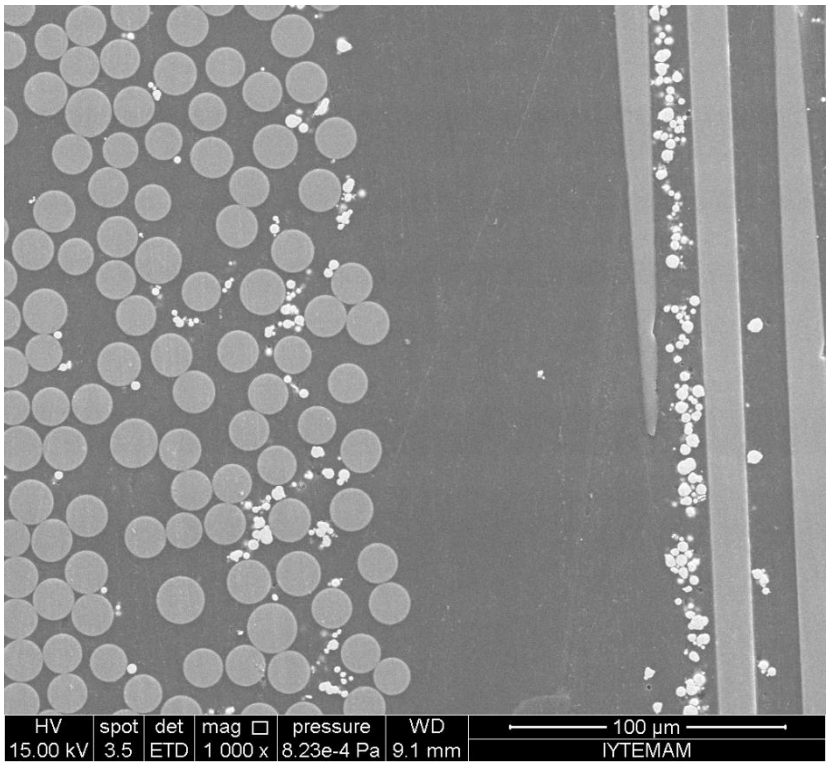

Figure 4.15. SEM image of CI distribution in 4th sample (1000X)

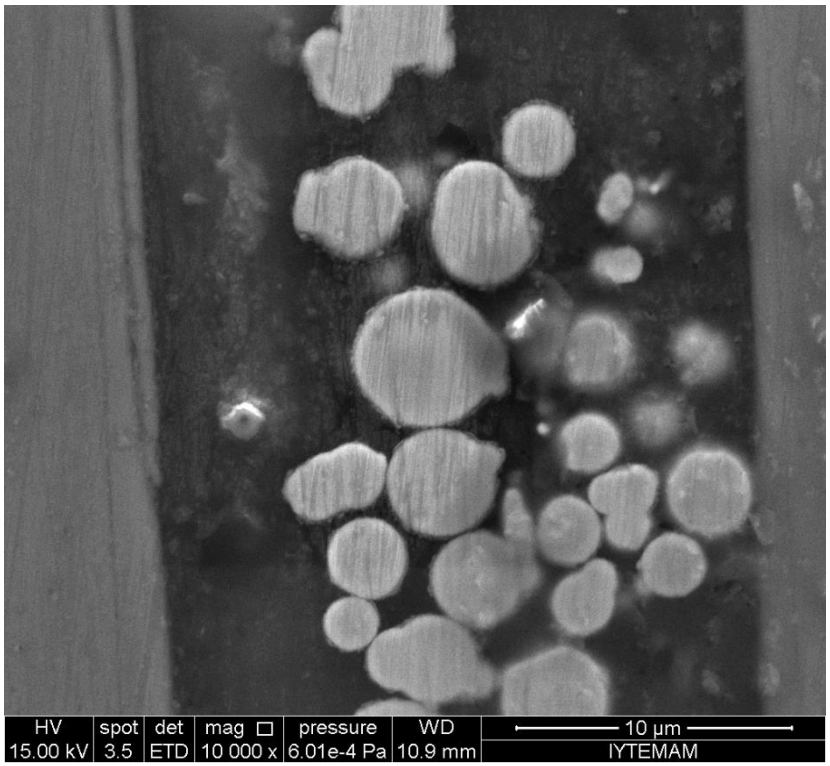

Figure 4.16. SEM image of CI particles in 5th sample (10000X)

Electron dispersive X-Ray (EDX) spectroscopy technique was exerted in order to investigate the chemical composition variations of manufactured structures from the cross sectional area.

Figure 4.17 shows elemental analysis of 0^{o} E-glass fabric from the cross section, which is dominated by silicon (Si), calcium (Ca), aluminium (Al) and oxygen (O) elements. Figure 4.18 also shows EDX spectrum that indicates dominant elements as Si, Ca, Al, O. Table 4.9 summarizes weight and atomic fractions of the conventional E-Glass fabric.

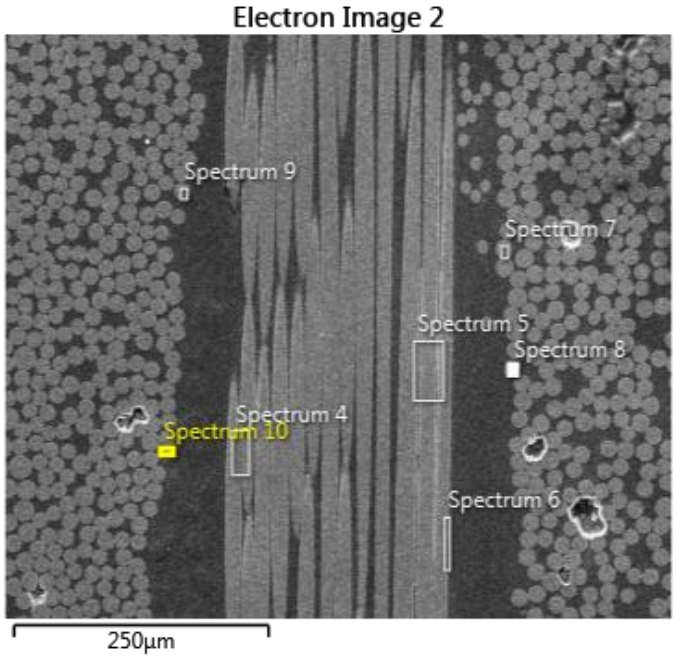

Figure 4.17. EDX analysis from the cross sectional area

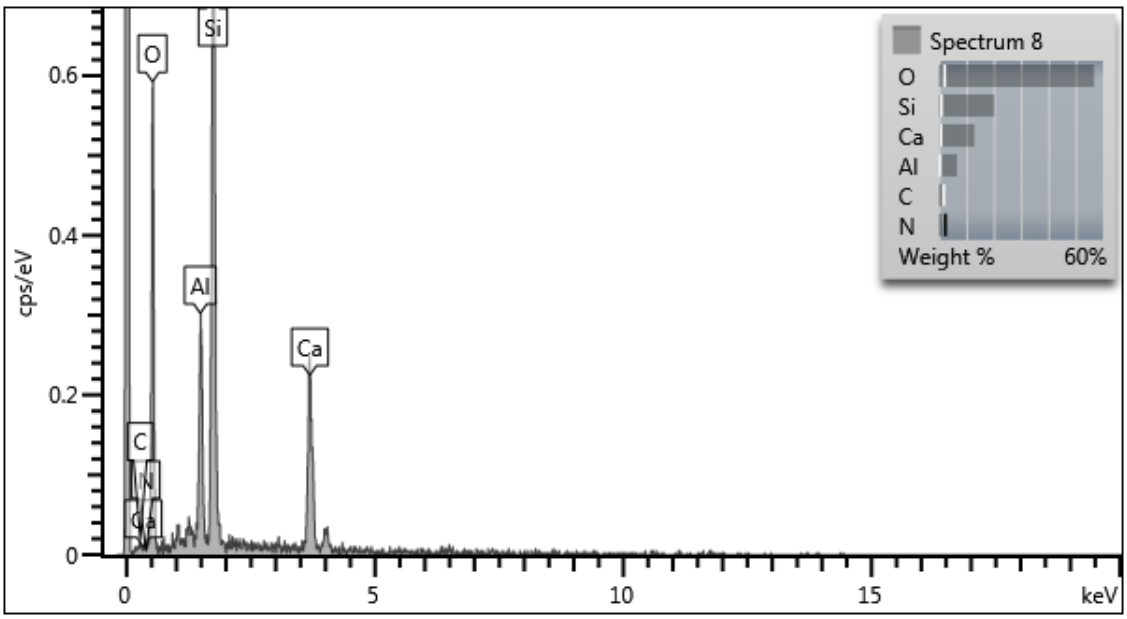

Figure 4.18. Chemical element analysis of 0^{o} E-Glass from cross section

Table 4.9. Weight and atomic percentages of uncoated E-Glass fabric

Element	**Wt%**	**Atomic %**
C	1.98	3.24
N	1.41	1.97
O	56.72	69.48
Al	6.59	4.79
Si	20.30	14.17
Ca	13.00	6.36
Total:	100.00	100.00

Figure 4.19 shows EDX result of ITO coated E-glass fabrics. Indium (In) as a component of ITO coating observed at the surface of the fabric. Figure 4.20 shows EDX spectrum of the ITO coated fabric surface. In addition to indium, a some amount of tin (Sn) is also visible. Table 4.10 summarizes weight and atomic percentages of ITO coated E-glass fabric.

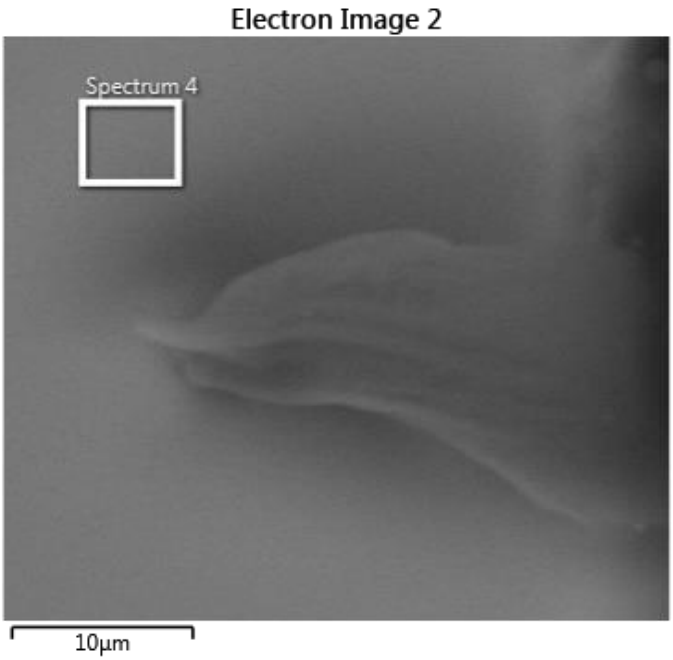

Figure 4.19. EDX analysis of surface of ITO coated E-glass

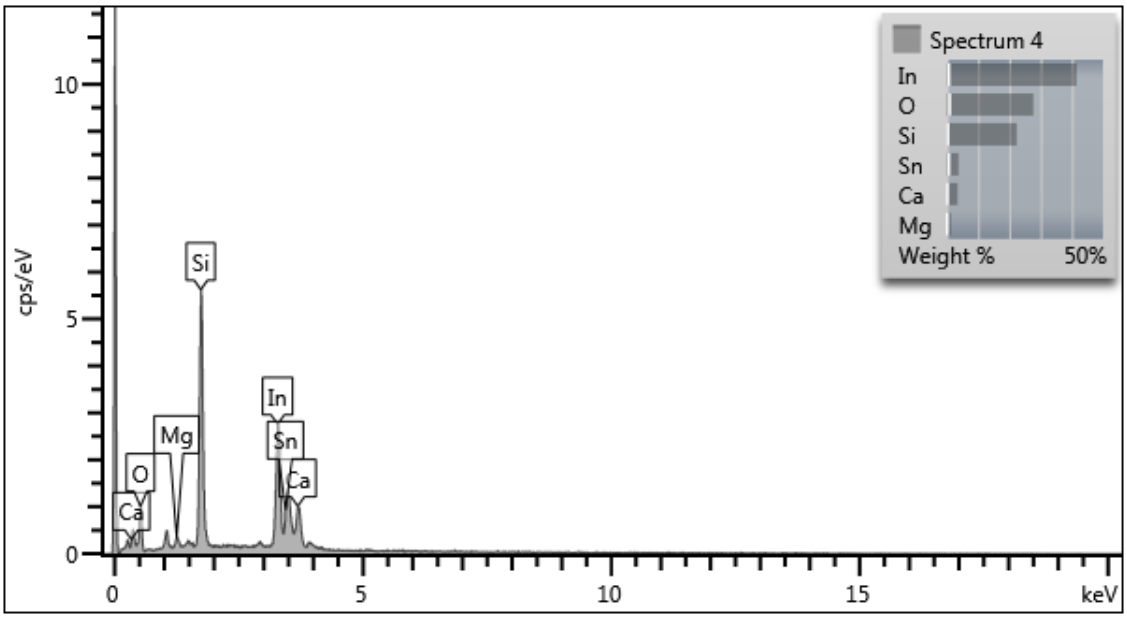

Figure 4.20. Chemical element analysis of ITO coated E-glass fabric

Table 4.10. Weight and atomic percentages of elements within ITO coated fabric

Element	Wt%	Atomic %
O	27.66	56.57
Mg	1.26	1.70
Si	22.39	26.07
Ca	3.42	2.79
In	41.54	11.84
Sn	3.72	1.03
Total:	100.00	100.00

Additionally, from the cross section, carbonyl iron micro particles were observed by using scanning electron microscopy. EDX analysis was done. In Figure 4.21 SEM image can be seen and in Figure 4.22 chemical element analysis of CI was shown. In Table 4.11, atomic percentages were given.

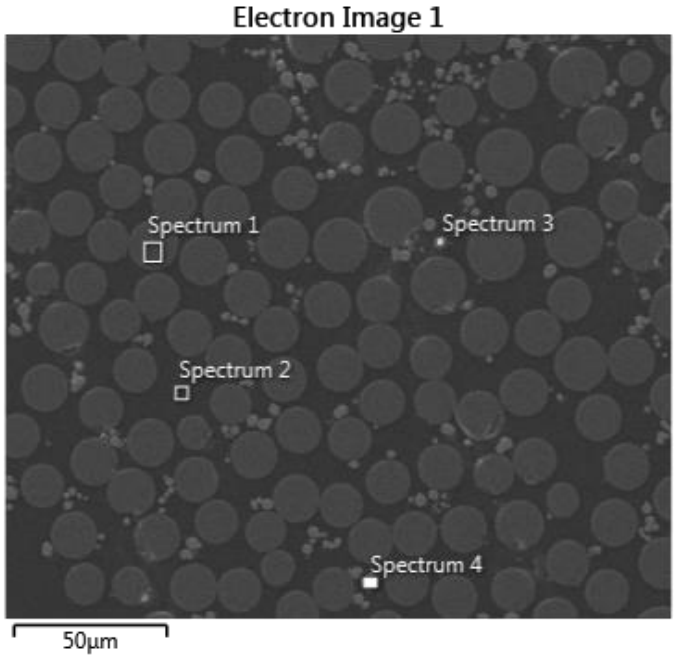

Figure 4.21. EDX analysis of surface of CI micro particle within the structure

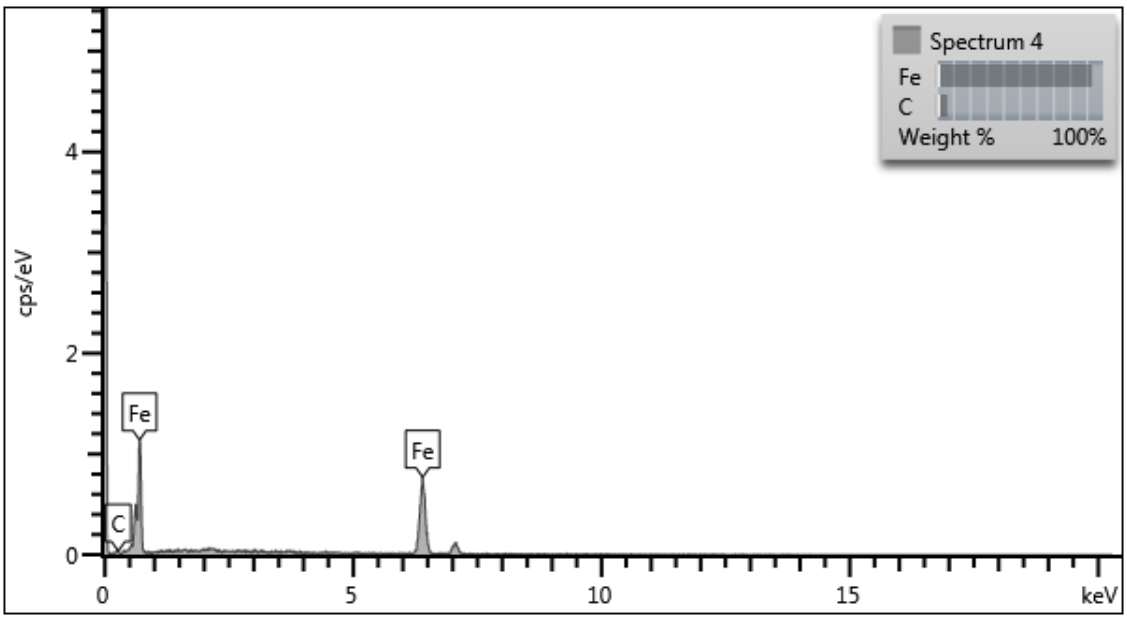

Figure 4.22.Chemical element analysis of CI micro particle within the structure

Table 4.11. Weight and atomic percentages of CI within the structure

Element	**Wt%**	**Atomic %**
C	6.64	24.85
Fe	93.36	75.15
Total:	100.00	100.00

Number 3 structure, which contain carbonyl iron additive, ITO coated resisitive sheet, E-glass fiber and epoxy resin, were prepared to apply it elemental mapping technique from the cross section. Figure 4.23 shows EDX mapping of the cross section sample. It can be seen from the image that, brightest particles are identified as carbonyl iron micro particles. Similar to to previous EDX, Si, Ca and Al elements that are dominant in fibers are visible. In addition to those, carbon as it is the primary element in epoxy chains, is visible within the EDX maps. Hovewer, there is no exact indium or thin elements in the elemental mapping. Because coated films on fabrics are so thin, and from the cross section, we can not see ITO elements of coatings.

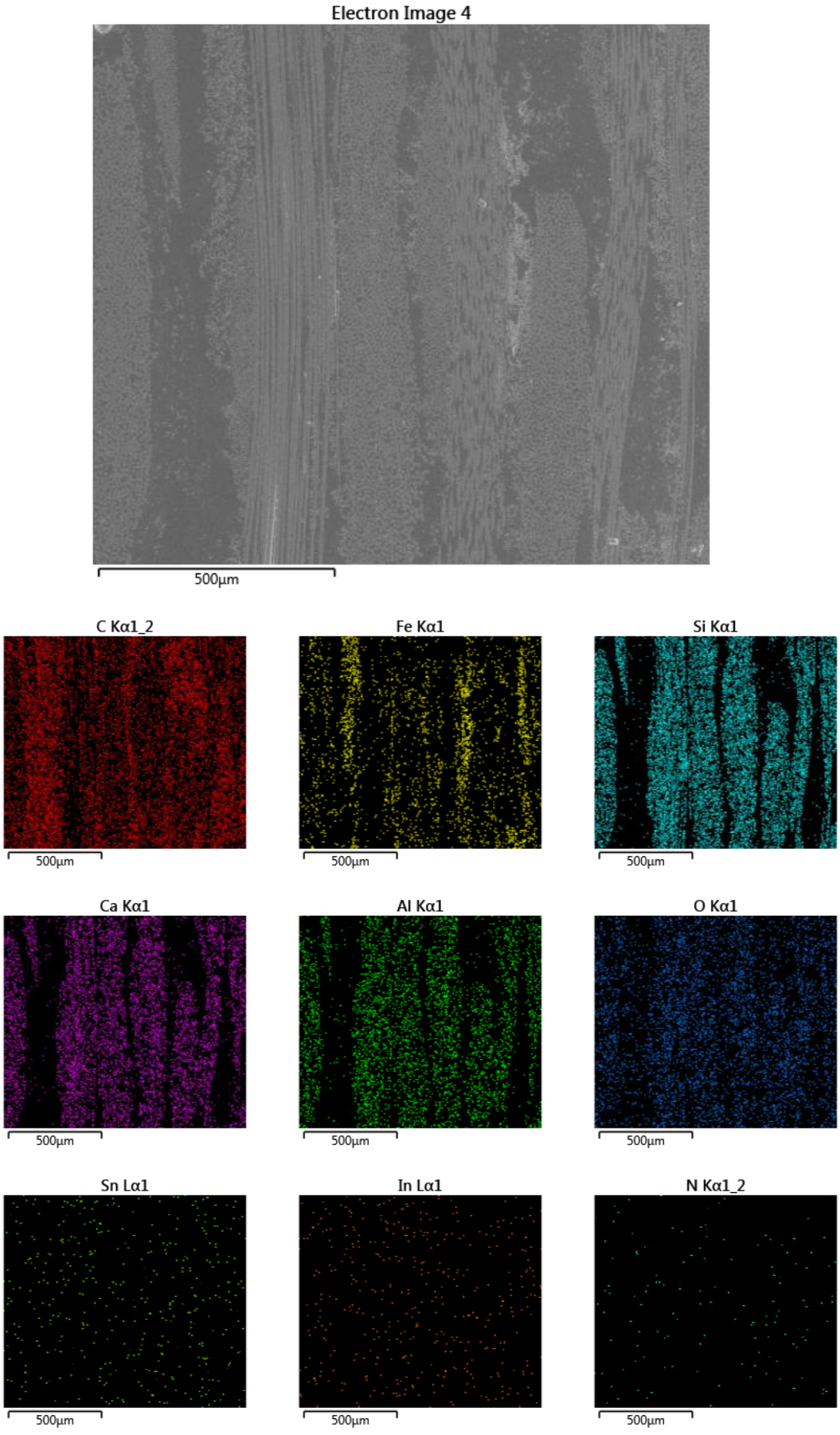

Figure 4.23. EDX mapping of number 3 structure from cross section

In order to investigate the tensile fracture surfaces of manufactured composites, scanning electron micrographs of tensile tests,were taken from the fructure surfaces. In Figure 4.23, specimen containing 0^o and 90^o oriented fibers, carbonyl iron and a layer of ITO coated fibers, are shown.

Figures 4.24 to 4.26 shows scanning electon micrographs of 1st sample with different magnifications, which had not any additive.

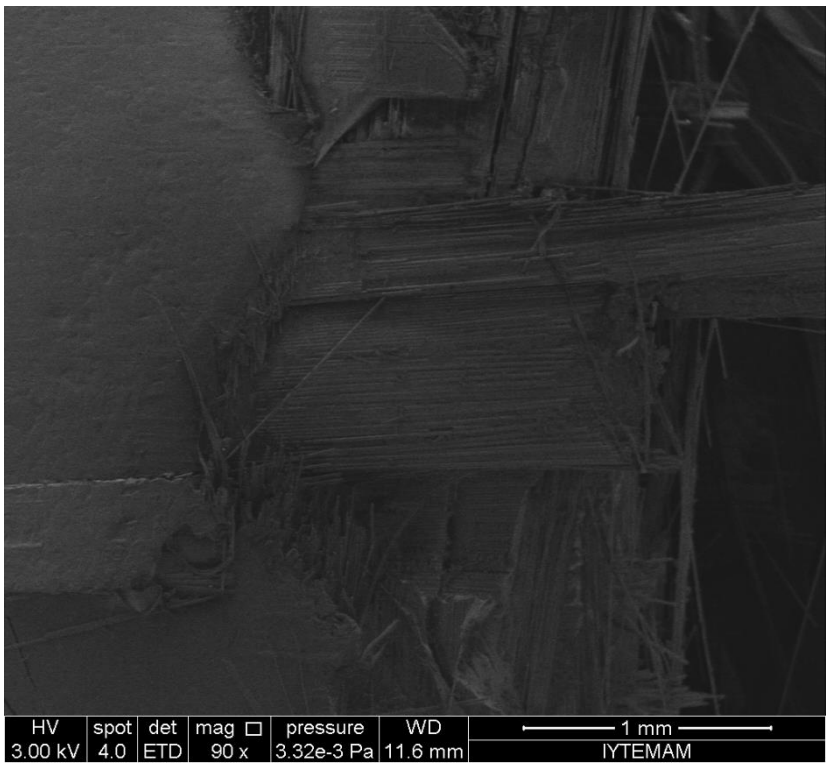

Figure 4.24. SEM image of 1st sample tensile test fracture (90X)

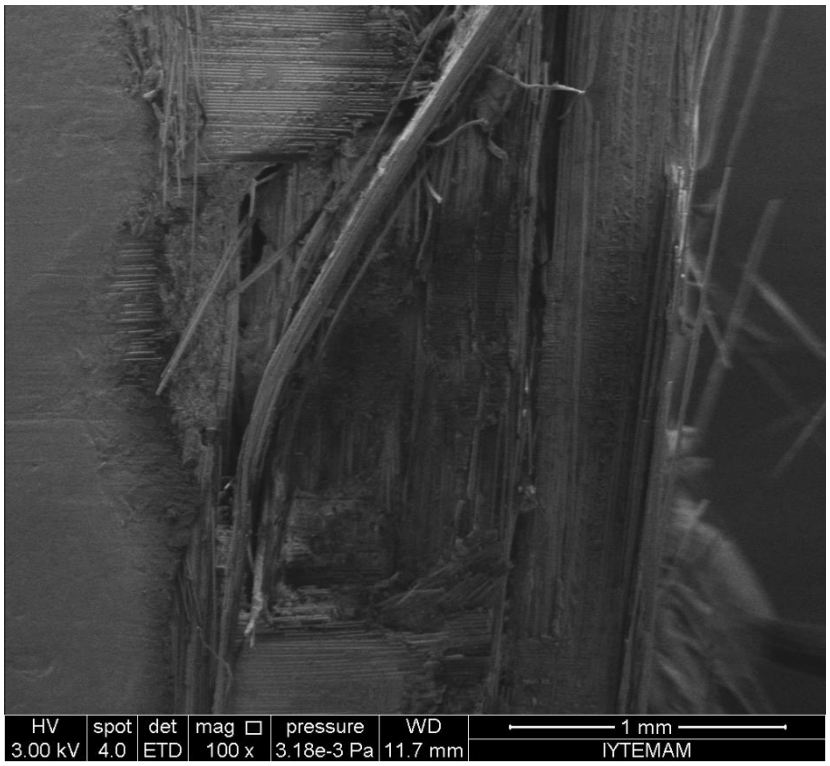

Figure 4.25. SEM image of 1st sample tensile test fracture (100X)

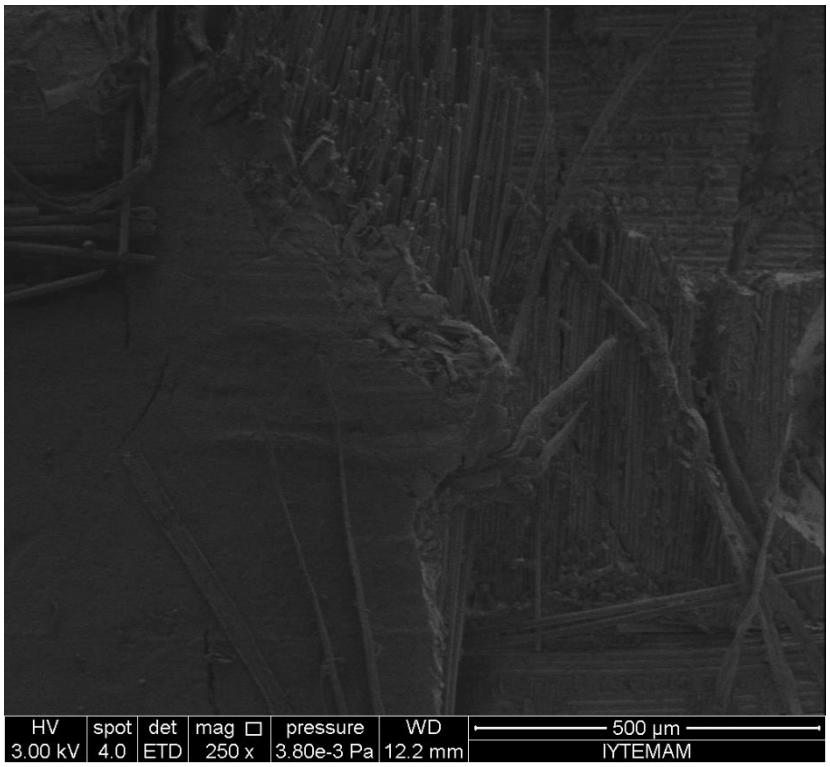

Figure 4.26. SEM image of 1st sample tensile test fracture (250X)

Moreover, tensile fracture SEM images were performed to the 2nd sample. Figures 4.27 to 4.29 show tensile fractures of 2nd manufactured sample. In this sample it had four Salisbury Screen resistive sheets and no CI additive.

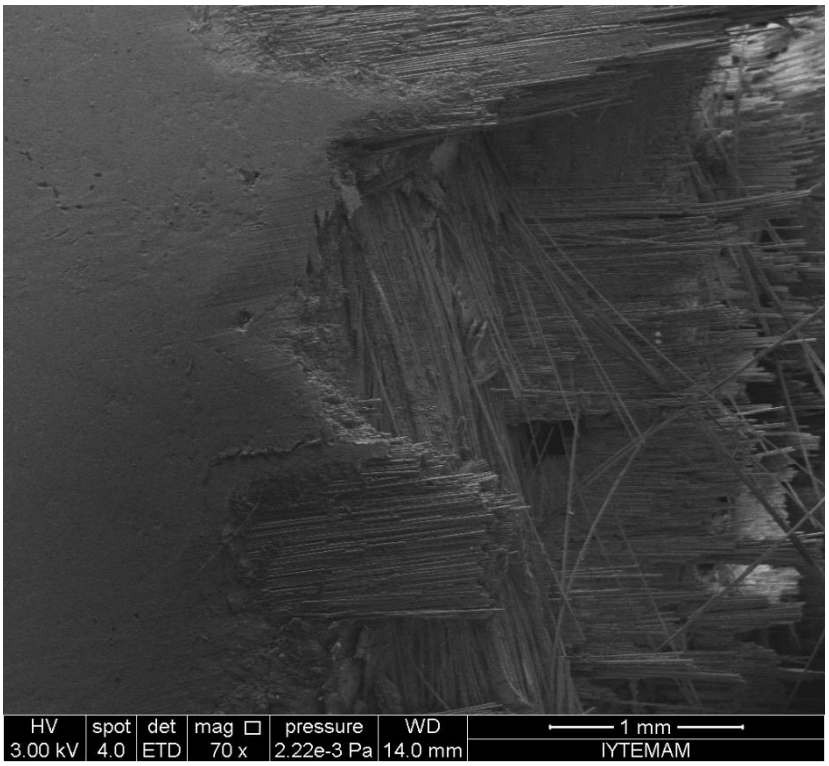

Figure 4.27. SEM image of 2nd sample tensile test fracture (70X)

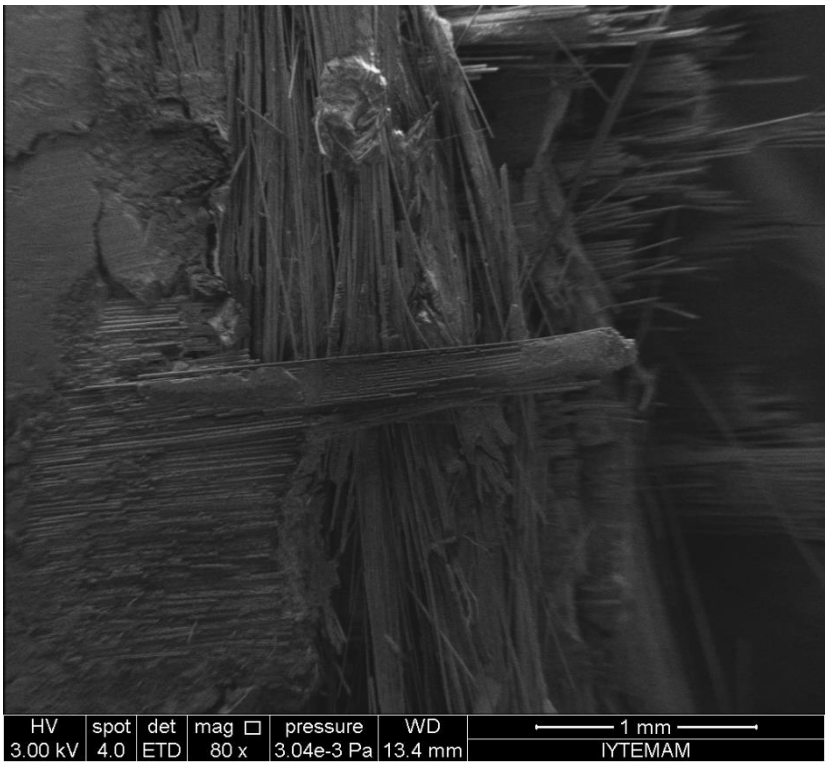

Figure 4.28. SEM image of 2nd sample tensile test fracture (80X)

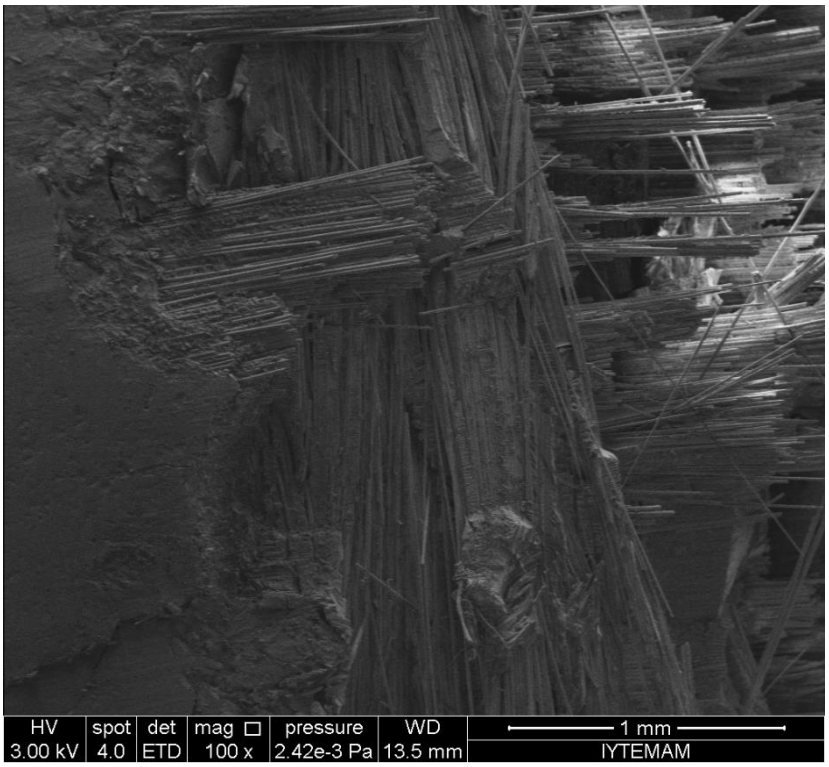

Figure 4.29. SEM image of 2nd sample tensile test fracture (100X)

Lastly, for the carbonly iron additive structure, tensile fraction scanning electron microscopy images were taken. It was not observed any unexpected situation when carbonly iron additive structure compared with 1st structure which was conventional E-glass polymeric composite structure.

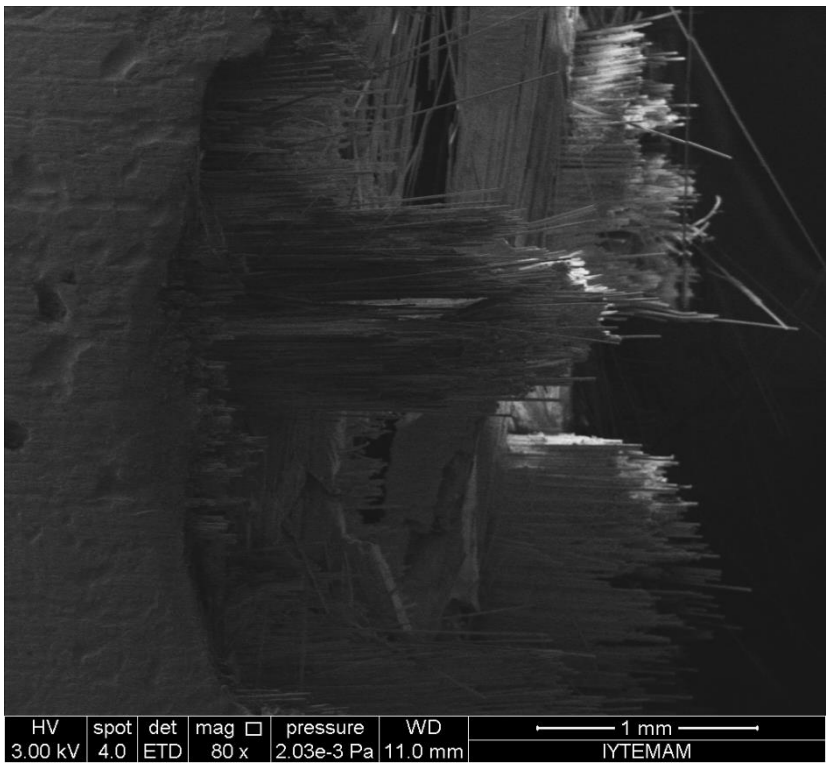

Figure 4.30. SEM image of 3rd sample tensile test fracture (80X)

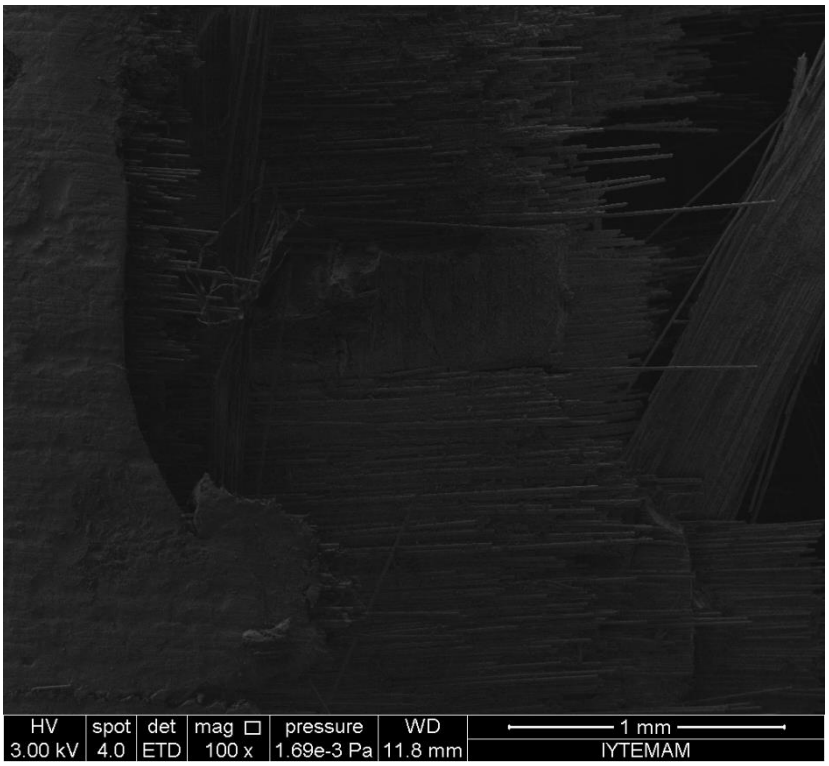

Figure 4.31. SEM image of 3rd sample tensile test fracture (100X)

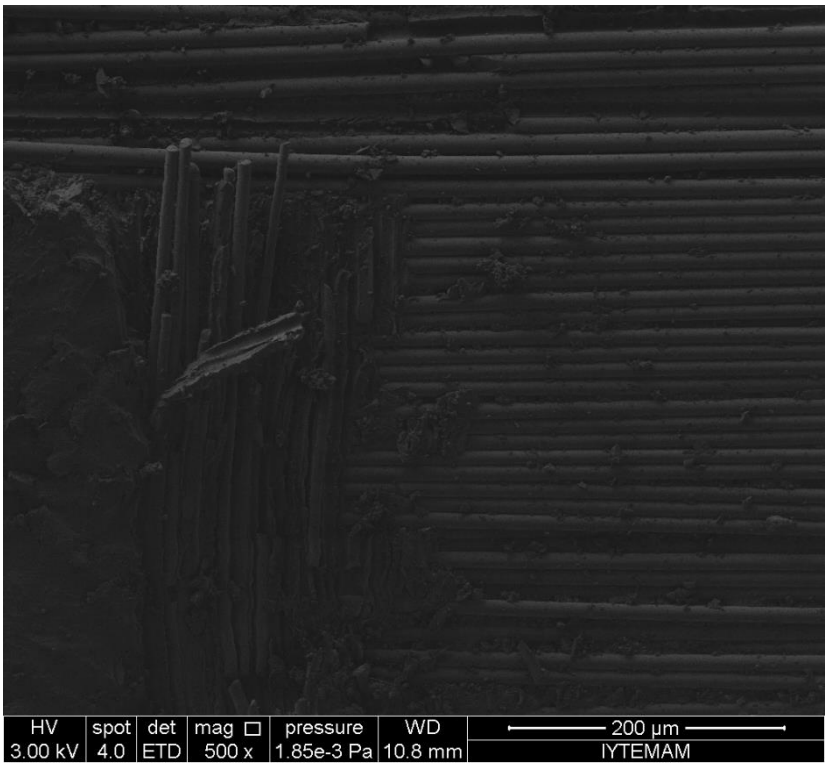

Figure 4.32. SEM image of 3rd sample tensile test fracture (500X)

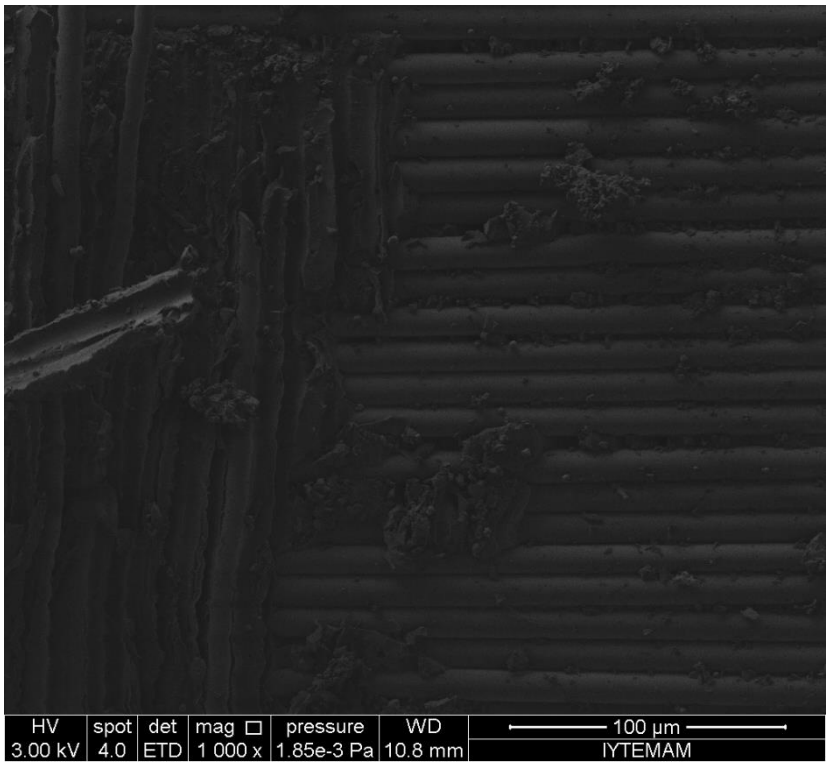

Figure 4.33. SEM image of 3rd sample tensile test fracture (1000X)

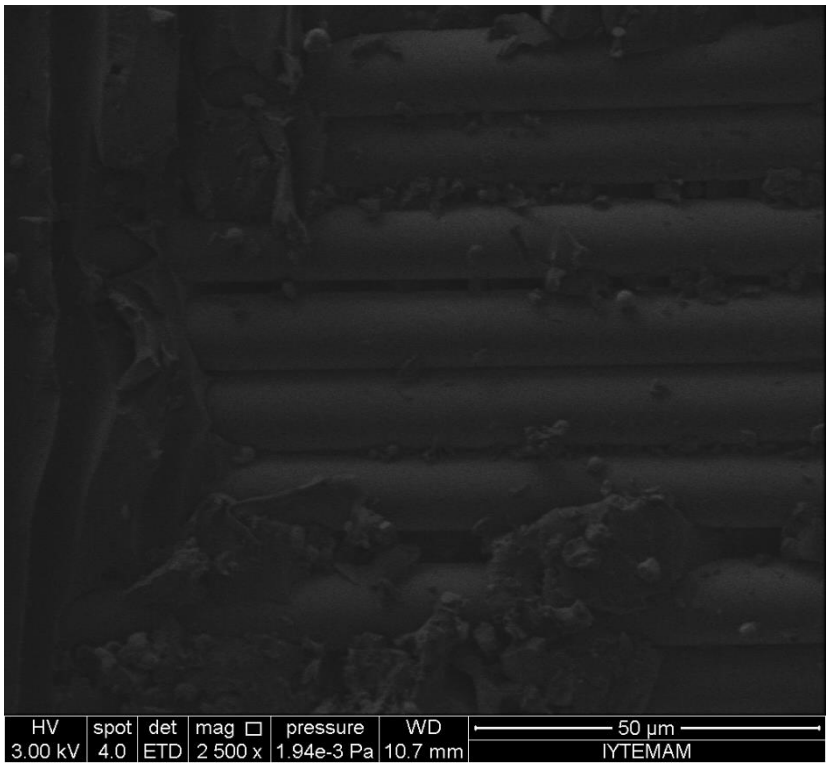

Figure 4.34. SEM image of 3rd sample tensile test fracture (2500X)

4.3.3. Optical Microscopy

In order to determine thicknesses between resistive sheets or between resistive sheet and surface, optical microcopy images were used. The purpose of using optical microscopy is the importance of the thickness parameters to design and manufacture radar absorbing structure with broadband attenuation. As mentioned before, for simulation results, the parameters taken from the optical microscopy were used. Because these values are more accurate if we compare them with calculated ones. In LabVIEW programming, these parameters were taken into account by using related transmission line theory formalization.

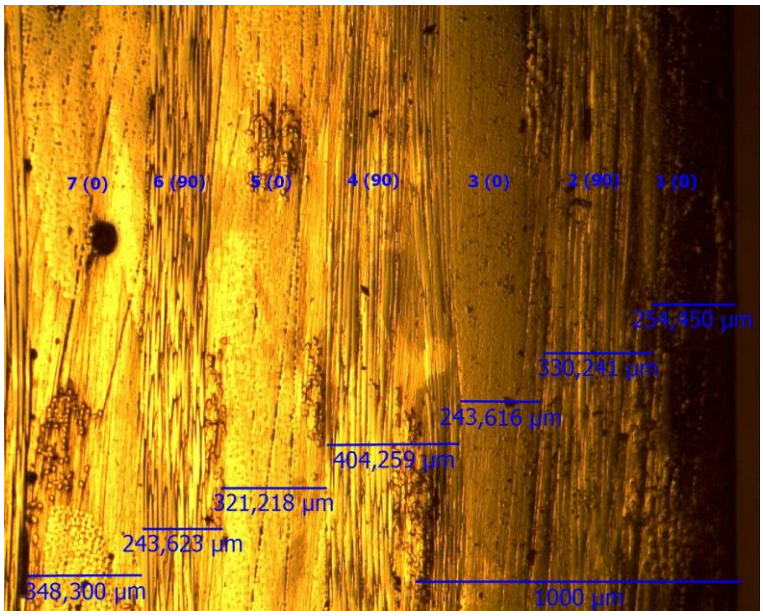

Figure 4.35. Optical image of seven layers in 1st structure

In Figure 4.35, thicknesses between sheets can be seen easily. For instance, by using this image, the important thickness parameters of reflection loss formalization can be used. In other words, these values can be used in LabVIEW programming system to see the confirmation between simulation and experimentally measured electromagnetic wave loss.

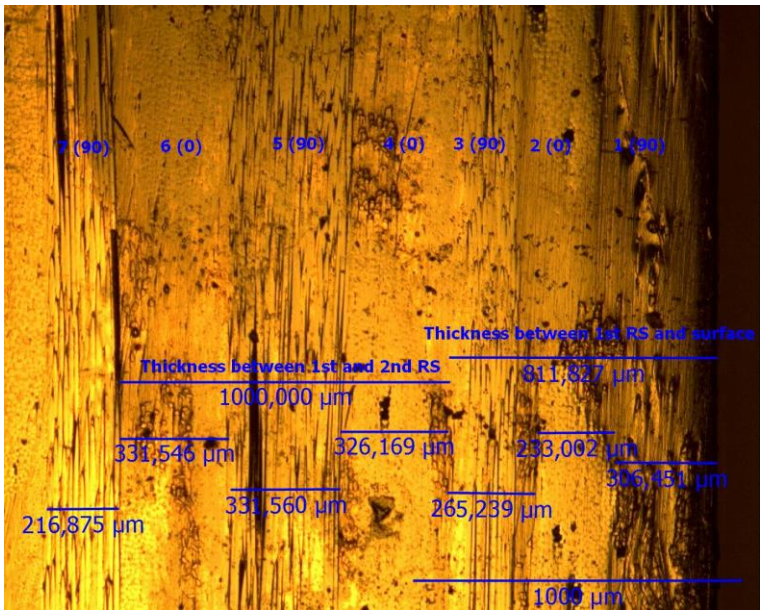

Figure 4.36. Optical image of 2nd structure for determination of thicknesses

Figure 4.36 gives exact information about the thicknesses between first resistive sheet and surface. Also, the thickness between surface and first resistive sheet can be seen easily.

For all absorbing structures, 16 E-glass fabrics were used and for second structure, 4 of them were conducting layers. On the time of manufacturing process of sample 2, 4th, 7th, 10th, and 13th structures were conducting layer. So, in Figure 4.36, first half of the structure cross section can be seen. Then, 3rd and 7th layers are resistive sheets.

In Figure 4.37 second half of the cross section image of sample 2 can be seen. Also, the thicknesses were easily determined.

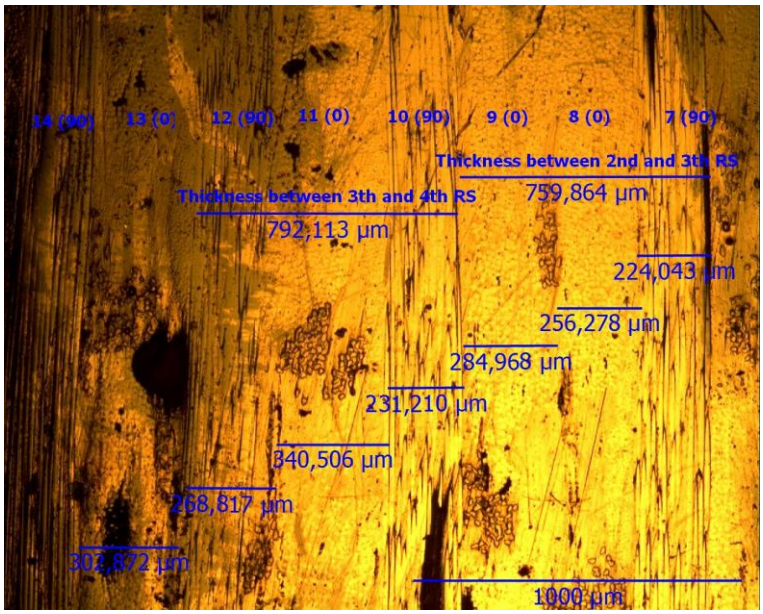

Figure 4.37. Optical image of 2nd structure (7.-14. layers)

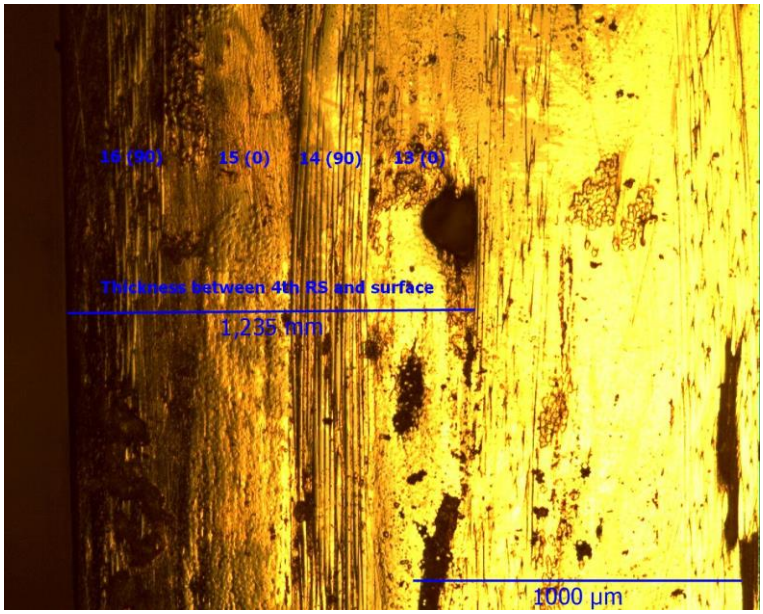

Figure 4.38. Optical image of 2nd structure (13.-16. layers)

4.4. Mechanical Characterization

Mechanical properties of the manufactured samples were examined by performing mechanical tests such as tensile, bending, compression and charpy impact. At least four specimens were prepared for testing for each test. Results, including strength, modulus,

strain at break values were reported based on tensile, bending and compression tests. Strain vs. stress graphs were plotted.

4.4.1. Tensile Properties

Through the Tables 4.11 to 4.15, tensile test results are summarized also in Figures 4.39 to 4.43, stress-strain graphs of all specimens are shown. One figure contains one structure data with four sample at least. All specimens show linear stress-strain curves nearly until break. None of them show plastic behaviour until failure.

If we take reference our first manufactured composite structure, which is conventional epoxy glass composite structure, it is observed that there is strength loss between 4% and 34% in all samples containing carbonyl iron micro particle. Also beside the strength, similar tendency is seen for modulus values. Modulus loss is between 2% and 19% in all specimens. Actually, there is no significant differences between modified structures. For instance, in samples 3 and 4, same percentage of CI additive was used in epoxy, so their strength and modulus values are nearly same. It can be said that these strength loss and modulus reduction comes from the CI filler so it is directly affects tensile properties of the composite structures. There is a bit increase in strength and modulus values in sample 2 which has ITO coated fabrics but no filler ingredient.

Table 4.12. Tensile properties of Sample 1

# of specimens	Tensile Strength (MPa)	Tensile Modulus (GPa)	Strain at Break (%)
1	332.92	19.23	2.14
2	317.80	18.38	1.97
3	319.07	18.56	2.09
4	327.46	19.27	1.9
Average	**324.31**	**18.86**	**2.03**
Std. Dev.	**7.16**	**0.46**	**0.11**

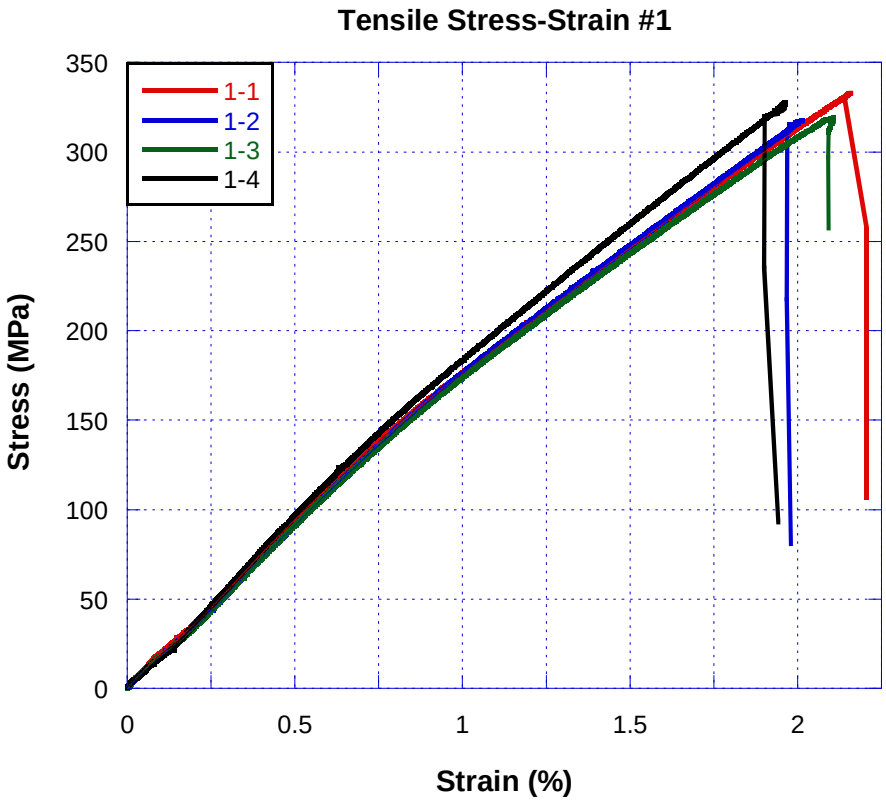

Figure 4.39. Tensile stress vs. strain graphs of Sample 1

Table 4.13. Tensile properties of Sample 2

# of specimens	Tensile Strength (MPa)	Tensile Modulus (GPa)	Strain at Break (%)
1	354.69	22.17	2.00
2	350.51	19.83	2.03
3	355.87	20.35	2.11
4	354.70	21.04	2.01
Average	**353.94**	**20.85**	**2.04**
Std. Dev.	**2.35**	**1.01**	**0.05**

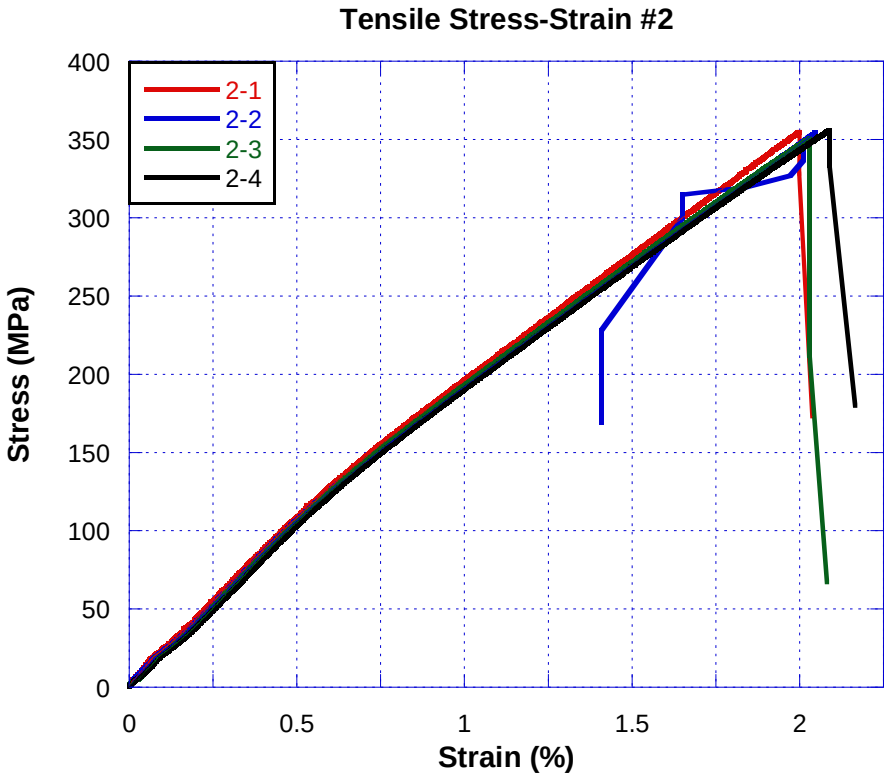

Figure 4.40. Tensile stress vs. strain graphs of Sample 2

Table 4.14. Tensile properties of Sample 3

# of specimens	Tensile Strength (MPa)	Tensile Modulus (GPa)	Strain at Break (%)
1	212.02	19.79	1.40
2	200.08	15.32	1.59
3	215.68	15.93	1.69
4	215.87	15.71	1.69
5	221.61	14.95	1.78
Average	**213.05**	**16.34**	**1.63**
Std. Dev.	**8.02**	**1.9**	**0.15**

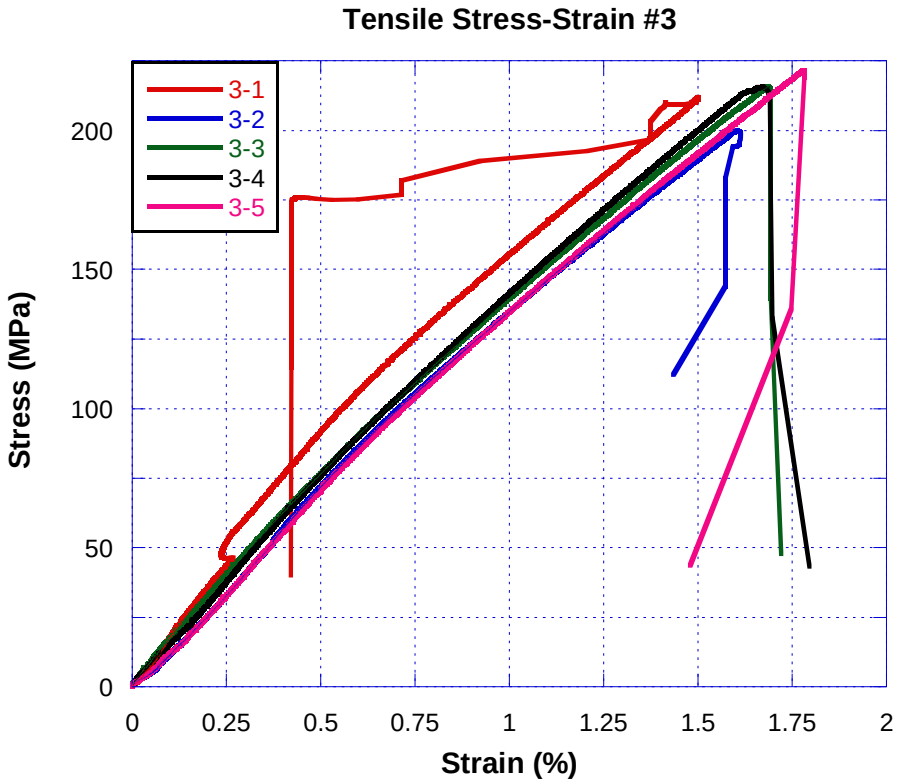

Figure 4.41. Tensile stress vs. strain graphs of Sample 3

Table 4.15. Tensile properties of Sample 4

# of specimens	Tensile Strength (MPa)	Tensile Modulus (GPa)	Strain at Break (%)
1	216.16	15.27	1.69
2	221.77	15.85	1.74
3	221.25	15.47	1.89
4	224.36	14.51	1.85
Average	**220.89**	**15.28**	**1.79**
Std. Dev.	**3.43**	**0.56**	**0.09**

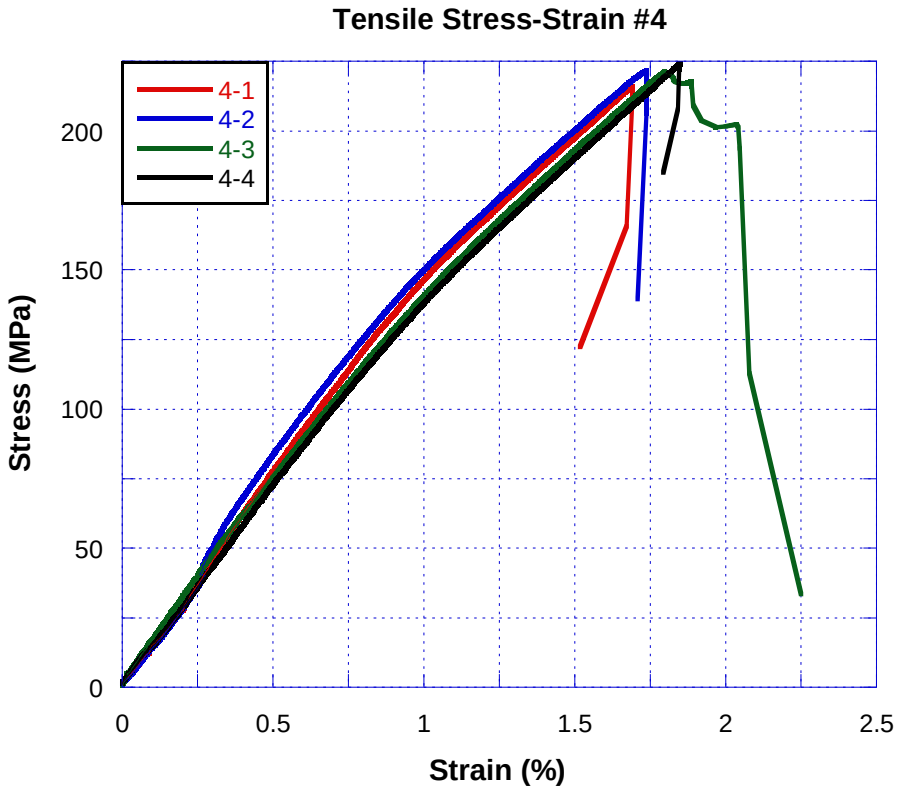

Figure 4.42. Tensile stress vs. strain graphs of Sample 4

Table 4.16. Tensile properties of Sample 5

# of specimens	Tensile Strength (MPa)	Tensile Modulus (GPa)	Strain at Break (%)
1	308.28	18.62	1.87
2	310.02	18.67	1.90
3	314.49	19.05	1.83
4	315.48	19.84	1.92
5	311.46	19.66	1.85
Average	**311.95**	**19.17**	**1.87**
Std. Dev.	**3.01**	**0.56**	**0.04**

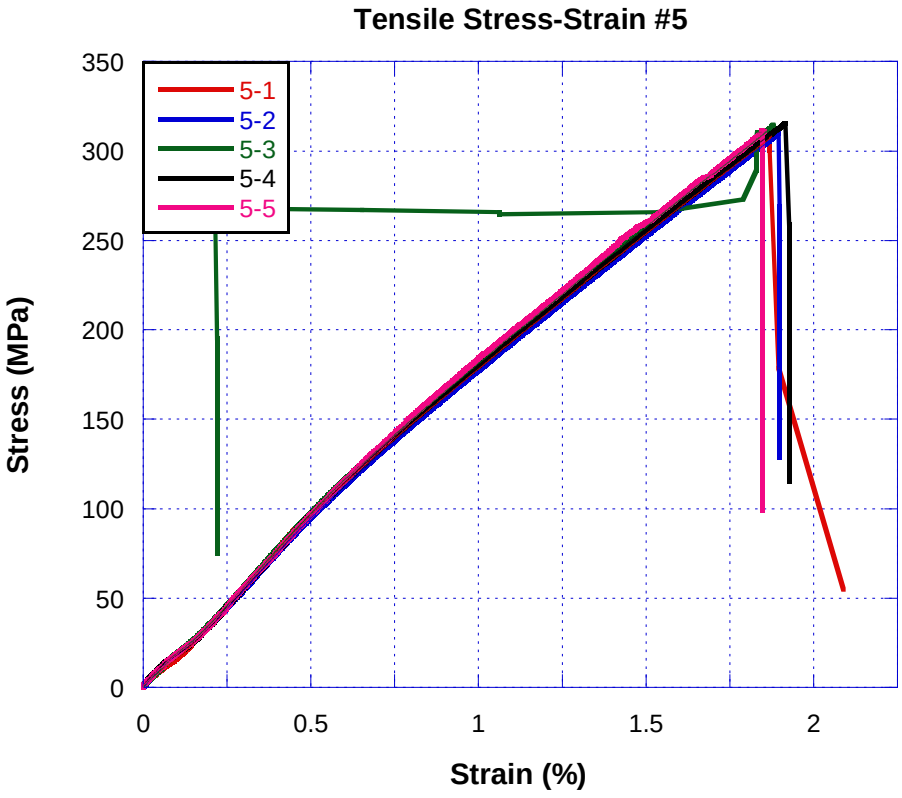

Figure 4.43. Tensile stress vs. strain graphs of Sample 5

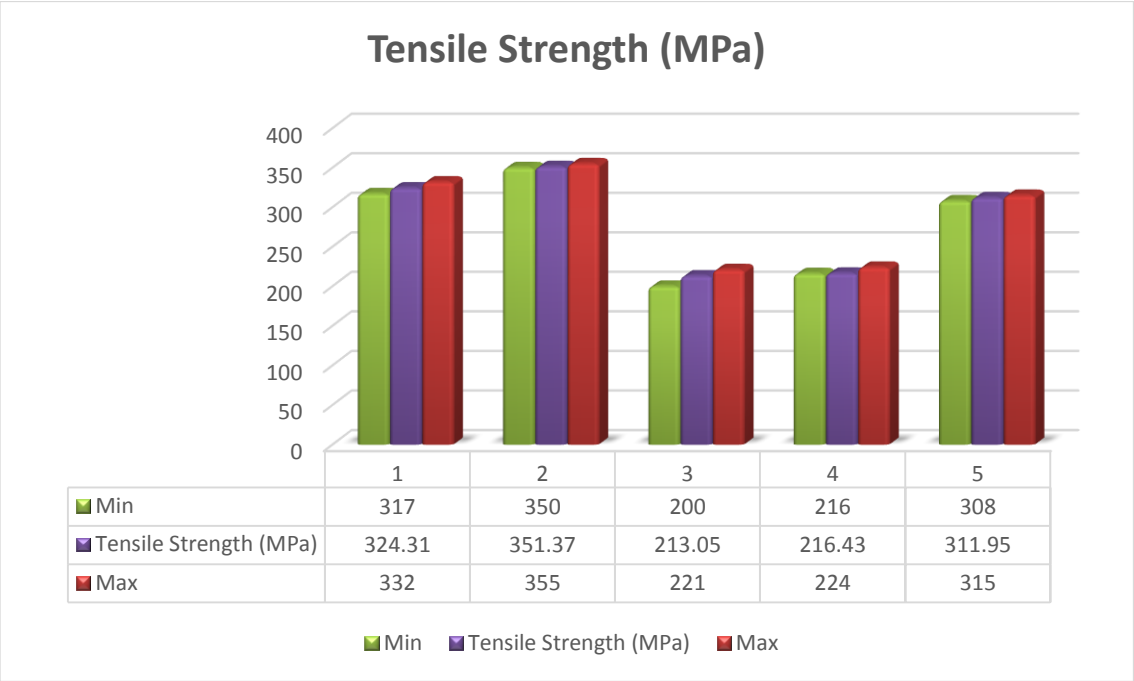

Figure 4.44. Tensile strength for all structures

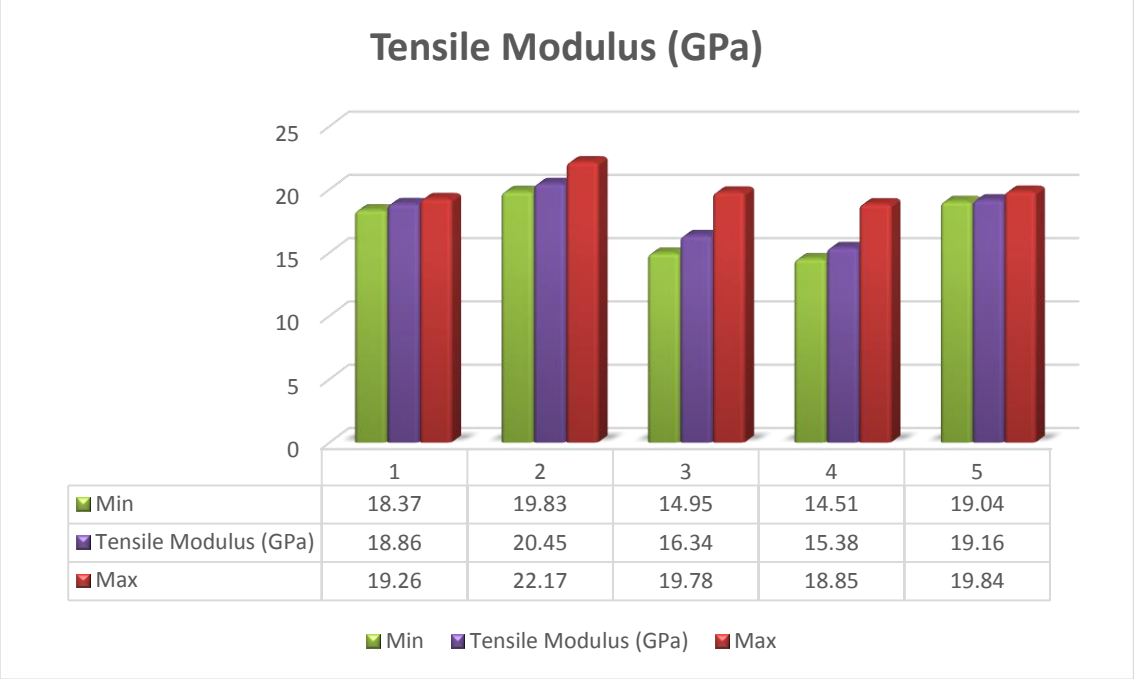

Figure 4.45. Tensile modulus for all structures

In Figures 4.44 and 4.45, tensile strength and tensile modulus of all structures are given. These values are average of at least 4 samples for all structures. It can be clearly

seen that carbonyl iron additive structures have trend of decreasing in tensile properties. But in sample 2 which contains four resistive sheets and no carbonyl filler has different behaviour. Mechanical properties are better than other structures. It can be from the effect of ITO thin film coating.

4.4.2. Flexural Properties

Tables from 4.17 to 4.21 show the results of performed flexural tests. Also, related graphs with these values are shown in Figure 4.46 to 4.50. Until the break, linear stress-strain curves are shown in all specimens. Moreover, it cannot be seen any plastic behaviour in any structure till failure.

It is observed that there is significant bending strength reduction and flexural modulus loss in carbonyl iron additive structures. If we take the first structure reference which is conventional epoxy glass polymeric composite structure, there is a 2-27 % strength reduction. Also modulus reduction is between 8 % and 36 %. If CI filler is increased, the effect of volume fraction of the samples are increased. For that reason, because of the carbonyl iron filler, flexural properties of structures are effected in a bad way. In sample 2 as in tensile property, there is a different effect of ITO thin film. Maybe, because of the modified glass fiber surface, bonding between epoxy and fabric get better. For that reason, flexural properties of structures for four resistive sheet and no CI additive, has better than other composites.

Table 4.17. Flexural properties of Sample 1

# of specimens	Bending Strength (MPa)	Flexural Modulus (GPa)	Flexural Strain at Break (%)
1	476.7	16.64	3.54
2	475.2	15.80	3.63
3	473.03	16.19	3.60
4	475.73	15.97	3.65
5	454.95	15.55	3.44
Average	**471.72**	**16.03**	**3.57**
Std. Dev.	**9.68**	**0.41**	**0.08**

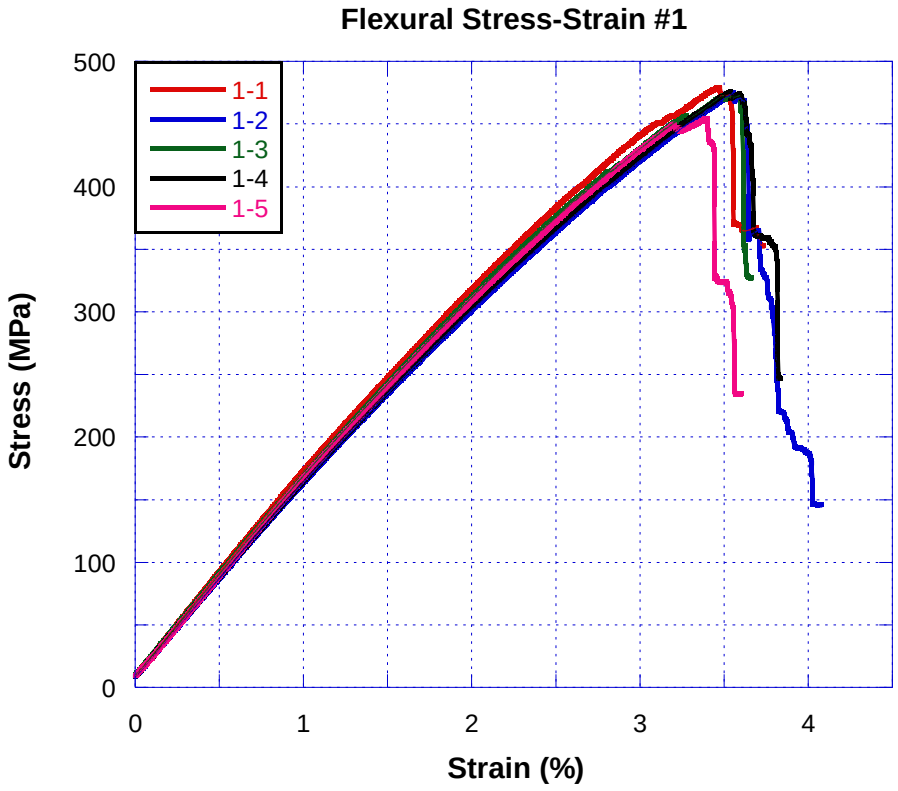

Figure 4.46. Flexural stress vs. strain graphs of Sample 1

Table 4.18. Flexural properties of Sample 2

# of specimens	Bending Strength (MPa)	Flexural Modulus (GPa)	Flexural Strain at Break (%)
1	603.82	21.90	3.13
2	602.81	21.83	3.14
3	579.35	21.53	3.21
4	601.35	21.91	3.33
5	616.12	21.87	3.16
Average	**600.69**	**21.80**	**3.19**
Std. Dev.	**13.3**	**0.15**	**0.08**

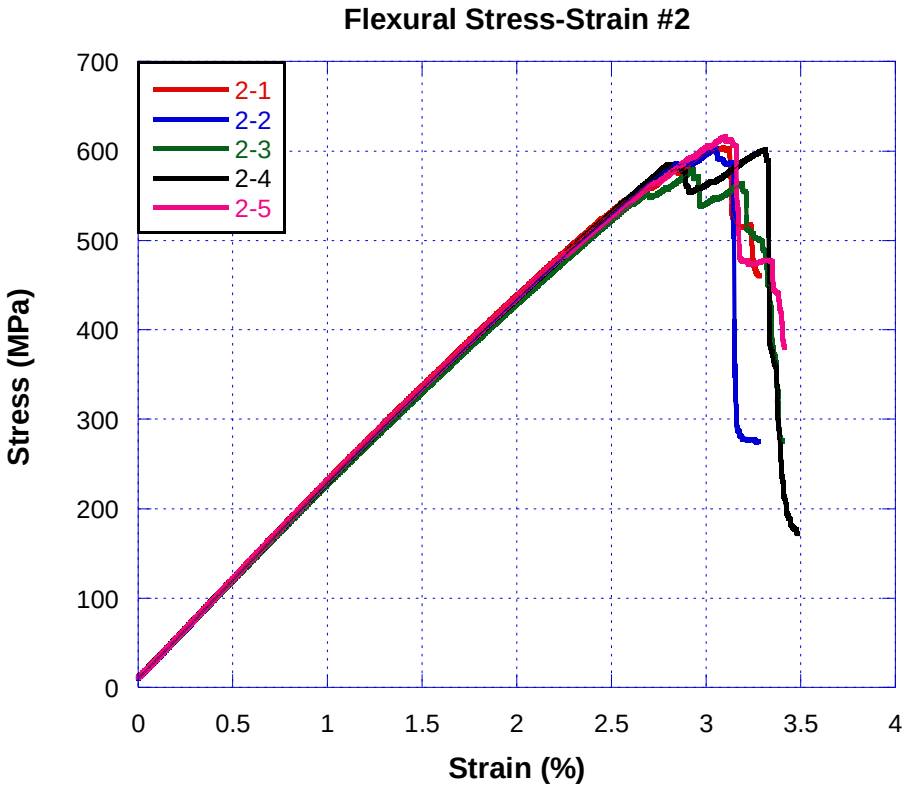

Figure 4.47. Flexural stress vs. strain graphs of Sample 2

Table 4.19. Flexural properties of Sample 3

# of specimens	Bending Strength (MPa)	Flexural Modulus (GPa)	Flexural Strain at Break (%)
1	364.61	13.60	3.06
2	359.82	13.71	3.05
3	364.70	14.22	3.02
4	352.01	13.96	2.89
5	333.57	13.99	2.83
Average	**354.94**	**13.89**	**2.97**
Std. Dev.	**13.01**	**0.24**	**0.1**

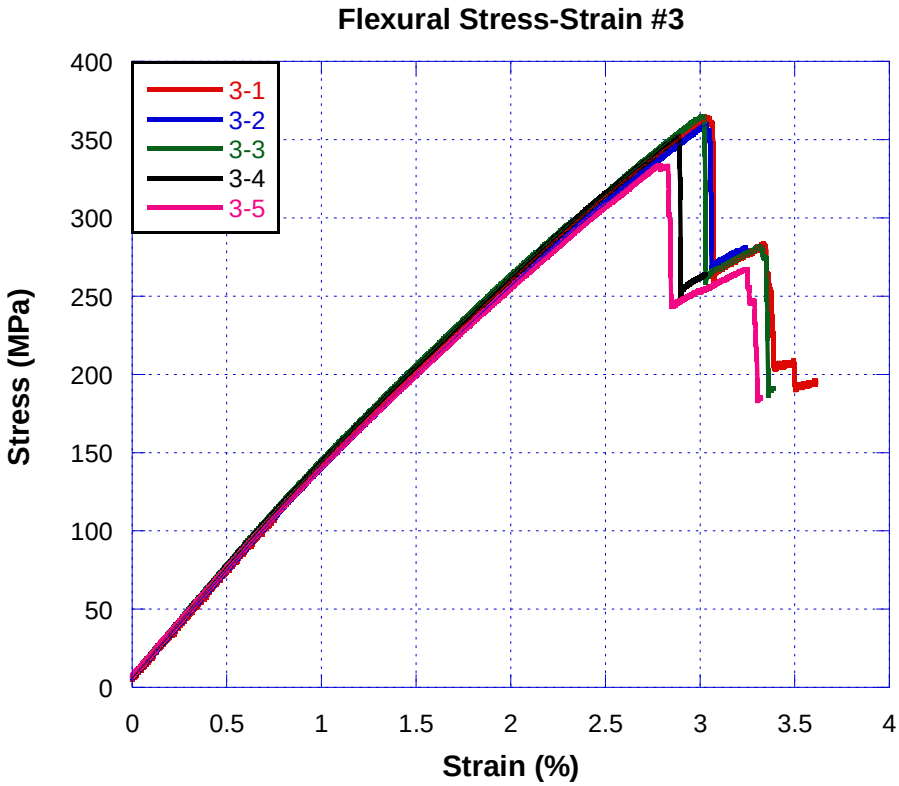

Figure 4.48. Flexural stress vs. strain graphs of Sample 3

Table 4.20. Flexural properties of Sample 4

# of specimens	Bending Strength (MPa)	Flexural Modulus (GPa)	Flexural Strain at Break (%)
1	472.93	17.75	2.80
2	476.02	17.99	2.81
3	465.06	18.05	2.76
4	454.30	17.58	2.76
5	451.53	17.17	2.79
Average	**463.96**	**17.70**	**2.78**
Std. Dev.	**10.89**	**0.35**	**0.02**

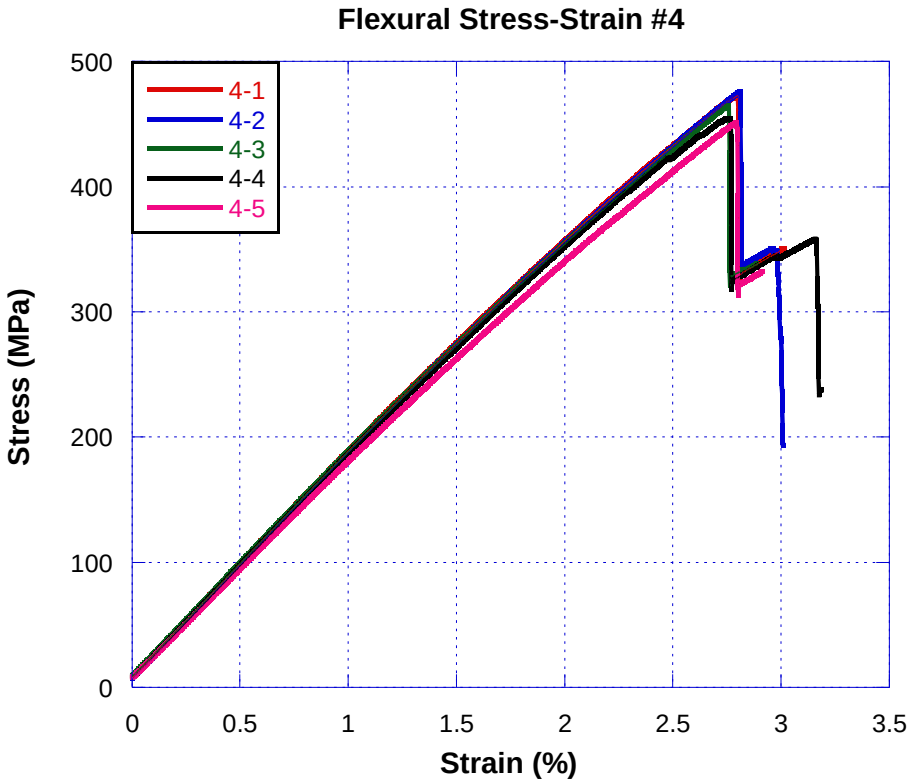

Figure 4.49. Flexural stress vs. strain graphs of Sample 4

Table 4.21. Flexural properties of Sample 5

# of specimens	Bending Strength (MPa)	Flexural Modulus (GPa)	Flexural Strain at Break (%)
1	431.84	17.21	2.87
2	436.45	17.80	2.83
3	422.54	17.38	2.73
4	446.80	17.22	2.98
5	420.14	17.18	2.84
Average	**431.55**	**17.35**	**2.85**
Std. Dev.	**10.81**	**0.25**	**0.08**

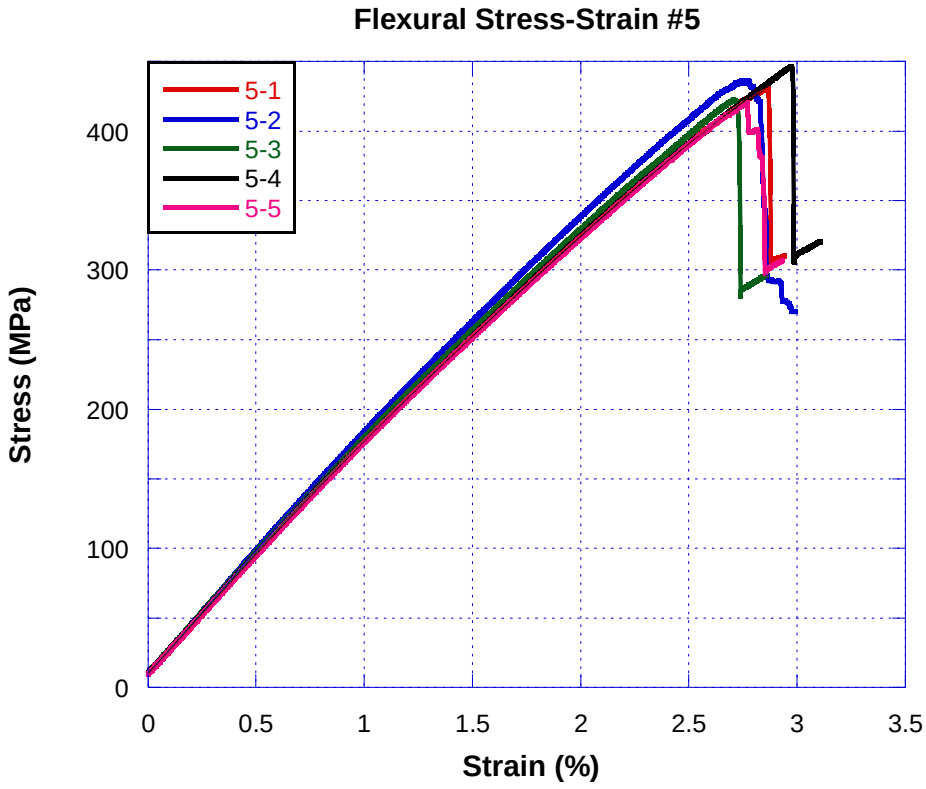

Figure 4.50 Flexural stress vs. strain graphs of Sample 5

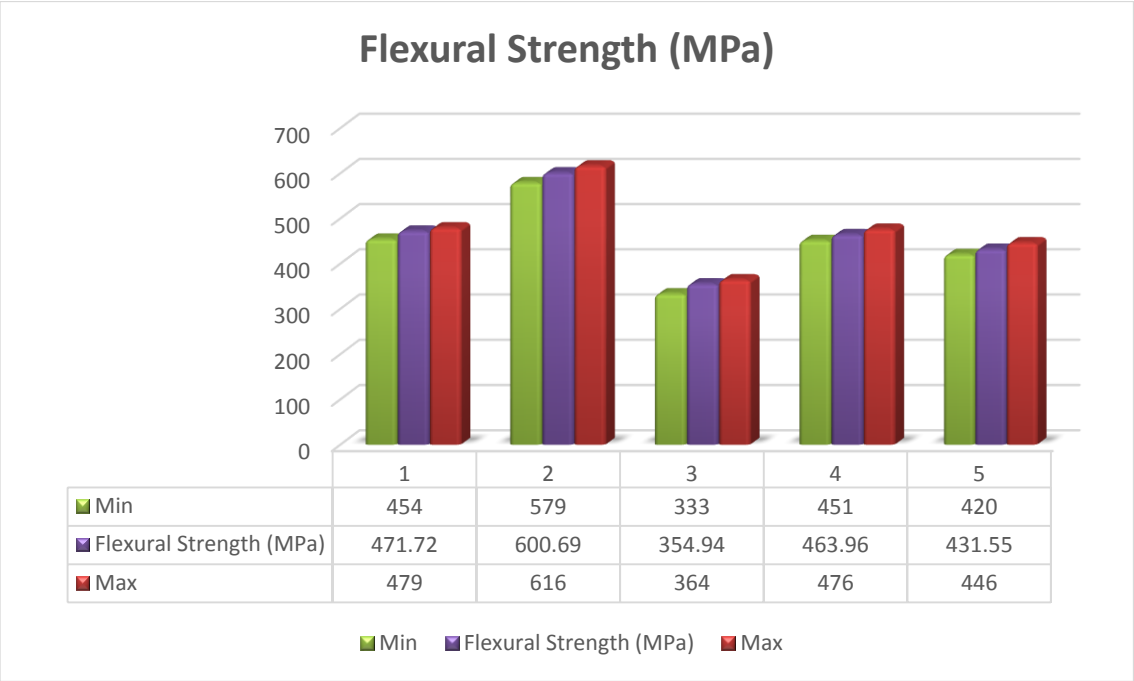

Figure 4.51. Flexural strength for all structures

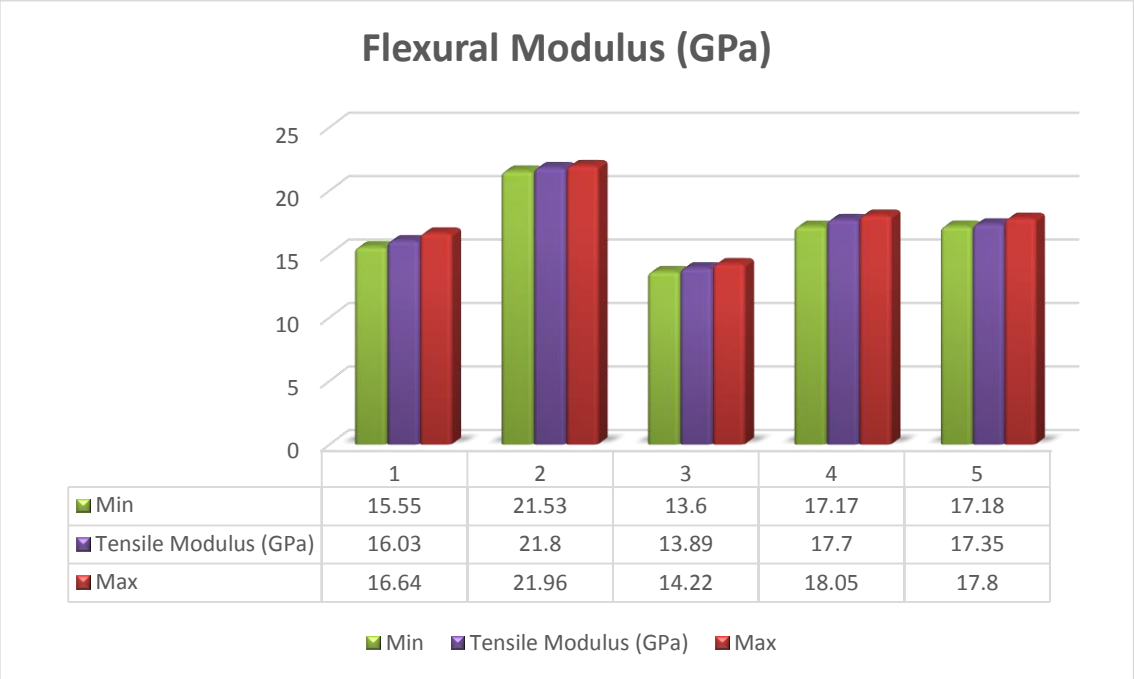

Figure 4.52. Flexural modulus for all structures

4.4.3. Compressive Properties

Tables from 4.22 to 4.26 show the results of performed compression tests. Also, related graphs with these values are shown in Figure 4.53 to 4.57. As it can be seen from the graphs there are band gaps between same samples specimens. This fluctuations are because of the nature of ASTM 6641 test, that both end loads and shear loads contributes to compressive stress. These fluctuations are taken into account when calculation of compressive modulus.

There is similar trend with tensile and flexural properties with lesser effect on reduction. Strength reduction about 4-12% and modulus reduction 10-37%.

Table 4.22. Compressive properties of Sample 1

# of specimens	Compressive Strength (MPa)	Compressive Modulus (GPa)	Compressive Strain at Break (%)
1	382.7	28.51	1.97
2	412.7	34.15	2.64
3	411.7	27.72	2.04
4	383.0	29.50	2.54
5	427.6	31.35	2.61
6	411.7	36.88	2.71
Average	**404.9**	**31.35**	**2.42**
Std. Dev.	**18.12**	**3.97**	**0.33**

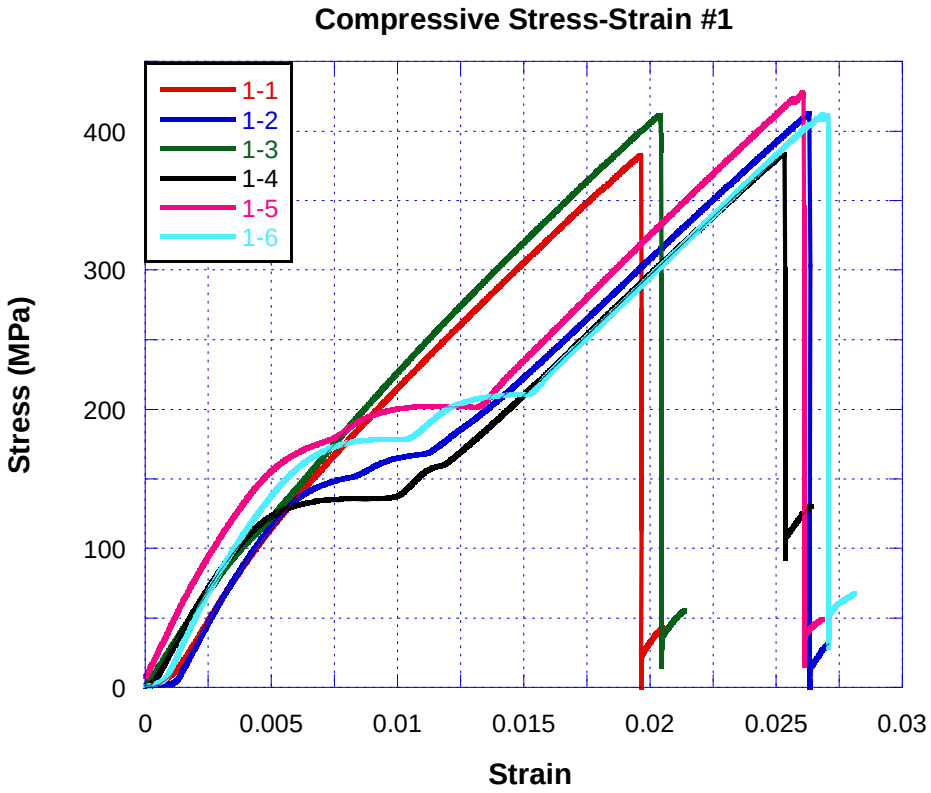

Figure 4.53. Compressive stress vs. strain graphs of Sample 1

Table 4.23. Compressive properties of Sample 2

# of specimens	Compressive Strength (MPa)	Compressive Modulus (GPa)	Compressive Strain at Break (%)
1	425.6	40.44	1.92
2	420.1	44.19	1.74
3	399.4	43.82	1.78
4	427.7	43.88	1.70
5	438.8	43.08	2.32
Average	**422.3**	**43.08**	**1.89**
Std. Dev.	**14.5**	**1.77**	**0.25**

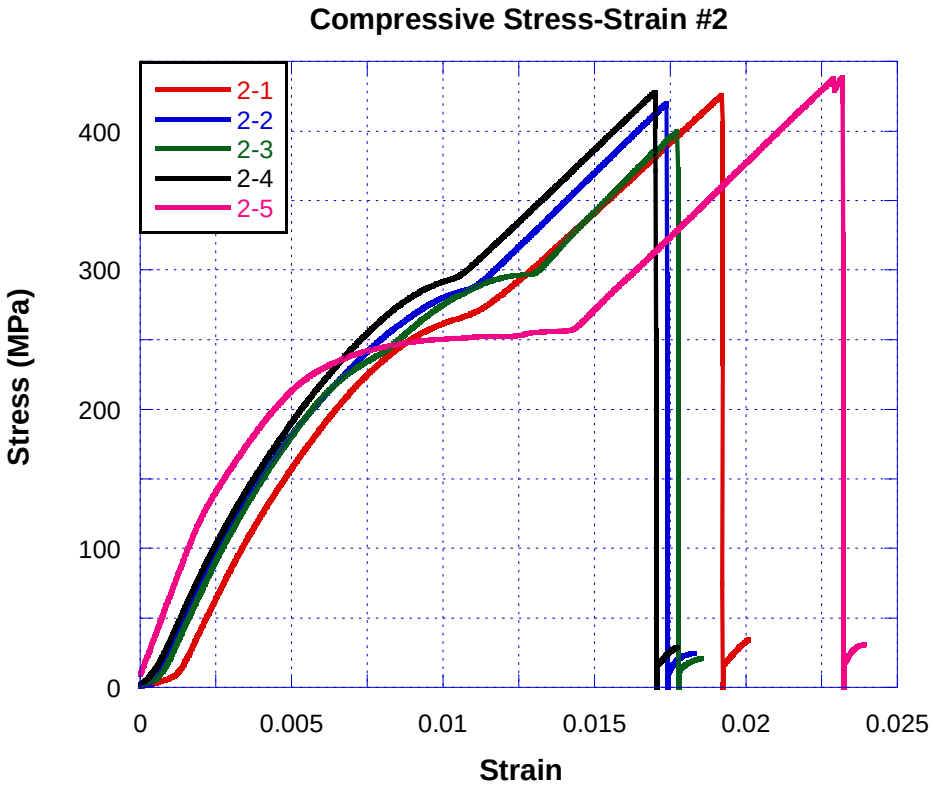

Figure 4.54. Compressive stress vs. strain graphs of Sample 2

Table 4.24. Compressive properties of Sample 3

# of specimens	Compressive Strength (MPa)	Compressive Modulus (GPa)	Compressive Strain at Break (%)
1	369.3	19.31	2.06
2	357.0	17.57	2.45
3	365.5	23.69	2.40
4	353.3	23.63	2.42
5	343.8	23.53	2.36
6	342.9	24.39	2.26
Average	**355.3**	**22.02**	**2.33**
Std. Dev.	**10.89**	**2.84**	**0.15**

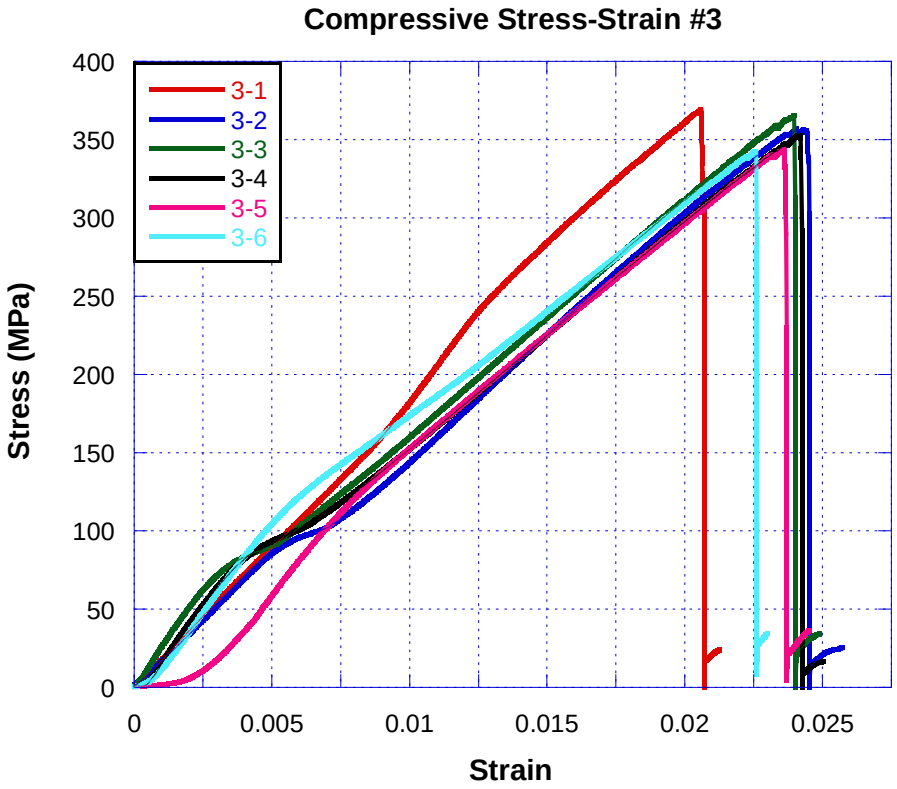

Figure 4.55. Compressive stress vs. strain graphs of Sample 3

Table 4.25. Compressive properties of Sample 4

# of specimens	Compressive Strength (MPa)	Compressive Modulus (GPa)	Compressive Strain at Break (%)
1	363.2	22.84	2.00
2	389.9	30.49	2.54
3	380.5	32.17	2.31
4	361.6	31.84	2.29
5	376.8	24.44	2.04
6	346.5	25.92	1.95
Average	**369.8**	**27.95**	**2.19**
Std. Dev.	**15.63**	**4.04**	**0.23**

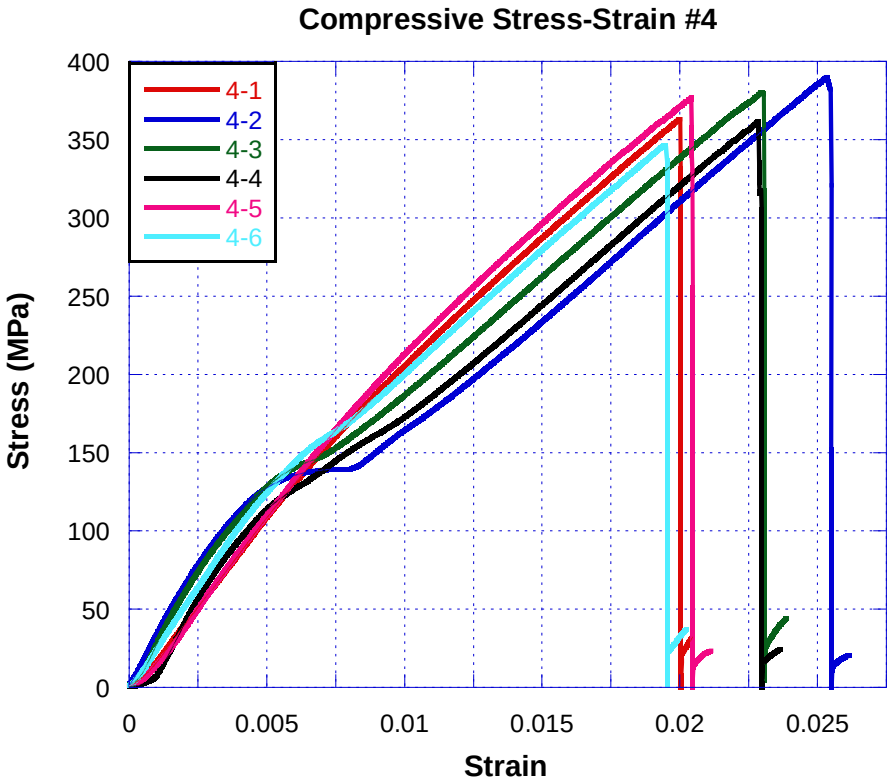

Figure 4.56. Compressive stress vs. strain graphs of Sample 4

Table 4.26. Compressive properties of Sample 5

# of specimens	Compressive Strength (MPa)	Compressive Modulus (GPa)	Compressive Strain at Break (%)
1	375.9	35.52	1.36
2	378.0	34.50	1.56
3	384.1	34.64	1.44
4	338.8	31.47	1.48
5	357.0	36.07	1.41
6	356.5	35.61	1.54
Average	**365.1**	**34.64**	**1.47**
Std. Dev.	**17.18**	**1.86**	**0.08**

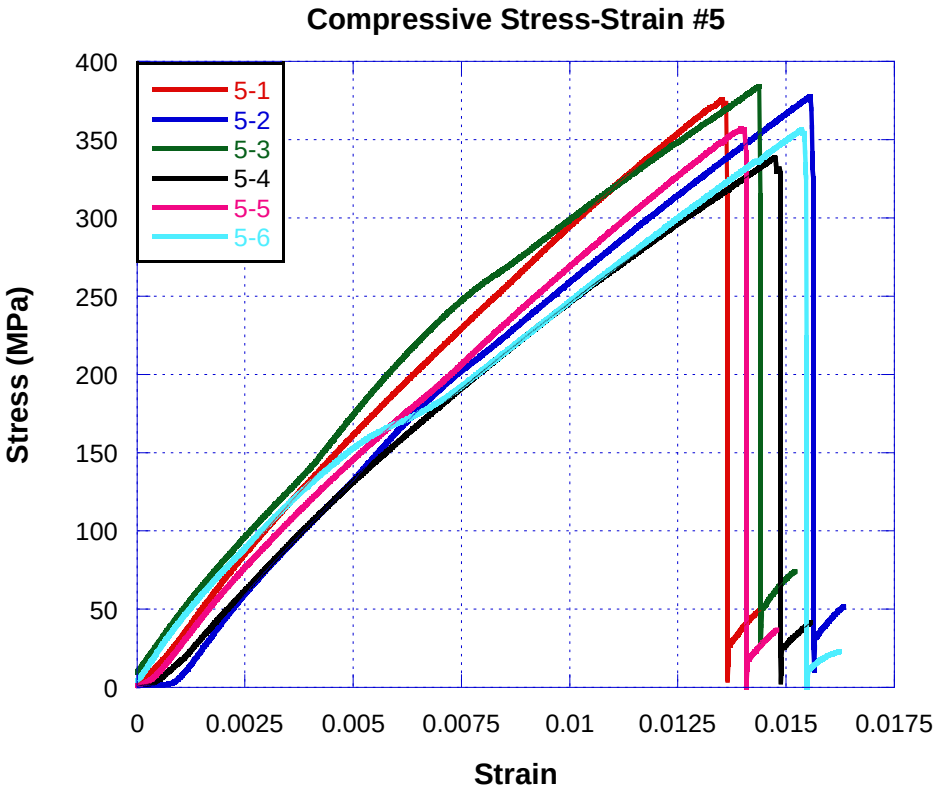

Figure 4.57. Compressive stress vs. strain graphs of Sample 5

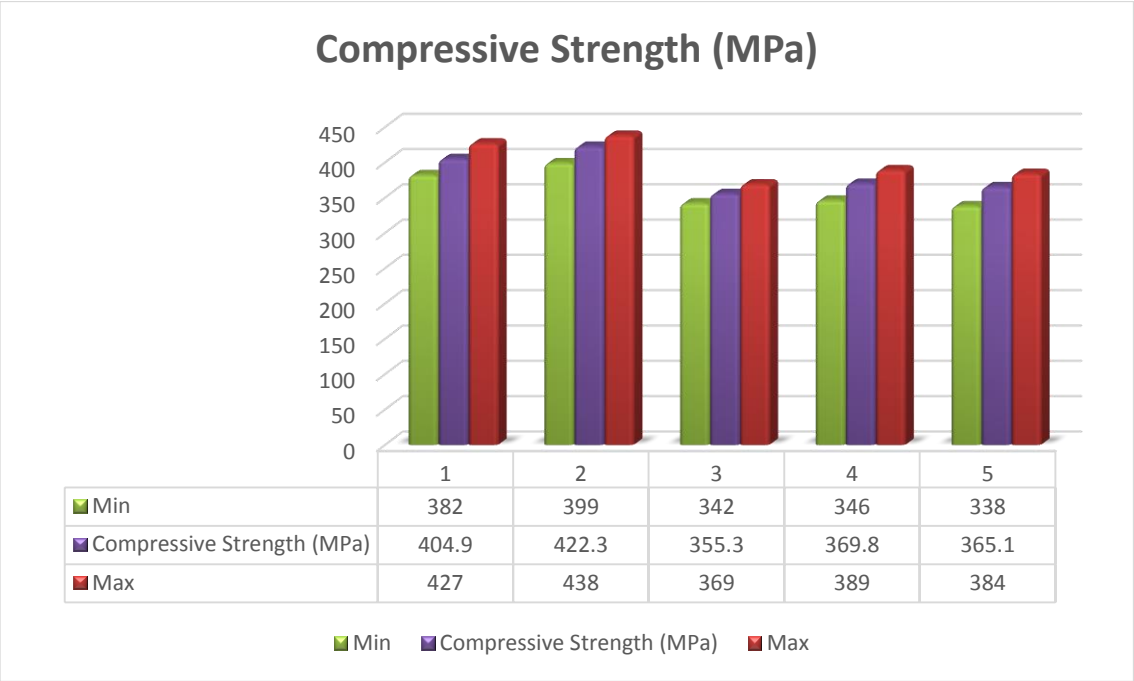

Figure 4.58. Compressive strength for all structures

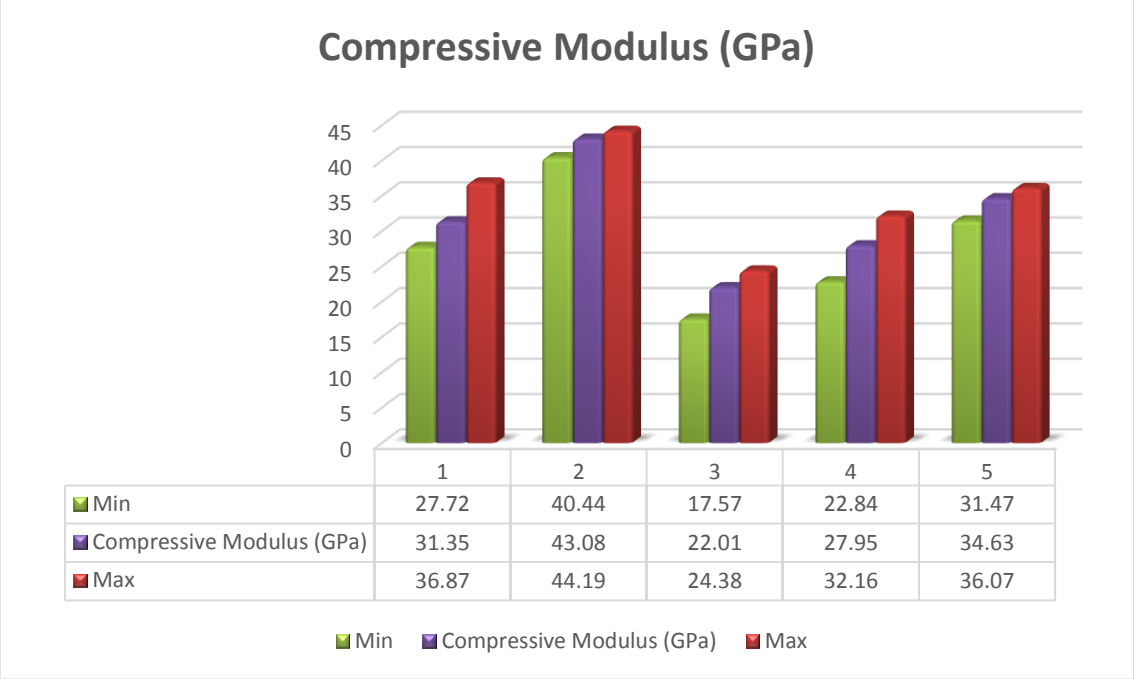

Figure 4.59. Compressive modulus for all structures

4.4.4. Impact Behaviour

For all manufactured samples impact energy and charpy impact strength results are ascertained. For each sample, at least 5 specimens were used in tests. Through the Tables 4.27 to 4.31 all specimens' results are summarized. Impact strength values are calculated by using impact energy values. For the result impact energy was divided to cross sectional area of the notched area. In the CI included samples there is a striking reduction in impact strength about 7% - 47% compared to conventional epoxy glass polymeric composite structures.

Table 4.27. Impact energy and strength of Sample 1

# of specimens	**Impact Energy (J)**	**Impact Strength (kJ/m^2)**
1	3.158	85.76
2	4.501	90.86
3	2.712	75.46
4	3.584	90.46
5	4.096	87.29
Average	**3.610**	**81.98**
Std. Dev.	**0.71**	**6.25**

Table 4.28. Impact energy and strength of Sample 2

# of specimens	**Impact Energy (J)**	**Impact Strength (kJ/m^2)**
1	3.206	105.06
2	2.851	97.20
3	2.264	83.33
4	3.250	101.19
5	2.680	98.12
6	2.890	92.88
Average	**2.857**	**96.58**
Std. Dev.	**0.36**	**7.56**

Table 4.29. Impact energy and strength of Sample 3

# of specimens	Impact Energy (J)	Impact Strength (kJ/m^2)
1	2.890	50.39
2	2.978	55.31
3	2.422	47.99
4	3.038	57.05
5	2.303	50.99
6	2.898	56.60
Average	**2.755**	**53.19**
Std. Dev.	**0.31**	**3.76**

Table 4.30. Impact energy and strength of Sample 4

# of specimens	Impact Energy (J)	Impact Strength (kJ/m^2)
1	3.010	56.33
2	2.438	53.60
3	3.354	58.58
4	3.358	61.45
5	2.364	57.29
6	3.640	61.83
Average	**3.027**	**58.35**
Std. Dev.	**0.53**	**3.14**

Table 4.31. Impact energy and strength of Sample 5

# of specimens	Impact Energy (J)	Impact Strength (kJ/m^2)
1	2.276	57.98
2	2.112	55.86
3	1.807	52.20
4	1.848	57.03
5	2.146	56.31
6	2.326	56.89
Average	**2.086**	**56.05**
Std. Dev.	**0.22**	**2.02**

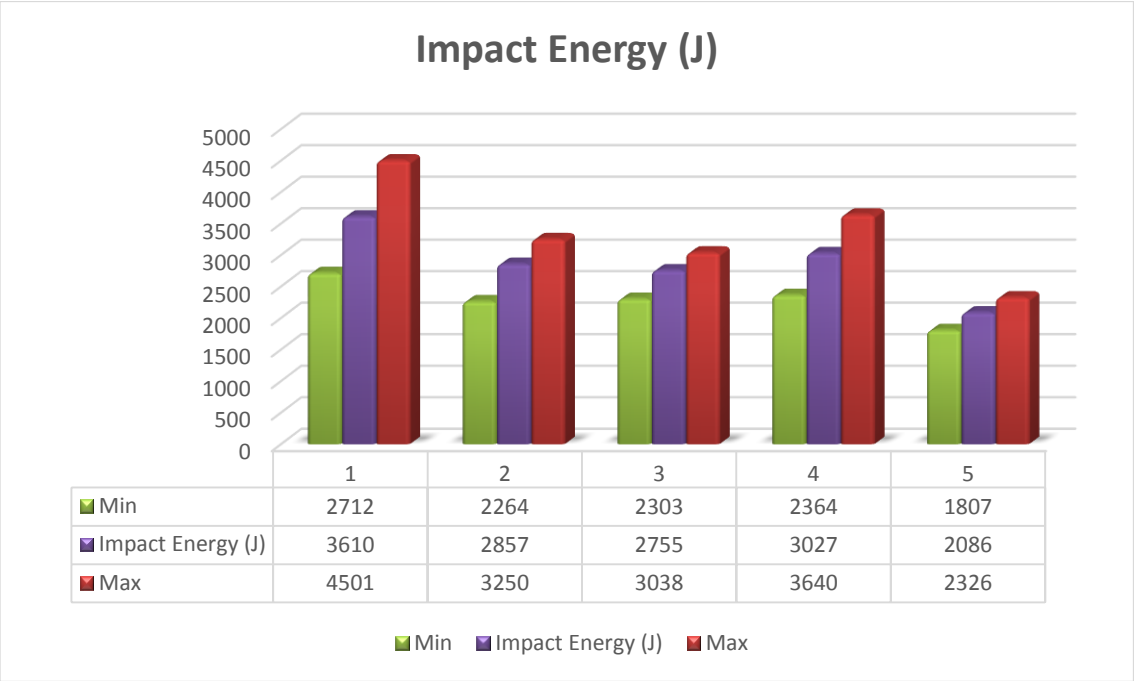

Figure 4.60. Impact energy for all structures

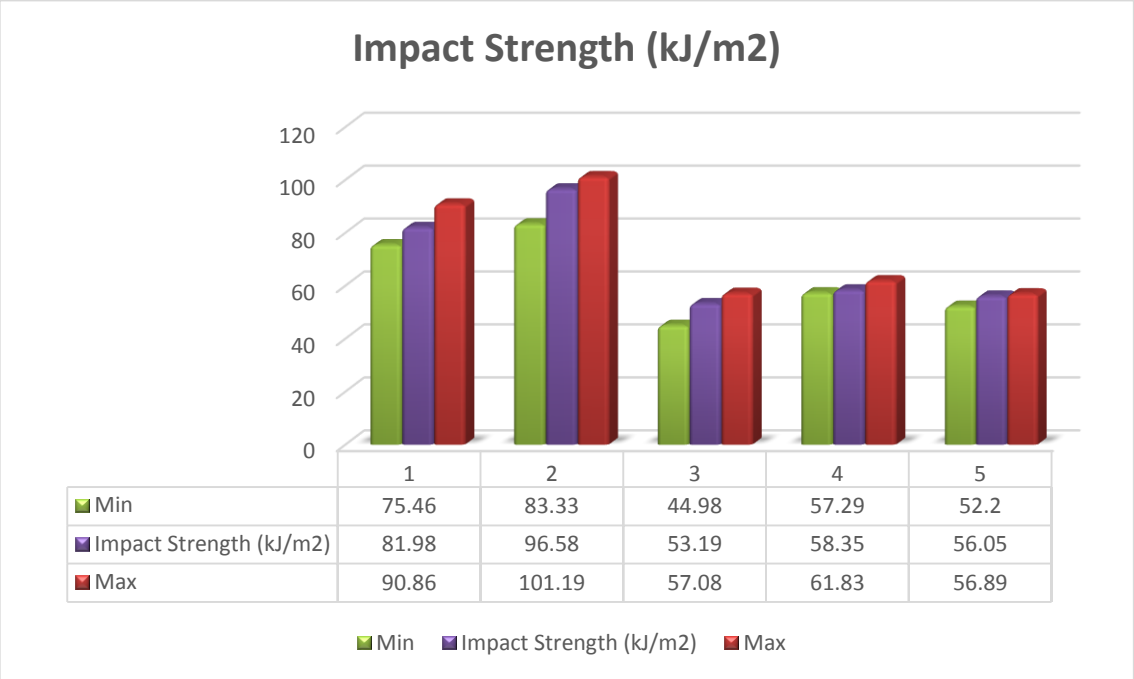

Figure 4.61. Impact strength for all structures

4.5. Radar Absorbing Properties

Before the fabrication process of radar absorbing structure, you need some parameters to construct the correct design and achieve the absorbance. Because of the importance of that reason, firstly MatLab simulation program was used to have an idea about thickness or resistive sheets or numbers of Jaumann type composite structure. By using this programming, structures were constructed. So it can be said we followed two main way. For the simulation process, nearly data acquired from the literature for permittivity and permeability. Also after manufactured the samples, by using the optical microscopy the thicknesses between resistive sheets and thickness between resistive sheet and surface of the structure determined exactly. Moreover, to confirm the measuring absorbance results, LabVIEW simulation programming also used.

In reflection loss measurements, calibrations were done to get correct results. In addition to the calibration, to get more accurate result, firstly metal back reflection measurements were performed. After this step, for each sample we continued to collect data from the structures. Metal back loss measurement is reference of all other structure. Metal back reference values substracted from the results taken from sutructures. Whereby we try to get more accurate result.

In Figure below, there are reflection loss measurements taken from the network analyzer which metal back results substract them.

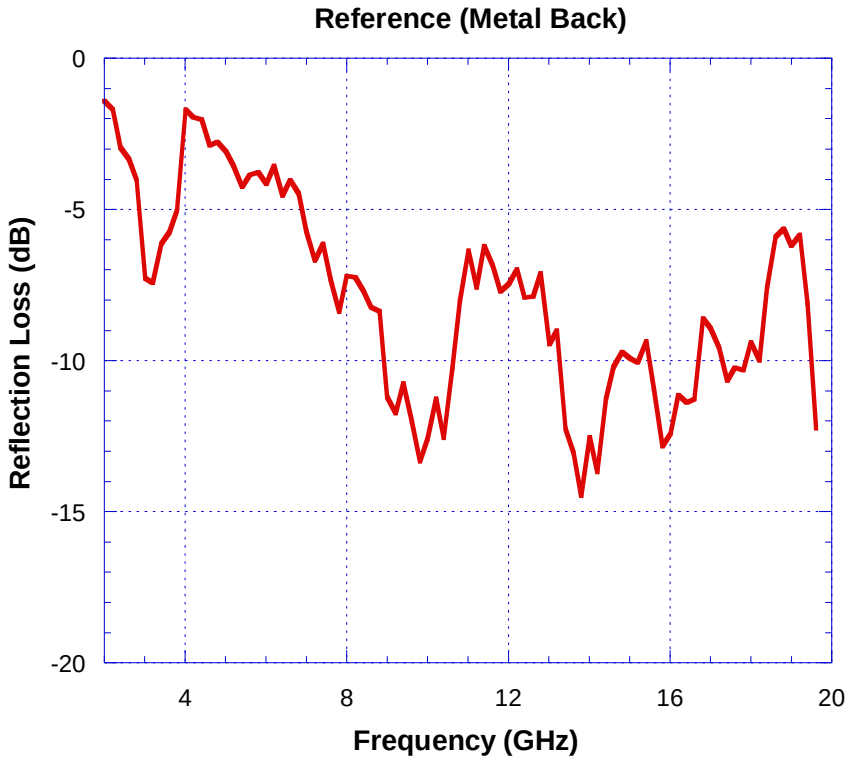

Figure 4.62. Reflection loss reference from metal back taken for accuracy

Metal back reflection measurement is used for each structure by subtracting it from samples absorbance measurements.

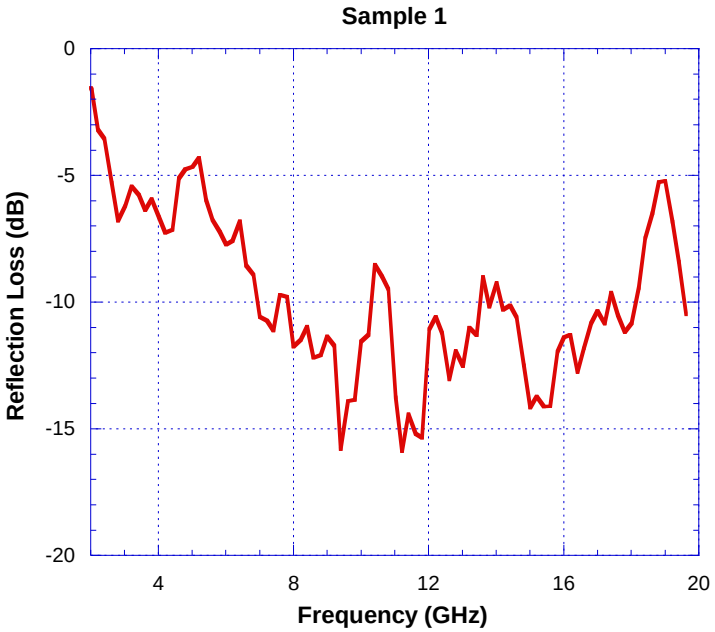

Figure 4.63. Reflection loss measurement of sample 1

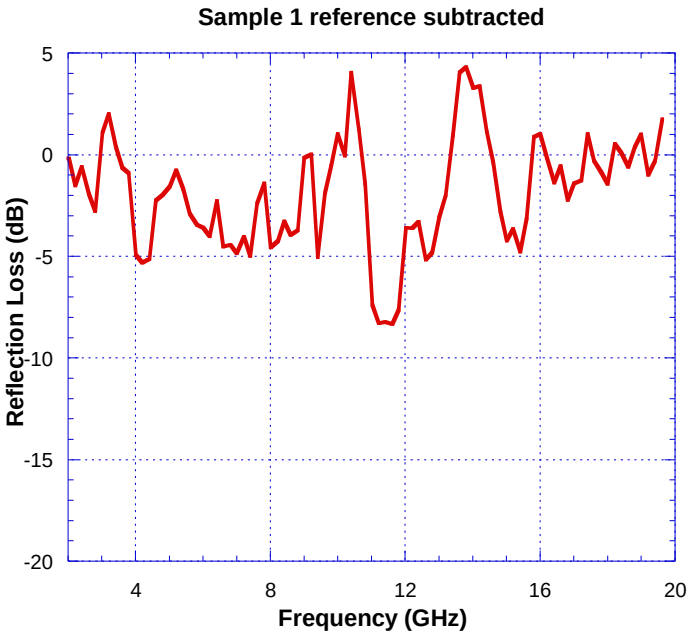

Figure 4.64. Actual absorbance property of Sample 1

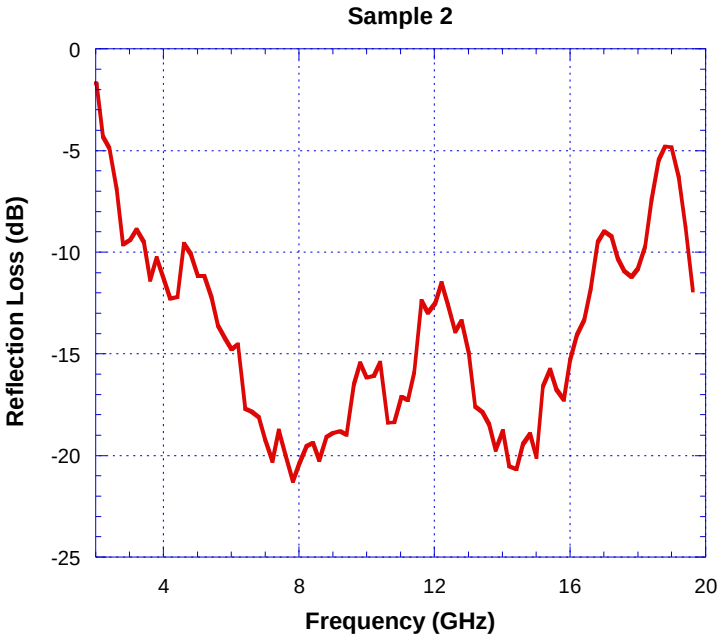

Figure 4.65. Reflection loss measurement of sample 2

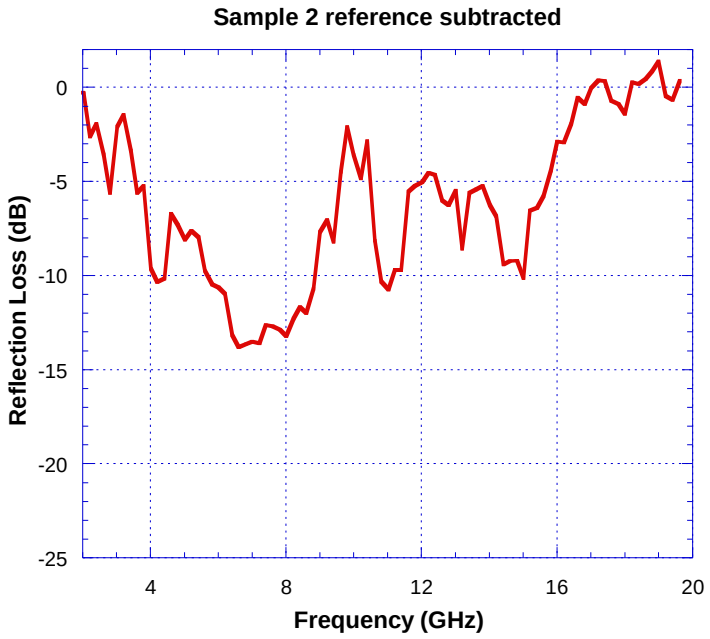

Figure 4.66. Actual absorbance property of Sample 2

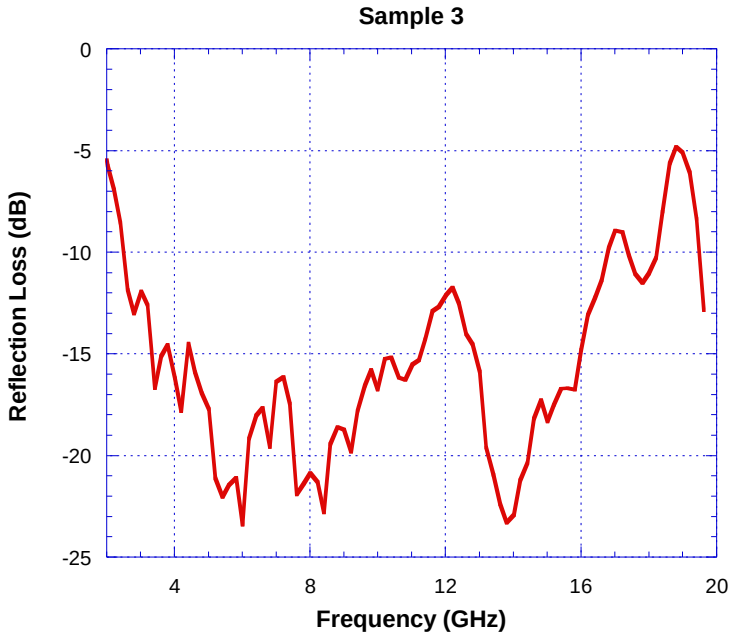

Figure 4.67. Reflection loss measurement of sample 3

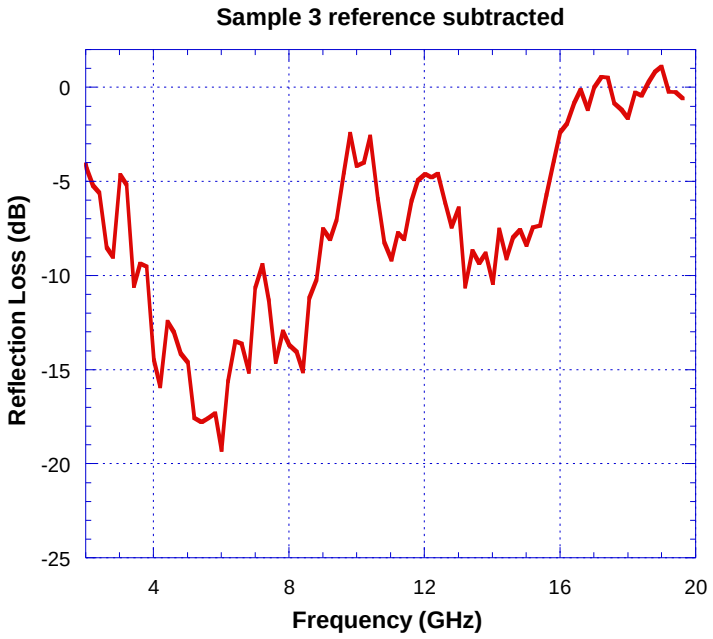

Figure 4.68. Actual absorbance property of Sample 3

As it is seen from the graphs, when the metal back reference subtracted from the reflection loss measurement of structure, the absorbance properties get worse. But still attenuation between 4 GHz and 8 GHz in C band below 15 dB.

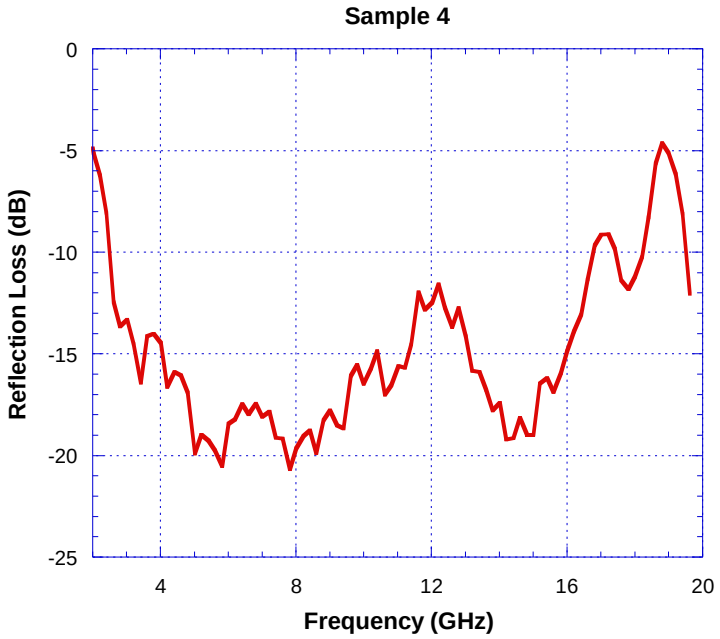

Figure 4.69. Reflection loss measurement of sample 4

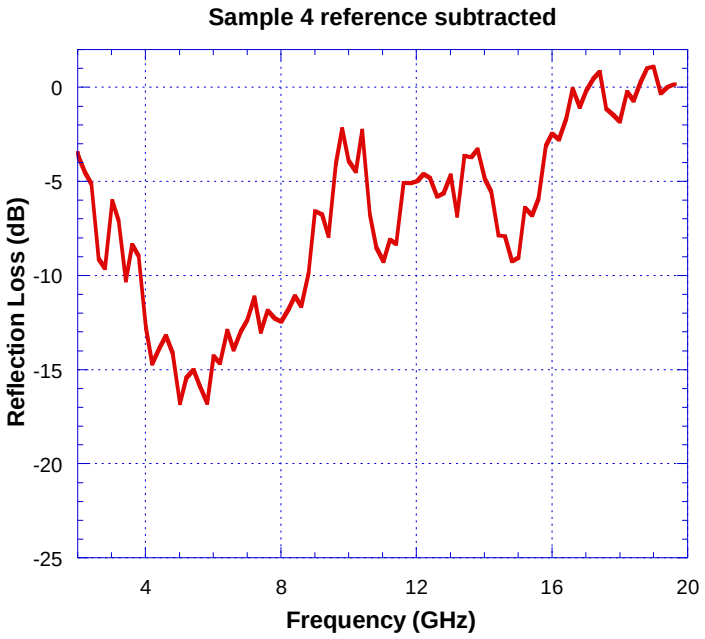

Figure 4.70. Actual absorbance property of Sample 4

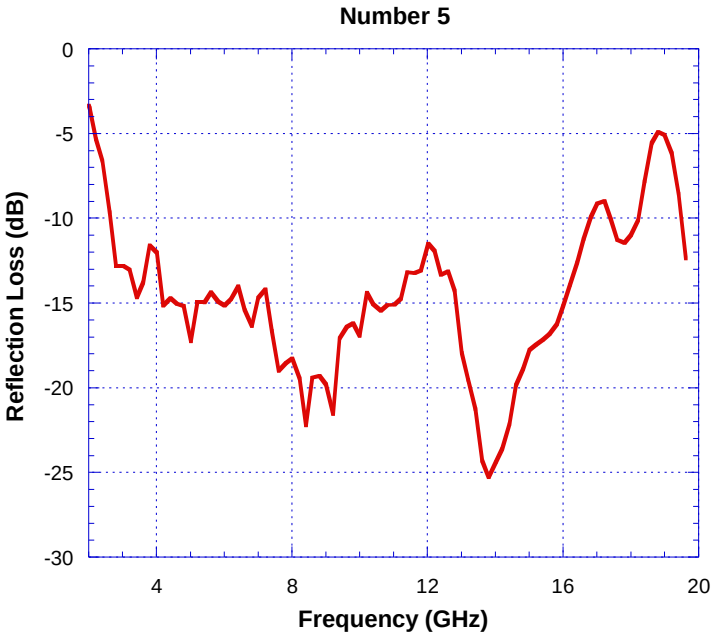

Figure 4.71. Reflection loss measurement of sample 5

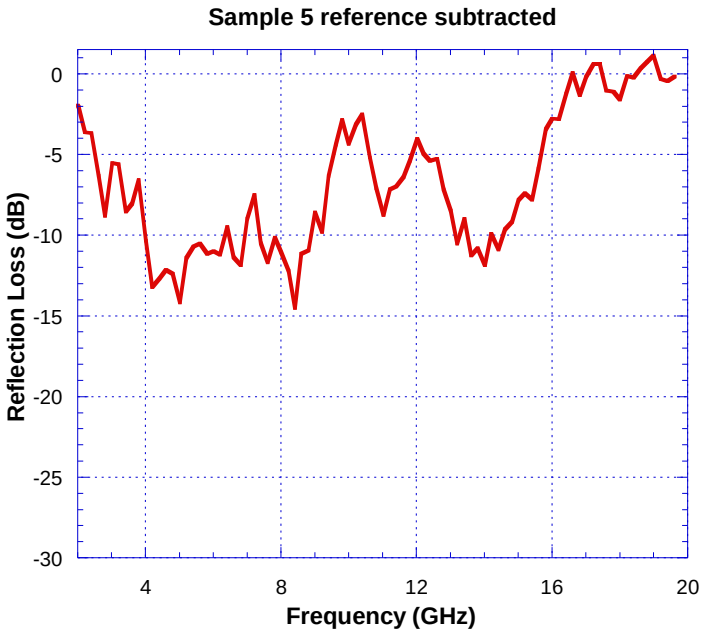

Figure 4.72. Actual absorbance property of Sample 5

Table 4.32. Summary about thicknesses of resistive sheets spacing in structure

Sample name	# of Layers	Filler	t_1 (mm)	t_2 (mm)	t_3 (mm)	t_4 (mm)	t_5 (mm)	Total t (mm)
1	16	No	--	--	--	--	--	5.6
2	16	No	1.3	0.9	0.9	0.9	0.9	4.9
3	16	25 wt% CI	1.2	1.5	1.2	1.5	0.8	6.3
4	16	25 wt% CI	1.7	1.2	1.2	1.2	1.2	6.5
5	16	25 wt% CI	1.27	0.96	0.96	0.96	0.96	5.1

Table 4.32 summarize the thicknesses between resistive sheets and also between surface and the first resistive sheet. These values were calculated by using total thickness of the structures. Then total thickness divided to 16 layers. The space of resistive sheets in the structure was known, and it multiplied with the sequence of the layer.

Table 4.33. Summary about resistance of resistive sheets in Jaumann structures

Sample name	# of Layers	Filler	R_1 (Ω/sqr)	R_2 (Ω/sqr)	R_3 (Ω/sqr)	R_4 (Ω/sqr)
2	16	No	45	100	340	410
3	16	25 wt% CI	75	120	300	430
4	16	25 wt% CI	30	35	41	245
5	16	25 wt% CI	75	110	330	350

Table 4.33 gives the information about resistive sheets used in composite structure.

It is observed from the graphs that, important parameters for absorbance are thicknesses, resistances and additives. Fillers effect intrinsic impedance of total structure. So, it means the other important parameters are permittivity and permeability values of structures. Additionally, from the transmission line theory it is seen that thickness

between resistive sheets are important. In our structures, spacing of the sheets in structure were changed. For each structure, different configuration was attempt. Moreover, the resistance values were chanced in different structures.

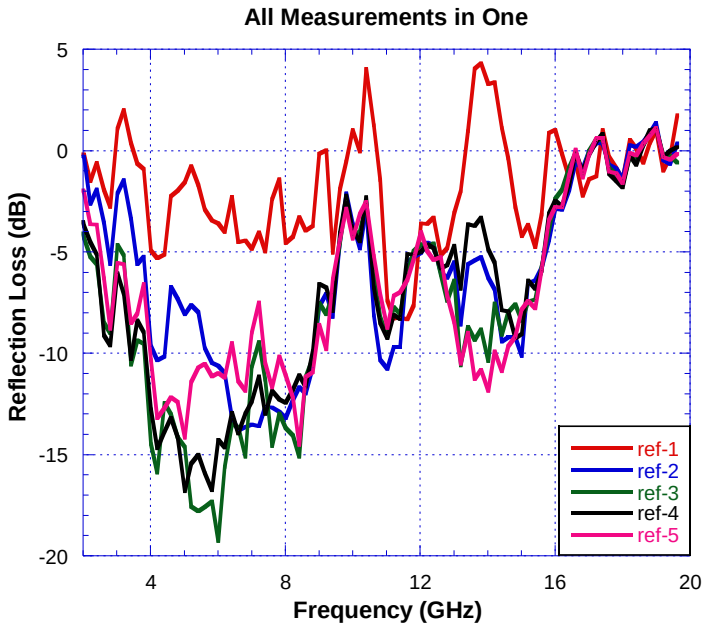

Figure 4.73. Absorbance measurements of all manufactured structures

It is seen from the reflection loss measurements that, there is a trend in the CI additive and comprising resistive sheet structures. These structures have a resonance frequency between 4 - 8 GHz C band and 12 - 16 GHz K_u band. In these ranges, sample 4 which has 25 wt% CI additive and four different resistive sheets, has maximum loss and better bandwidth with respect to the other samples.

4.5.1. LabVIEW Confirmation

To confirm our measured reflection loss graphs, LabVIEW programming was used by using transmission line theory which constructed for four resistive sheet Jaumann type structures.

Resistance parameters which measured by using four probe system were used in program. Thicknesses were taken from optical microscopy images for the exact values.

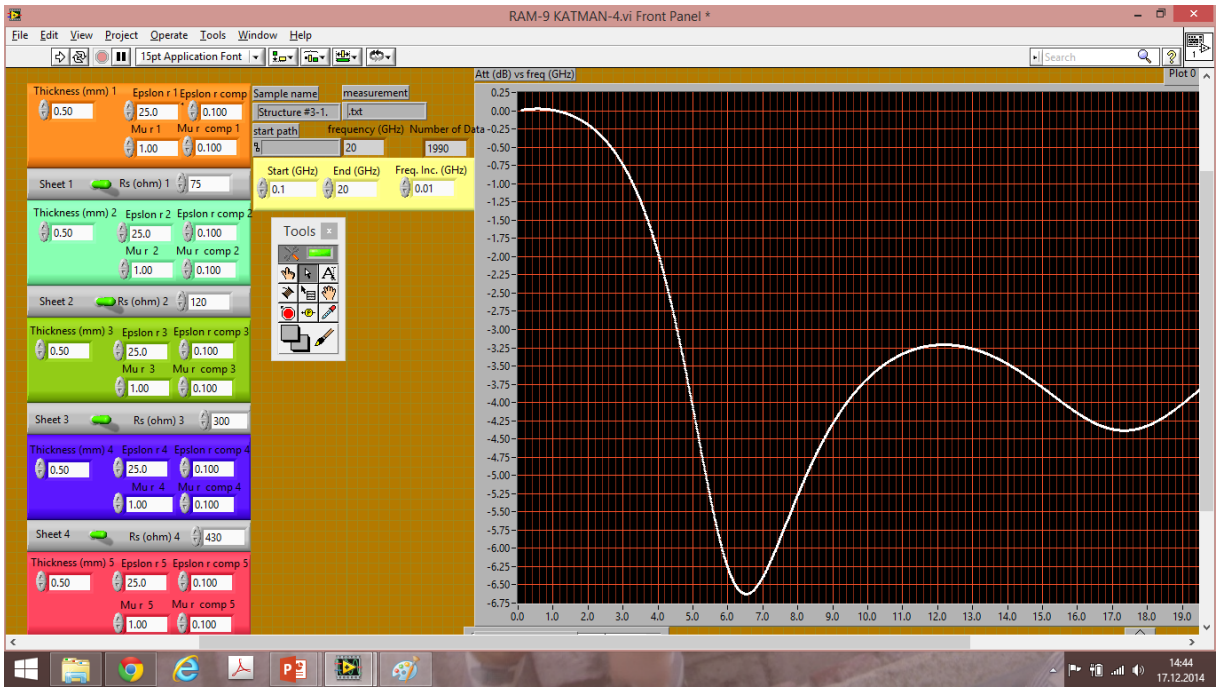

Figure 4.74. Front page of LabVIEW simulation programme

Moreover, permittivity and permeability values were used from the literature to plot the reflection loss graphs.

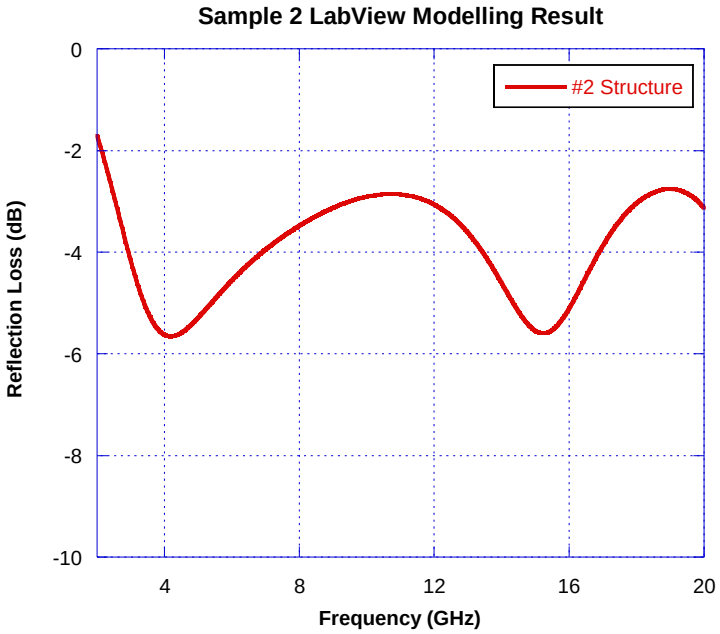

Figure 4.75. LabVIEW simulation result of sample 2

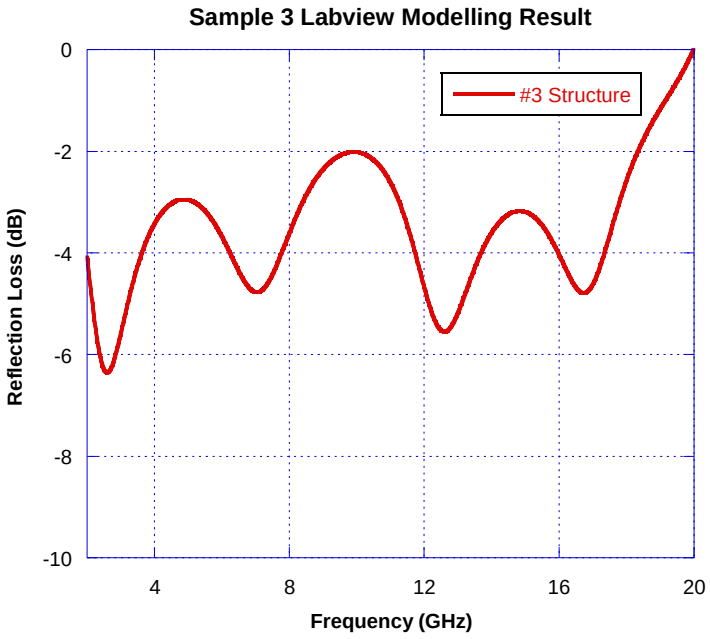

Figure 4.76. LabVIEW simulation result of sample 3

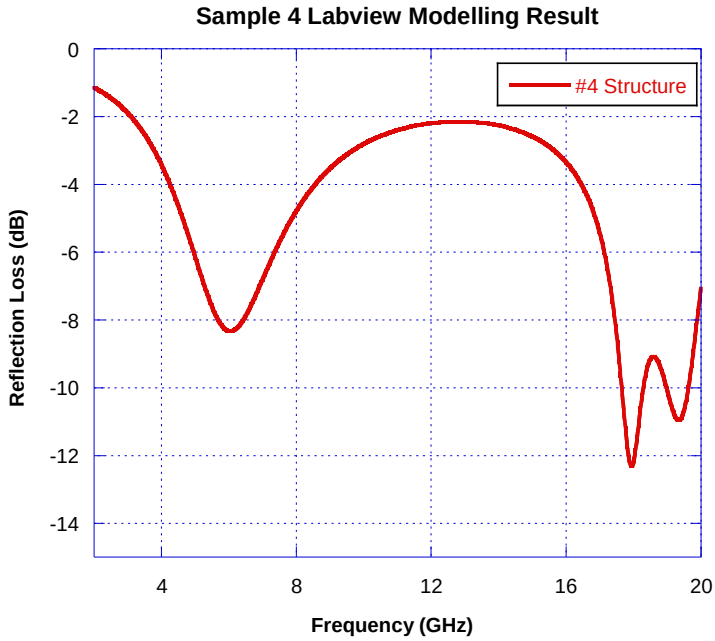

Figure 4.77. LabVIEW simulation result of sample 4

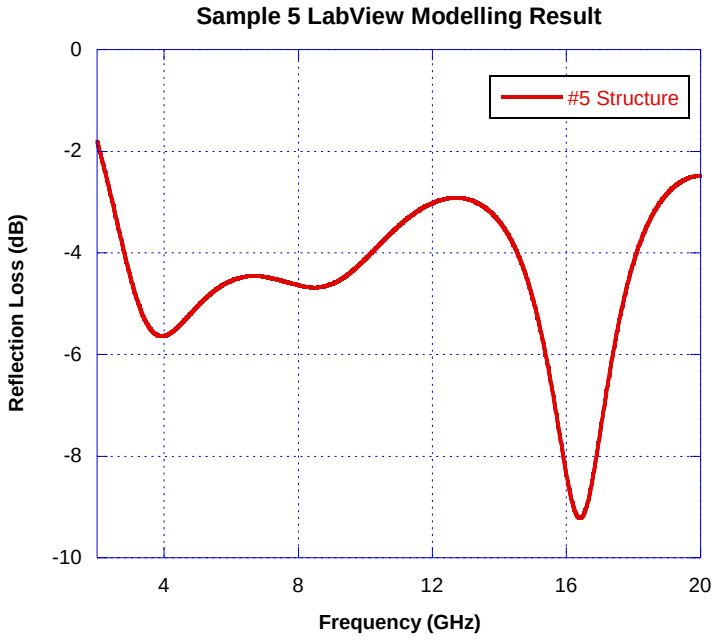

Figure 4.78. LabVIEW simulation result of sample 5

There are main differences between simulation and measured reflection losses. It is about the bandwidth of absorbance and amount of reflection loss. So many reasons can be listed for this observation.

First of all, resistive sheets considered as a uniform surface and conductivity same everywhere. In fact some fluctuations can be observed on the surface of the sheet. Because of that reason, it can be some differences between measured and simulation one.

Another difference is the resistive sheet spacing in the structure. Because of the manual clamping of the mould at the end of the manufacturing process, it is very difficult to obtain same and constant thickness for all samples.

Moreover, permittivity and permeability values taken from the literature can be different from manufactured ones. Because as an additive maximum 25 wt% CI micro particles were used in our studies. But in the data, structure contain 50 wt% minimum CI without any E-glass reinforcement.

CHAPTER 5

CONCLUSION

In this study, glass fiber reinforced epoxy based radar absorbing structures were manufactured. Carbonyl iron micro particles were used to change the intrinsic impedance of the structure to increase the absorption. Also, to increase the bandwidth of the absorption, Salisbury screen resistive sheets were prepared to use in composites. Reflection loss measurements were performed to characterize the structures. Additionally, physical property of structures were investigated. These tests include, microstructural evaluation by SEM analysis and optical microscopy, determination of fiber volume content by burnt out method, characterization of charpy impact strength and evaluation of mechanical properties such as ultimate strength, modulus and strain at break for tensile, flexural and compression test configurations. Lastly electromagnetic wave absorption properties were examined.

LabVIEW simulation programme were written by using transmission line theory to confirm or compare with the measured reflection loss results. Parameters taken from the manufactured structures were used. For this aim resistance values, thicknesses were measured from the constructed structures. In the last step, for the permittivity and permeability values, containing 50 wt% CI additive structure parameters were adapted to use them in transmission line theory.

When CI micro particles mixed with the epoxy resin, it dispersed in matrix. But after layup it on the surface of the fabric, because of the higher density property of the CI, it is seen in the SEM analysis that, it precipitated on the fabric. It caused the negative effect for the radar absorbing structure. In CI additive structures mechanical properties were effected and they showed similar decreasing tendency for the final and modulus values with respect to the conventional fiber reinforced polymeric composite structure. Impact strength shows similar behaviour as flexural, compressive and tensile tests with reduction of impact strength loss is more explicit.

In all conducted tests, modified composite structure with only ITO coated resistive sheet, showed the best property.

There are some distinct behaviour in the measurement results of simulated and manufactured samples. These differences is caused by many reasons such as, non-homogeneous resistive sheet layers, differences of permittivity and permeability values acquired from literature, spacing differences of the resistive sheets in the structure, thicknesses between resistive sheets or thickness between resistive sheet and surface of the structure, total thickness of the structures and measurement errors resulting from the measurement set up. As long as these problems solved, more consisting results between simulation and measurements can obtained.

For our manufactured composite structures, it is seen from the reflection loss measurements that, there is a trend in the CI additive and comprising resistive sheet structures. These structures have a resonance frequency between 4 - 8 GHz C band and 12 - 16 GHz K_u band. In these ranges, sample 4 which has 25 wt% CI additive and four different resistive sheets, has maximum loss and better bandwidth with respect to the other samples.

In literature there are some other additives used in structures such as magnetic materials which I mentioned about it in Chapter 2. These magnetic materials can be used as an absorber additive in structures. Barium hexaferrite, carbon nanotubes, carbon short fibers, carbon nano fibers, graphite are examples of some magnetic materials. In further studies, these materials could be preferred. Additionally, multilayer configurations with different types of matrices might be a possible candidate for wide band absorbers.

Moreover, incident wave angles should be taken in to account as in real life situations. Different angle of incident waves can be tested and in this context solutions should be created for the maximum absorbance and broad bandwidth.

REFERENCES

Adams Jr, L.W., M.W. Gilpatrick, and R.V. Gregory. 1994. Method for generating a conductive fabric and associated product. Google Patents.

B, M.E. 1958. Microwave radiation absorbers. Google Patents.

Barry Jr, C.N. 1993. Method for enhancing polyaniline conductivity. Google Patents.

Barton, D.K., and S.A. Leonov. 1998. Radar technology encyclopedia.

Bjorklund, R.B., and I. Lundström. 1984. Some properties of polypyrrole-paper composites. *Journal of Electronic Materials*. 13:211-230.

Bohren, C.F., R. Luebbers, H.S. Langdon, and F. Hunsberger. 1992. Microwave-absorbing chiral composites: Is chirality essential or accidental? *Applied optics*. 31:6403-6407.

Bornemann, J. 1993. Computer-aided design of multilayered dielectric frequency-selective surfaces for circularly polarized millimeter-wave applications. *Antennas and Propagation, IEEE Transactions on*. 41:1588-1591.

Broderick, J.F., N.J. Tessier, M.S. Heafey, and M.T. Kocsik. 1996. Electromagnetic energy absorber. Google Patents.

Campbell Jr, F.C. 2003. Manufacturing processes for advanced composites. Elsevier.

Capaccioli, S., M. Lucchesi, P. Rolla, and G. Ruggeri. 1998. Dielectric response analysis of a conducting polymer dominated by the hopping charge transport. *Journal of Physics: Condensed Matter*. 10:5595.

Carlton, P.B. 1961. Nondirectional, metal-backed, electromagnetic radiation-absorptive films. Google Patents.

Chakravarty, S., R. Mittra, and N.R. Williams. 2001. On the application of the microgenetic algorithm to the design of broad-band microwave absorbers comprising frequency-selective surfaces embedded in multilayered dielectric media. *Microwave Theory and Techniques, IEEE Transactions on*. 49:1050-1059.

Chakravarty, S., R. Mittra, and N.R. Williams. 2002. Application of a microgenetic algorithm (MGA) to the design of broadband microwave absorbers using multiple frequency selective surface screens buried in dielectrics. *Antennas and Propagation, IEEE Transactions on*. 50:284-296.

Chambers, B., and A. Tennant. 1996. Optimised design of Jaumann radar absorbing materials using a genetic algorithm. *IEE Proceedings-Radar, Sonar and Navigation*. 143:23-30.

Chambers, B., and A. Tennant. 2003. Progress in smart radar absorbers. *P Soc Photo-Opt Ins*. 5055:344-355.

Charles, A., M. Towers, and A. McCowen. 1996. Computation in Electromagnetics. *In* Third International conference on (Conf. Publ. No 420). Vol. 117.

Charles, A., M. Towers, and A. McCowen. 1999. Microwaves, Antennas & Propagation. *In* IEEE Proceedings. Vol. 146. 257.

Cheldavi, A., and M. Kamarei. 1997. Microwave Symposium Digest, 1997. *IEEE MTT-S International*. 3:1555.

Child, A.D. 1998. Method of enhancing the stability of conductive polymers. Google Patents.

Child, A.D., and A.R. DeAngelis. 1999. Patterned conductive textiles. Google Patents.

Child, A.D., A.R. DeAngelis, and D.E. Green. 1997. Patterned conductive textiles. Google Patents.

Child, A.D., A.R. DeAngelis, and D.E. Green. 1998. Method of making patterend conductive textiles. Google Patents.

Cloete, J.H., and C.F. Dutoit. 1989. Ridged Cavity Backed Slot Antenna with Dielectric Loading. *Electron Lett*. 25:323-324.

Collins, G.E., and L.J. Buckley. 1996. Conductive polymer-coated fabrics for chemical sensing. *Synthetic Metals*. 78:93-101.

Connolly, T.M., and E.J. Luoma. 1977. Microwave absorbers. Google Patents.

Cuddihee, M.E., R.V. Gregory, and W.C. Kimbrell Jr. 1992. Electrically conductive polymer material having conductivity gradient. Google Patents.

Dallenbach, W., and W. Kleinsteuber. 1938. Reflection and absorption of decimeter-waves by plane dielectric layers. *Hochfreq. u Elektroak*. 51:152-156.

De Rosa, I.M., A. Dinescu, F. Sarasini, M.S. Sarto, and A. Tamburrano. 2010. Effect of short carbon fibers and MWCNTs on microwave absorbing properties of polyester composites containing nickel-coated carbon fibers. *Composites Science and Technology*. 70:102-109.

Deng, L., and M. Han. 2007. Microwave absorbing performances of multiwalled carbon nanotube composites with negative permeability. *Applied physics letters*. 91:023119-023119-023113.

Diaz, R.E., and W.E. McKinzie. 2003. Multi-resonant, high-impedance electromagnetic surfaces. Google Patents.

du Toit, L., and J. Cloete. 1989. Antennas & Propagation Society International Symposium, 1989. *AP-S. Digest*. 3:1558.

du Toit, L., and J. Cloete. 1990. Advances in the design of Jaumann absorbers. *In* Antennas and Propagation Society International Symposium, 1990. AP-S. Merging Technologies for the 90's. Digest. IEEE. 1212-1215.

Emerson, W.H. 1973. Electromagnetic Wave Absorbers and Anechoic Chambers through Years. *Ieee T Antenn Propag*. Ap21:484-490.

Eugene, F.K., and T. Michael. 2004. Radar cross section. SciTech Publishing, Inc Raleigh, NC.

Fante, R.L., and M.T. Mccormack. 1988a. Reflection Properties of the Salisbury Screen. *Ieee T Antenn Propag*. 36:1443-1454.

Fante, R.L., and M.T. Mccormack. 1988b. Reflection properties of the Salisbury screen. *Antennas and Propagation, IEEE Transactions on*. 36:1443-1454.

Foroozesh, A., A. Cheldavi, and F. Hodjat. 2000. Antennas, Propagation and EM Theory, 2000. *In* Proceedings. ISAPE 2000. 5th International Symposium on. Vol. 227.

Gama, A.M., and M.C. Rezende. 2010. Complex permeabillity and permittivity variation of carbonyl iron rubber in the frequency range of 2 to 18 GHz. *Journal of Aerospace Technology and Management*. 2:59-62.

Gaylor, K. 1989. Radar Absorbing Materials-Mechanisms and Materials. DTIC Document.

Genies, E., C. Petrescu, and L. Olmedo. 1991. Conducting materials from polyaniline on glass textile. *Synthetic Metals*. 41:665-668.

Gregory, R., W. Kimbrell, and H. Kuhn. 1989. Conductive textiles. *Synthetic Metals*. 28:823-835.

Halpern, O. 1960. Method and means for minimizing reflec. Google Patents.

Hashimoto, O., A. Takumi, R. Satake, M. Kaneko, and Y. Hashimoto. 1995. Design and Manufacturing of Resistive-Sheet Type Wave Absorber at 60GHz Frequency Band. *IEICE transactions on communications*. 78:246-252.

Heafey, M., R.S. Kasevich, and M. Kocsik. 1993. Broadband electromagnetic energy absorber. Google Patents.

Jaggard, D.L., and N. Engheta. 1989. Chirosorb as an Invisible Medium. *Electron Lett*. 25:173-174.

Janos, W.A. 1994. Synthetic dielectric material for broadband-selective absorption and reflection. Google Patents.

Jenn, D.C. 2005. Radar and laser cross section engineering. American Institute of Aeronautics and Astronautics.

Johnson, J.M., and V. Rahmat-Samii. 1997. Genetic algorithms in engineering electromagnetics. *Antennas and Propagation Magazine, IEEE*. 39:7-21.

Kasevich, R.S., and J.F. Broderick. 1993. Broadband electromagnetic energy absorber. Google Patents.

Kim, J.-B., S.-K. Lee, and C.-G. Kim. 2008. Comparison study on the effect of carbon nano materials for single-layer microwave absorbers in X-band. *Composites Science and Technology*. 68:2909-2916.

Kim, S.-S., Y.-C. Yoon, and K.-H. Kim. 2003. Electromagnetic wave absorbing properties of high-permittivity ferroelectrics coated with ITO thin films of 377 Ω. *Journal of electroceramics*. 10:95-101.

Kimbrell Jr, W.C., and H.H. Kuhn. 1989. Electrically conductive textile materials and method for making same. Google Patents.

Kimbrell Jr, W.C., and H.H. Kuhn. 1991. Method for making electrically conductive textile materials. Google Patents.

Kocsik, M.T., and P.E. Rowe. 2000. Radar absorber and method of manufacture. Google Patents.

Kuehl, S., S. Grove, E. Kuehl, M. Bingle, and J. Cloete. 1997. Manufacture of microwave chiral materials and their electromagnetic properties. *In* Advances in complex electromagnetic materials. Springer. 317-332.

Kuhn, H.H. 1992. Anthraquinone-2-sulfonic acid doped conductive textiles. Google Patents.

Kuhn, H.H., A.D. Child, and W.C. Kimbrell. 1995. Toward real applications of conductive polymers. *Synthetic Metals*. 71:2139-2142.

Kuhn, H.H., and E.H. Pittman. 1992. Electrically conductive textile fabric having conductivity gradient. Google Patents.

Kunihiro, S. 1971. Superwide band wave absorber. Google Patents.

Lederer, P. 1986. An introduction to radar absorbent materials (RAM). *NASA STI/Recon Technical Report N*. 87:13594.

Lederer, P. 1992. Modelling of practical Salisbury screen absorbers. *In* Low Profile Absorbers and Scatterers, IEE Colloquium on. IET. 1/1-1/4.

Lee, S.-E., J.-H. Kang, and C.-G. Kim. 2006. Fabrication and design of multi-layered radar absorbing structures of MWNT-filled glass/epoxy plain-weave composites. *Composite structures*. 76:397-405.

Long, A.C. 2005. Design and manufacture of textile composites. Elsevier.

Machell, G., and M.A. Thomas. 1975. Process of modifying textile materials with polymerizable monomers. US Patent 3,909,195.

Mallick, P.K. 1993. Fiber-reinforced composites: materials, manufacturing, and design. CRC press.

Marchant, S., F. Jones, T. Wong, and P. Wright. 1998. Free-space microwave characteristics of polypyrrole coated glass fibre. *Synthetic metals*. 96:35-41.

Mazumdar, S. 2001. Composites manufacturing: materials, product, and process engineering. CrC press.

McDonald, J.J., B.C. Brock, S.E. Allen, P.G. Clem, and J.A. Paquette. Radar-Cross-Section Reduction of Wind Turbines (Part 1).

Meshram, M., N.K. Agrawal, B. Sinha, and P. Misra. 2004. Characterization of M-type barium hexagonal ferrite-based wide band microwave absorber. *Journal of Magnetism and Magnetic Materials*. 271:207-214.

Meyer, E., H. Severin, and G. Umlauft. 1954. Resonanzabsorber für elektromagnetische Wellen. *Zeitschrift für Physik*. 138:465-477.

MICHELI, D. 2011. Design of Microwave Absorbing Structure and Microwave Shielding Structure by using Composite Materials, Nanomaterials and Evolutionary Computation.

Micheli, D., C. Apollo, R. Pastore, and M. Marchetti. 2010. X-Band microwave characterization of carbon-based nanocomposite material, absorption capability comparison and RAS design simulation. *Composites Science and Technology*. 70:400-409.

Mosallaei, H., and Y. Rahmat-Samii. 2000. RCS reduction of canonical targets using genetic algorithm synthesized RAM. *Antennas and Propagation, IEEE Transactions on*. 48:1594-1606.

Motevasselian, A. 2010. On the scattering reduction of an aircraft wing profile enclosing an antenna. KTH.

Munk, B.A. 2005. Frequency selective surfaces: theory and design. John Wiley & Sons.

Nahmias, M.E. 1977. Method and means for reducing reflections of electromagnetic waves. Google Patents.

Neher, L.K. 1953. NONREFLECTING BACKGROUND FOR TEST. Google Patents.

Newman, P.R., L.F. Warren Jr, and E.F. Witucki. 1986. Process for producing electrically conductive composites and composites produced therein. Google Patents.

Nortier, J.R., C.A. Vanderneut, and D.E. Baker. 1987. Tables for the Design of Jaumann Microwave Absorber. *Microwave J*. 30:219-222.

Oh, J.-H., K.-S. Oh, C.-G. Kim, and C.-S. Hong. 2004. Design of radar absorbing structures using glass/epoxy composite containing carbon black in X-band frequency ranges. *Composites Part B: Engineering*. 35:49-56.

Oh, K.W., K.H. Hong, and S.H. Kim. 1999. Electrically conductive textiles by in situ polymerization of aniline. *Journal of applied polymer science*. 74:2094-2101.

Oikonomou, A., T. Giannakopoulou, and G. Litsardakis. 2007. Design, fabrication and characterization of hexagonal ferrite multi-layer microwave absorber. *Journal of Magnetism and Magnetic Materials*. 316:e827-e830.

Olmedo, L., P. Hourquebie, and F. Jousse. 1995. Microwave properties of conductive polymers. *Synthetic Metals*. 69:205-208.

Otto, H., J.M.H. Johnson, and R.W. Wright. 1960. Isotropic absorbing layers. Google Patents.

Parida, R.C., D. Singh, and N. Agarwal. 2007. Implementation of multilayer ferrite radar absorbing coating with genetic algorithm for radar cross-section reduction at X-band. *INDIAN JOURNAL OF RADIO AND SPACE PHYSICS*. 36:145.

Park, K.-Y., J.-H. Han, J.-B. Kim, and S.-K. Lee. 2011. Two-layered electromagnetic wave-absorbing E-glass/epoxy plain weave composites containing carbon nanofibers and NiFe particles. *Journal of Composite Materials*. 45:2773-2781.

Park, K.-Y., S.-E. Lee, C.-G. Kim, and J.-H. Han. 2006. Fabrication and electromagnetic characteristics of electromagnetic wave absorbing sandwich structures. *Composites science and technology*. 66:576-584.

Petrov, V.M., and V.V. Gagulin. 2001. Microwave absorbing materials. *Inorg Mater+*. 37:93-98.

Pratt, B.C. 1961. NONDIRECTIONAL. Google Patents.

Qing, Y., W. Zhou, S. Jia, F. Luo, and D. Zhu. 2010. Dielectric properties of carbon black and carbonyl iron filled epoxy–silicone resin coating. *Journal of materials science*. 45:1885-1888.

Qing, Y., W. Zhou, F. Luo, and D. Zhu. 2009. Microwave-absorbing and mechanical properties of carbonyl-iron/epoxy-silicone resin coatings. *Journal of Magnetism and Magnetic Materials*. 321:25-28.

Ramo, S., J.R. Whinnery, and T. Van Duzer. 2007. Fields and waves in communication electronics. John Wiley & Sons.

Reinert, J., J. Psilopoulos, J. Grubert, and A.F. Jacob. 2001. On the potential of graded-chiral Dallenbach absorbers. *Microwave and Optical Technology Letters*. 30:254-257.

Rhode, W., and H.F. Sparks Jr. 2001. Radar dispersion fabrics. Google Patents.

Ruck, G. Radar cross section handbook, 1981. Plenum Press.

Salati, O.M. 1954. Electromagnetic-wave energy absorber. Google Patents.

Severin, H. 1956. Nonreflecting absorbers for microwave radiation. *Antennas and Propagation, IRE Transactions on*. 4:385-392.

Simovski, C.R., M. Kondratiev, and S. He. 2000. Array of C-shaped wire elements for the reduction of reflection from a conducting plane. *Microwave and Optical Technology Letters*. 25:302-307.

Tang, C.W., and S.A. Vanslyke. 1987. Organic Electroluminescent Diodes. *Applied Physics Letters*. 51:913-915.

Tanner, H.A. 1961. Fibrous microwave absorber. Google Patents.

Terracher, F., and G. Berginc. 2000. Thin electromagnetic absorber using frequency selective surfaces. *In* Antennas and Propagation Society International Symposium, 2000. IEEE. Vol. 2. IEEE. 846-849.

Thieblemont, J., M. Planche, C. Petrescu, J. Bouvier, and G. Bidan. 1993. Stability of chemically synthesized polypyrrole films. *Synthetic metals*. 59:81-96.

Truong, V.-T., and J.G. Ternan. 1995. Complex conductivity of a conducting polymer composite at microwave frequencies. *Polymer*. 36:905-909.

Tuna, O., Y. Selamet, G. Aygun, and L. Ozyuzer. 2010. High quality ITO thin films grown by dc and RF sputtering without oxygen. *J Phys D Appl Phys*. 43.

Vanderplas, G., A. Barel, and E. Schweicher. 1989. A Spectral Iteration Technique for Analyzing Scattering from Circuit Analog Absorbers. *Ieee T Antenn Propag*. 37:1327-1332.

Varadan, V., R. Ro, and V. Varadan. 1994. Measurement of the electromagnetic properties of chiral composite materials in the 8–40 GHz range. *Radio science*. 29:9-22.

Vinoy, K.J., and R.M. Jha. 1995. Trends in radar absorbing materials technology. *Sadhana-Acad P Eng S*. 20:815-850.

Vinoy, K.J., and R.M. Jha. 1996. Radar absorbing materials: From theory to design and characterization. Kluwer academic publishers Boston.

W, T.J. 1948. Phase adjuster for fixed-branch wave guide. Google Patents.

Warren, L.F., D.S. Klivans, and L. Maus. 1986. Electrodepositing polypyrrole polymer or dielectric porous substrate, flexibility. Google Patents.

Wettermark, U.G., and G.H. Worrell. 1996. Method for producing a dimensionally graded conductive foam. Google Patents.

Woldanski, G.L. 2001. Process for making a low density foam filled reticulated absorber by means of vacuum. Google Patents.

Wright, P., T. Wong, B. Chambers, and A. Anderson. 1994. Electrical characteristics of polypyrrole composites at microwave frequencies. *Advanced Materials for Optics and Electronics*. 4:253-263.

Xu, Y., D. Zhang, J. Cai, L. Yuan, and W. Zhang. 2013. Microwave absorbing property of silicone rubber composites with added carbonyl iron particles and graphite platelet. *Journal of Magnetism and Magnetic Materials*. 327:82-86.